New maps of global geological provinces and tectonic plates

D. Hasterok[a], J. Halpin[b], A.S. Collins[a], M. Hand[a], C. Kreemer[c], M. Gard[a,d], S. Glorie[a]

[a]Mawson Geoscience Centre and Department of Earth Sciences, University of Adelaide, Adelaide, Australia

[b]Institute of Marine and Antarctic Studies, University of Tasmania, Hobart, Australia

[c]Nevada Bureau of Mines and Geology, and Seismological Laboratory, University of Nevada, Reno, Nevada, USA

[d]Geoscience Australia, Canberra, Australia

This manuscript was submitted to Earth Science Reviews on March 18th 2022. This is a non-peer reviewed preprint submitted to EarthArXiv. Subsequent versions of this manuscript may differ. If accepted, the final version of this manuscript will be available via the 'Peer-reviewed Publication DOI' link on the EarthArXiv webpage for this manuscript. Please feel free to contact any of the authors; we welcome feedback.

Address all correspondence to D. Hasterok (derrick.hasterok@adelaide.edu.au)

Email address: derrick.hasterok@adelaide.edu.au (D. Hasterok)

New maps of global geological provinces and tectonic plates

D. Hasterok[a,*], J. Halpin[b], A.S. Collins[a], M. Hand[a], C. Kreemer[c], M. Gard[a,d], S. Glorie[a]

[a]*Mawson Geoscience Centre and Department of Earth Sciences, University of Adelaide, Adelaide, Australia*
[b]*Institute of Marine and Antarctic Studies, University of Tasmania, Hobart, Australia*
[c]*Nevada Bureau of Mines and Geology, and Seismological Laboratory, University of Nevada, Reno, Nevada, USA*
[d]*Geoscience Australia, Canberra, Australia*

Abstract

Accurate spatial models of tectonic plates and geological terranes are important for analyzing and interpreting a wide variety of geoscientific data and developing compositional and physical models of the lithosphere. We present a global compilation of active plate boundaries and geological provinces in a shapefile format with interpretive attributes (e.g., crust type, plate type, province type, last orogeny). The initial plate and province boundaries are constructed from a combination of published global and regional models that we refine using a variety of geoscientific constraints including, but not limited to, relative GPS motions, earthquakes, mapped faults, potential field characteristics, and geochronology. These new plate model show improved correlation to observed earthquake and volcano occurrences within deformation zones and microplates, compared to existing models, capturing 73 and 80% of these criteria, respectively. We estimate 57.7% of the Earth's surface is covered by oceanic crust, which is a slight increase relative to the most recent seafloor age model. The model of last orogenies agrees well with peaks in the globally summed geochronology data. There is room for improvement in future editions of our global plate and geologic provinces model where basins, ice, or lack of geological data fidelity obscure bedrock geology, particularly in the eastern Central Asian Orogenic Belt, much of Africa, East Antarctica, and eastern Australia. Additionally, some province types—orogens, shields, and cratons that are homogenized within our global scheme—can likely be partitioned into smaller terranes with more precise geodynamic attributes. Despite some of these shortcomings, the digital maps presented here form a self-consistent data standard for adding spatial metadata to geoscientific databases. The database is available on GitHub where the geoscience community can provide updates to improve the models and their contemporaneity as new knowledge is acquired. The files are also released in formats suitable for use in Generic Mapping Tools and GoogleEarth.

*Corresponding author
Email address: derrick.hasterok@adelaide.edu.au (D. Hasterok)

Keywords: tectonic plate, tectonic province, orogenic system, orogeny, geodynamics, geospatial analysis

---

Contents

1. Introduction

The structural architecture, tectonic environment, and temporal evolution of rocks at the surface of the Earth is frequently are frequently correlated with the chemical and physical characteristics of the enclosing lithosphere (Gard et al., 2019b; Artemieva, 2019; Tang et al., 2020; Tetley et al., 2020). As a result, it is useful to have spatially accurate maps of geologic provinces and terrane boundaries that encompass a pragmatically uniform set of common geological characteristics for comparative global studies. Such maps also form the foundation for accurate plate reconstructions (Merdith et al., 2021). While there are some regional models of tectonic provinces that are digital (Artemieva, 2006; Laske et al., 2013), there are few accurate global models easily accessible to the geoscience community built on a multiplicity of comparative attributes that approach self-consistency.

In this paper, we present two basic models: (1) a global set of geologic provinces and (2) a model for present-day plate boundaries. Both models are presented in a vector format with accompanying metadata that can be used to improve and simplify the process of global tectonic data analysis and/or modeling across a diverse range of geoscientific phenomena. These models have been produced using a wide variety of geologic and geophysical data and have been partially validated, wherever possible, using igneous and metamorphic age dates allied with additional geophysical datasets. Our hope is these models can be used as a data standard for common classification across the variety of geological databases that currently exist. The global models presented below are freely available in open-source and form a basic digital architecture that can be progressively updated as geological data and interpretations continue to improve.

2. Existing Global Models of Tectonic Plates and Provinces

Previous global plate and province models have been published that incorporate tectonic setting, juvenile age, or thermotectonic age (e.g., Artemieva, 2006; Goutorbe et al., 2011; Laske et al., 2013; Szwillus et al., 2019). Ideally, the digital nature of these maps makes them easy to use and allows one to add desirable attributes to underlying datasets. However, the raster

format of these models is often an impediment to accurate spatial analysis at or near province boundaries due to their low resolution and pixelated nature. Even though some plate and province maps include age and province type, it may not be possible to separate individual terranes that potentially have distinctive chemical and physical characteristics. For example, a terrane-type map (Laske et al., 2013, e.g.,) can be useful for identifying data within a volcanic arc setting, but it can be difficult to separate individual volcanic arcs to compare temporal and spatial geochemical patterns that illuminate the geodynamic character. Furthermore, while some of these maps have been included in peer-reviewed publications as part of global studies, it is unclear to what degree the maps themselves have been examined in detail because the underlying geological data used to construct the maps is not available to the geological community. In some cases, it is difficult to obtain digital versions from the authors, making it challenging to validate or improve the models as a geoscientific community and achieve widespread use. As a consequence, some of these maps of global geological provinces are essentially artistic and have opaque underlying rationale that cannot be interrogated.

A few global shapefiles of province polygons do exist (Klett et al., 1997; Torsvik and Cocks, 2016; Matthews et al., 2016), but they cannot be accurately matched to the province boundaries as they are identified in regional studies. For example, the Klett et al. (1997) proposed geologic provinces were developed to assess global hydrocarbon reserves. Therefore, a narrow perceived attribute rather than broad actual attributes were used to delineate geological provinces. The models by Torsvik and Cocks (2016), Matthews et al. (2016), and Merdith et al. (2021) are based on tectonic blocks as they were developed to perform plate reconstructions (Figure 1b), but they are typically shape-defined by contemporary global geography. Some terrane boundaries agree well with published models (e.g., Africa, McCourt et al. (2013); South America, Ibañez-Mejia et al. (2011)), while others appear greatly simplified and/or do not closely follow geophysical trends for reasons that are not given (e.g., western United States, Hasterok and Chapman (2007)). Furthermore, many models are time diluted. For example, models by Matthews et al. (2016) and Merdith et al. (2021) were developed for reconstructions to 400 Ma and 1000 Ma, respectively. As a result, most Mesoproterozoic and older regions are not divided into separate terranes except where they behave as separate entities during the plate model timeframe, despite a wealth of data that would otherwise allow the organization of these older participants to be

illuminated.

In addition to the lack of globally a comprehensive and self-consistent scheme for the depiction of geological provinces, there are still ambiguities and lack of self-consistency in contemporary plate tectonic maps. Bird (2003) released a widely used plate boundary shapefile (Figure 1a). Since its release, several additional microplates have been proposed, generally on the basis of GPS motion data. The new proposed microplates are the Adria Microplate (Battaglia et al., 2004; Breton et al., 2017), the Danakil Microplate (Eagles et al., 2002; McClusky et al., 2010), the Yakutat Microplate (Fletcher and Freymueller, 1999; Bruhn et al., 2012), the Sierra Nevada Microplate (Dixon et al., 2000; Schweickert et al., 2004), several microplates around the Caribbean (DeMets and Wiggins-Grandison, 2007; Sun et al., 2020), and few microplates on the Somali Plate (Saria et al., 2014; Stamps et al., 2021). The Bird model is also missing a few microplates proposed at the time of publication including the Capricorn Microplate and Indo-Australian Deformation zone (Royer and Gordon, 1997), the Coiba and more recently associated Malpelo Microplates (Hardy, 1991; Zhang et al., 2017). The Bird model included some plate boundary deformation zones, but many zones of known deformation were excluded from the model (e.g., Gordon, 1998). Additional improvements can be gained by incorporating more recent kinematic models of strain within plate boundaries to discriminate between discrete and more continuously deforming zones (Kreemer et al., 2014).

Beyond the global models discussed above, there exists a plethora of regional geologic province and terrane maps that are downloadable. Many of these models are more precise because they may incorporate a variety of datasets as constraints (e.g., topography, bedrock geology, seismic tomography, and crustal faults or shear zones), but they are poorly designed for digital processing as they are only available as raster images in papers despite many being created using geographic software. While these depictions are sufficient for presentation in publications, the rationale and metadata are generally not available for scrutiny. Consequently, interpreted tectonic boundaries are often inconsistent between publications, especially when boundaries are envisaged beneath cover. In many publications (e.g., Gee and Stephenson, 2006; Xu et al., 2016; He et al., 2018), a province or terrane map is often secondary to the main point of the paper, and boundary definition may be schematic rather than rigorous and is commonly simply adopted from pre-existing publications. An obvious example is the

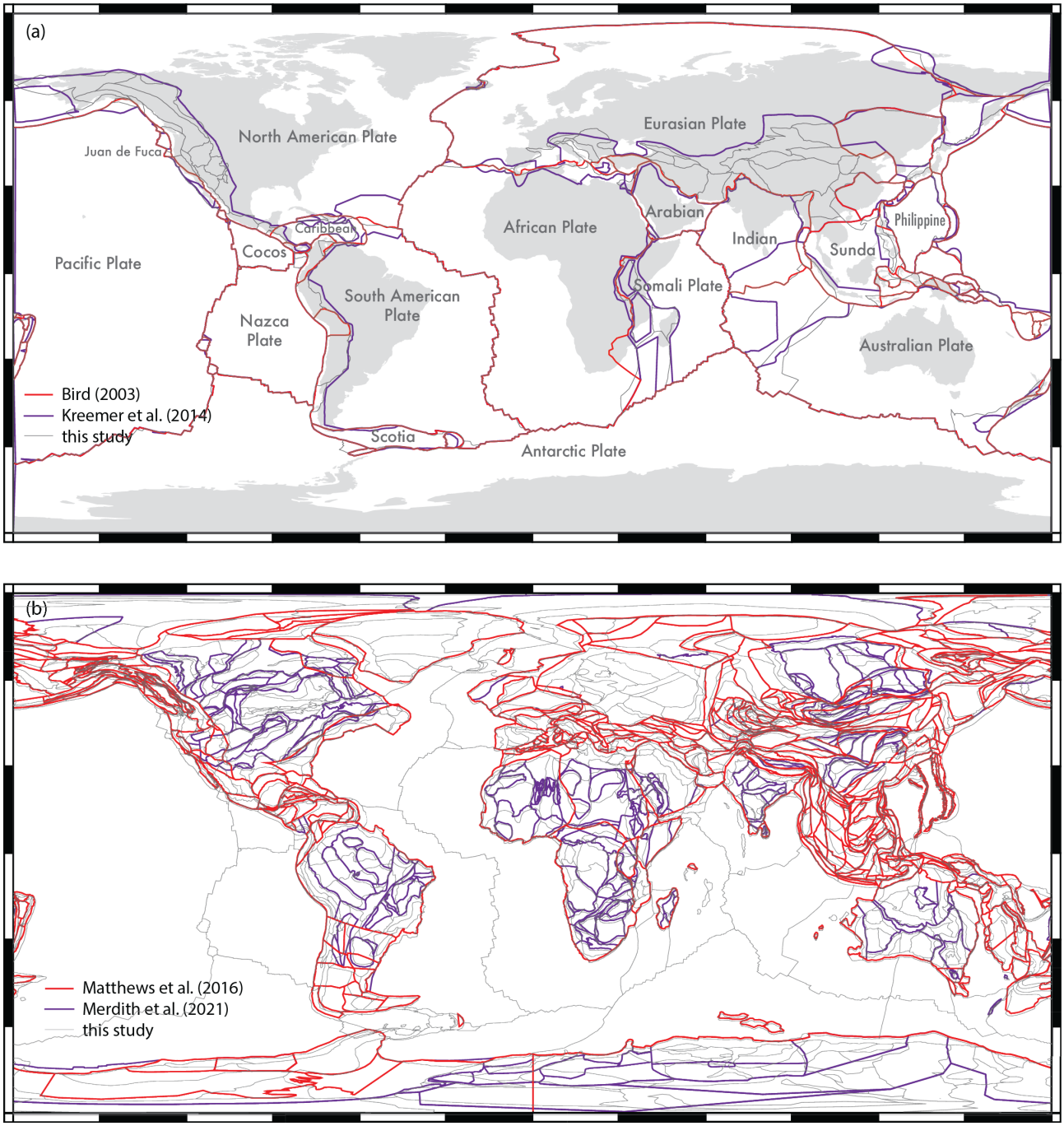

Figure 1: Tectonic plate and geologic province models. (a) A comparison between the Bird (2003) plate model, limit of modeled plate boundary zones (Kreemer et al., 2014) and the plate model from this study. Note that the limit of the deformation model domain is not an exact limit of the deformation, in many cases wider than the true deformation zone. (b) A comparison between the Matthews et al. (2016) and Merdith et al. (2021) plate models and province models from this study.

depiction of the Sahara Metacraton (Figure 14 and Figure 1 of Liégeois et al., 2013; Kwékam et al., 2020, respectively). Furthermore, the locations and level of detail lack continuity between publications, such that province boundaries cannot be easily matched up between maps of adjacent regions, even when apparently depicted in the same map projection scheme (e.g., wei Zhou and Murphy, 2005; Blayney et al., 2019).

The objective of the work we present here is to try and smooth deficiencies between existing models for tectonic province and plate boundaries by delineating a set boundaries in a vectorized format that incorporates attributes derived from geophysical, geochemical and geochronological data. Our models represent an attempt to extend tectonic boundaries back to ca. 2.3 Ga and possibly further in some cases, incorporating numerous existing geologic interpretations. Some of these interpretations are modified slightly to meet additional observational constraints from global geophysics, geologic maps and geochronology. Our goal is to create an adaptable and interactive environment that allows the geoscience community to improve delineation of geological provinces and the behaviors of their boundaries and interiors during Earth evolution. In particular, we hope creating an interactive data environment will bring more illumination to the Mesoproterozoic and older Earth, which hosts a significant fraction of metallic resources.

3. Method of Construction

The maps constructed in this study come from four separate shapefiles—also released in GMT and KML formats for use in Generic Mapping Tools and GoogleEarth, respectively. These files include the plate polygons, tectonic province polygons, the oceanic–continental crustal boundary, and plate boundary types. The ocean–continent boundary and plate boundary types are both developed in conjunction with the plate polygons. Each of these files contains a number of attributes that include a variety of contextual information. The metadata for each file are described in Table 1.

Vector format shapefiles have several advantages over the raster maps that dominate the existing literature. The polygons and lines created across the four shapefiles are seamless, i.e., they use common boundaries where geologically appropriate. Vectorized data permit multiple attributes to be assigned to each polygon, line, or point, which can be unique. Raster models allow only a single attribute per pixel, often requiring multiple maps (generally from separate

Table 1: A description of shapefile attributes for the plate and province files released in this study.

Field name	Field description
	Plate polygons (plates.shp)
id	unique polygon identifier
poly_name	unique polygon name
plate	major plate, includes microplates and deformation zones
plate_id	numeric subplate id
plate_code	subplate abbreviation
subplate	separates microplates and deformation zones from major plates
plate_type	rigid plate, microplate, or deformation zone
crust_type	continental or oceanic crust
sea_name	name of ocean or sea
domain	oceanic domain for geochemical grouping purposes
area	polygon area in square kilometers
plate_ref	reference for initial plate polygon
	Plate boundaries (plate_boundaries.shp)
feature_id	unique boundary segment identifier
feature	name of boundary segment
type	type of boundary segment
plate1 and plate2	subplates on either side of boundary segment
level	assigns an integer value, 1 = major plate boundaries and 2 = minor plate boundaries
comment	specific comments about a boundary segment
length	length of segment in kilometers
	Ocean–continent boundary (oc_boundary.shp)
id	line segment identification number
length	length of segment in kilometers
	Province polygons (geologic_provinces.shp)
id	unique polygon identifier
prov_name	unique province name
prov_type	dominant tectonic character of a tectonic province
prov_group	name for multiple polygons with a shared geological history, may contain multiple tectonic styles
lastorogen	most recent significant orogenic event
continent	continent name if on a continent
crust_type	continental, oceanic, or transitional
area	polygon area in square kilometers
comment	specific comments about a province
prov_ref	reference for initial province polygon

studies), which could lead to non-causal juxtaposition of such attributes. For example, slight differences in the boundaries of different attributes from unrelated studies could result in oceanic crust being incorporated into a continental orogenic belt or continental crust being excluded from the same orogenic system. Vector format files are also typically more memory efficient than raster images. Thus the seamless nature of the polygons in this project is a distinct advantage when constructing physical and/or compositional models of the lithosphere.

We recognize the study presented here attempts to do on a global scale, what a large number of studies have done at a variety of subordinate scales. Therefore we are aware of an element of hypocrisy in being somewhat critical of continuity between existing studies. However our goal isn't to be correct, it's to create an environment where decisions about tectonic provinces and their boundaries are globally determined where possible, using the same style of data sets and their interpretation. Where our study differs from predecessors, is the compiled data used is freely available and adoptable by more informed practitioners because the models are available on GitHub (`https://github.com/dhasterok/global_tectonics`) where community users can correct errors and omission and propose refinements.

3.1. Plate Model

The plate model consists of two separate shapefiles including the plate polygons and the boundary lines (Table 1; Figure 2). The plate shapefiles were created in QGIS using global vector and raster datasets (Table 2). We used the widely-distributed model by Bird (2003) as the initial plate boundaries to construct the shapefile (Figure 1a). Newer models that incorporate proposed past plates and microplates for use with plate reconstruction software such as GPlates were also used for reference (i.e., Zahirovic et al., 2014; Matthews et al., 2016). Although Bird's model is an excellent framework, increased spatial coverage of GPS and an additional 18 years of earthquake observations has improved our ability to recognize additional microplates and identify presently deforming regions. The strain-rate model by Kreemer et al. (2014) is also used as an initial constraint on the boundaries of microplates and deformation zones and as a way to distinguish between the two (Figure 1). Digital elevation models and global models of active faults have also improved since Bird's model (Amante and Eakins, 2009; Styron and Pagani, 2020), which allow for more accurate and precise positioning of the boundaries.

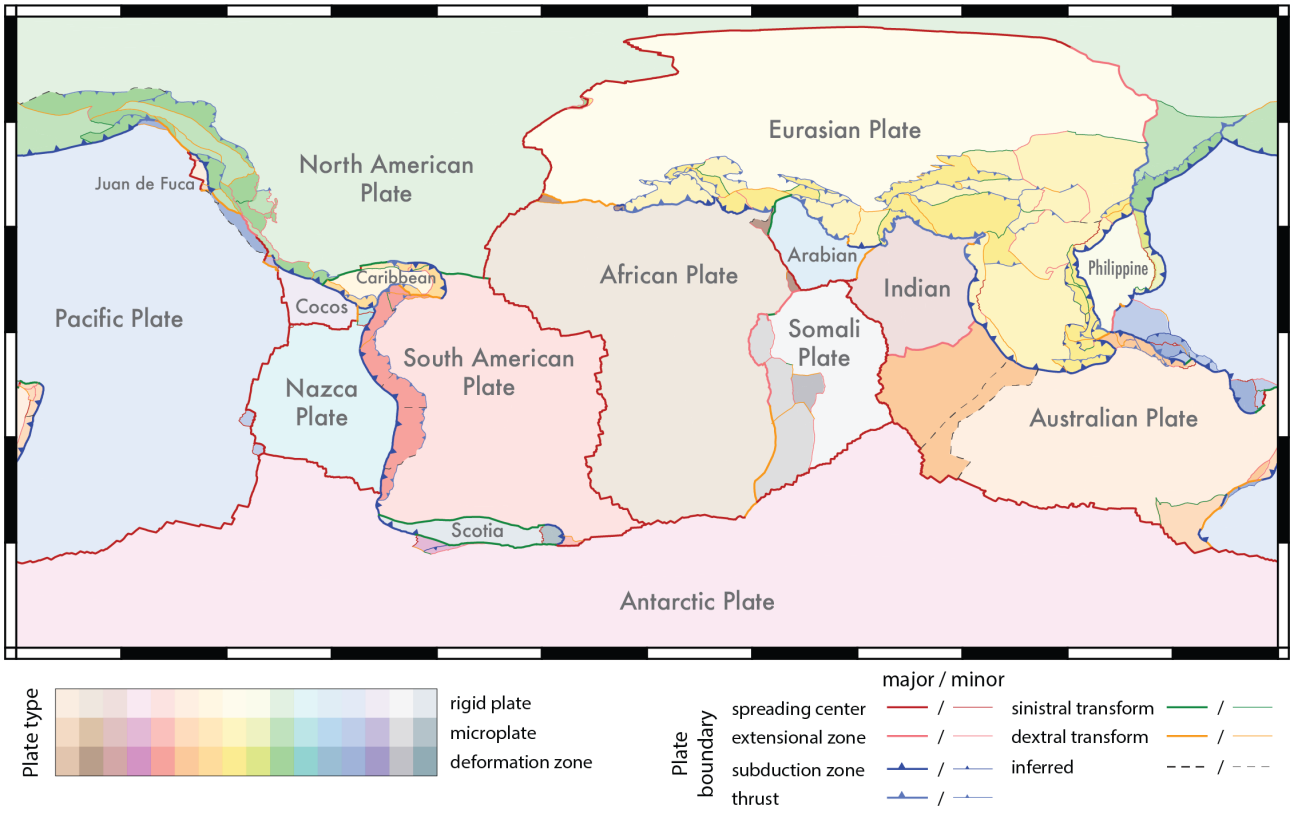

Figure 2: An updated plate model along with the plate boundary types. Microplates and deformation zones are illustrated as darker shades of the same hue as the major plate that they are most closely associated with.

Where there is ambiguity in the location of the plate boundary from topography and its gradient, the location was chosen to fit with the pattern of recent seismicity (Figure 3). We found it helpful to compute a spatial histogram of earthquakes because it is easier to identify zones of high seismicity relative to a simple scatter plot. To produce the histogram, we use global seismicity M5.5+ for 1970–1990 and M3.5+ for 1990–2020 extracted from the US Geological Survey's Advanced National Seismic System (ANSS) global seismic catalog. The earthquake density accurately traces out much of the mid-ocean ridge systems (Figure 3).

3.1.1. Plate Type

We include metadata with the plate model, including a plate_type field. The following definitions are used to distinguish plate types:

fixed plate, a region with distinct plate boundaries generally defined by seismicity, little internal deformation, distinct motion relative to several other plates, and generally large area;

microplate, a region with distinct plate boundaries generally defined by seismicity, little internal deformation, motion controlled by surrounding plates, and generally small area;

Table 2: Datasets used to develop and evaluate the plate, plate boundary, and oceanic–continental boundary models.

Region	Data Type	Description	Resolution	Reference
global	plate model	shapefile		Bird (2003)
global	plate model	GPlates shapefile		Zahirovic et al. (2014)
global	plate model	GPlates shapefile		Matthews et al. (2016)
global	earthquakes	1990-2020, <30 km, M3-M5.5		ANSS (2020)
global	earthquakes	1970-2020, <30 km, M5.5+		ANSS (2020)
global	earthquakes	heat map (ANSS data above)	0.1 degree	
global	volcanic centers			Global Volcanism Program (2013)
global	topography	ETOPO1	1 arcmin	Amante and Eakins (2009)
global	topographic gradient[a]	derived from ETOPO1	1 arcmin	
global	seafloor age		1 arcmin	Seton et al. (2020)
global	shear wave tomography	EMC-3D2018_08Sv at 70 km depth	2 degree	Debayle et al. (2016), Debayle et al. (2019)
global	active faults	GEM GAF-DB	various	Styron and Pagani (2020)
global	GPS velocities	computed as a fixed-plate reference frame for each major plate		Kreemer et al. (2014)
global	strain rate		0.25 degree	Kreemer et al. (2014)
Azores Microplate	GPS velocities	global model		DeMets et al. (2010)
Adria Microplate	GPS velocities	case study		Breton et al. (2017)
Alaska and northwest Canada	GPS velocities	case study		Elliott and Freymueller (2020)
Danakil Microplate	GPS velocities	case study		McClusky et al. (2010)
Somali Plate	GPS velocities	case study		Saria et al. (2014), Stamps et al. (2021)
Greater Antilles	GPS velocities	case study		DeMets and Wiggins-Grandison (2007), Sun et al. (2020)
Lesser Antilles	magnetics and seismic	case study		Allen et al. (2019)
Coiba and Malpelo Microplates	GPS velocities	case study		Zhang et al. (2017)
New Zealand (North Island)	Seismicity	case study		Shi et al. (2019)
Sierra Nevada Microplate	GPS velocities	case study		Schweickert et al. (2004)
Philippines and East Indonesia	GPS velocities	case study		Zahirovic et al. (2014)
Yakutat Microplate	GPS velocities	case study		Bruhn et al. (2012)

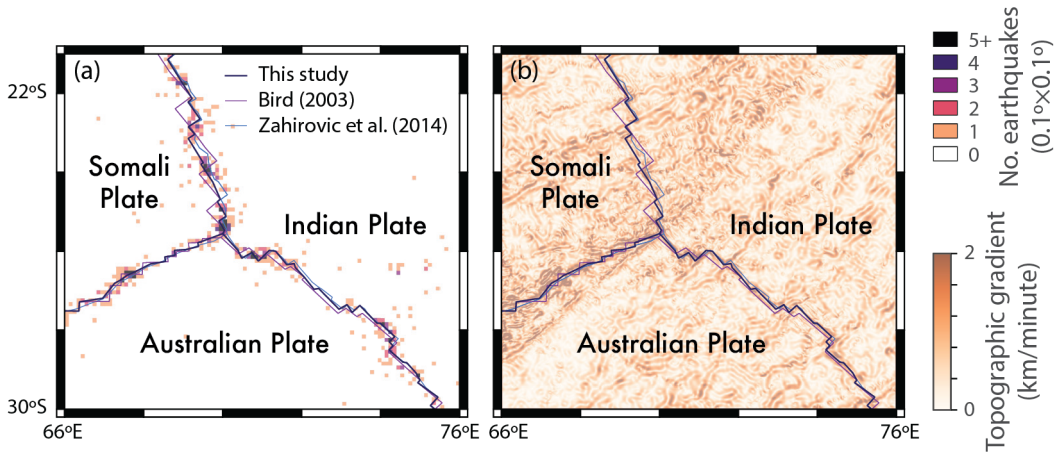

Figure 3: Refining locations of mid-ocean ridges relied heavily on the earthquake catalog, shown as histogram in (a), and topography along with its gradient (b).

and

deformation zone, a zone identified by GPS motions as distinct from, yet controlled by surrounding plates/microplates with significant internal deformation and seismicity.

The microplates and deformation zones are are associated with a parent plate for instances where a simpler model is required (Figure 2).

3.1.2. Plate Boundary Type

Plate boundaries are frequently formed by a series of several fault zones that accommodate a portion of the plate motion rather than a single discrete structure. However, there is often one fault zone that accommodates the majority of the motion, which is chosen as the boundary for the plate and plate boundary shapefiles. This choice means that in some cases, the presently most-seismically active fault may not mark the plate boundary as defined here, as it may not have accumulated the greatest displacement. For some extensional plate boundaries, the deformation is distributed over hundreds of kilometers. In these cases, we chose the boundaries by the major structures that bound the extension.

There are several plate boundary types defined in our model:

subduction zone, convergent plate boundaries, kinematically active footwall, plate1 field is the upper plate;

thrust, compression-dominated plate boundaries, kinematically active hanging wall, plate1 field is the upper plate;

ridge, divergent plate boundaries, type reserved for mid-ocean spreading centers (includes transform segments);

extensional zone, extension dominated plate boundaries, plate1 field is the upper plate;

dextral transform, right-lateral transform boundary;

sinistral transform, left-lateral transform boundary; and

inferred, unknown boundary types, or location.

Our definitions are simplified as they do not include transpressional or transtensional styles, which are classified most commonly as transform boundaries, but these may be considered in future versions.

To construct the plate boundary shapefile, we converted the plate polygons to lines and removed duplicate lines. We then split the boundaries so that each line segment represents the boundary between two plates, microplates, or deformation zones (Figure 2). Plate attributes including the boundary type are then added and stylized in QGIS. In order to ensure that thrusts and subduction zone boundaries had the barbs displayed on the upper plate, some lines were topologically reversed in direction.

3.1.3. Ocean–Continent Boundary

We split the plate polygons into continental and oceanic parts because the ocean–continent boundary is colocated with many plate boundaries. For example, subduction zones generally form the boundary between plates as well as oceanic and continental regions. However, rifts and transform boundaries may form boundaries between plates but rarely form ocean–continental boundaries. Passive margins do not represent plate boundaries but do contain the ocean–continent transition.

A single depth contour cannot be used to identify the ocean–continent transition because the depth differs from region to region as a result of variations in sediment thickness and isostatic state. To create the initial model for the ocean-continent boundary, we created a polygon that defines the global distribution from the global seafloor age model (Seton et al., 2020). This initial polygon was then modified to provide a better match to the base of steep topographic gradients (continental slope) computed from ETOPO1 (Figure 4).

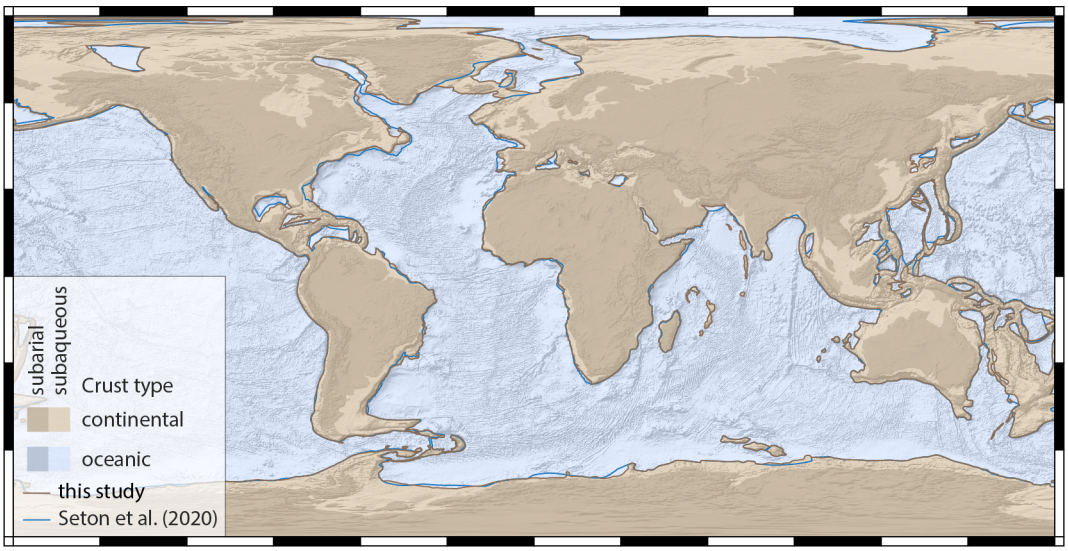

Figure 4: A model of continental and oceanic crustal domains. Plate boundaries as defined in Figure 2.

The ocean–continent boundary model could be improved with the addition of crustal thickness and/or seismic velocity estimates across the ocean–continent transition. Presently, global seismic models are of insufficient resolution to precisely identify the boundary. A compilation of seismic profiles is beyond the scope of the present work.

3.1.4. Oceanic Domain

There appear to be differences in chemistry between ocean basins (domains). For example, Brandl et al. (2013) documents a difference in basaltic geochemistry between the Atlantic and Pacific Oceans, possibly related to temperatures of melt generation. Back-arc basins, separated from the major oceans by continental ribbons behind subduction zones, tend to contain enriched basalts compared with mid-ocean ridge basalts (Langmuir et al., 2006). Thus, it is desirable to have a way to quickly divide geoscientific data into these separate domains.

For the oceanic-type crustal polygons a mantle chemical domain is included in the plates shapefile attributes table (Table 1). We have separated the oceans into nine separate domains (Figure 5). The domains are intended to make separation of data from the different ocean basins easier for geochemical and geophysical studies. However, the divisions are speculative rather than data driven, specifically the exact boundaries of these chemical domains. The only boundary that has been tested geochemically lies between the Indian and Pacific oceanic mantle (Pyle et al., 1992). This study used isotopic analyses of Sr, Nd, and Pb to place the Indian–Pacific boundary of Australia along the mid-ocean ridge at approximately 126°E. Similarly, there is also evidence for a more complex chemistry in the seafloor basalts of the Philippine

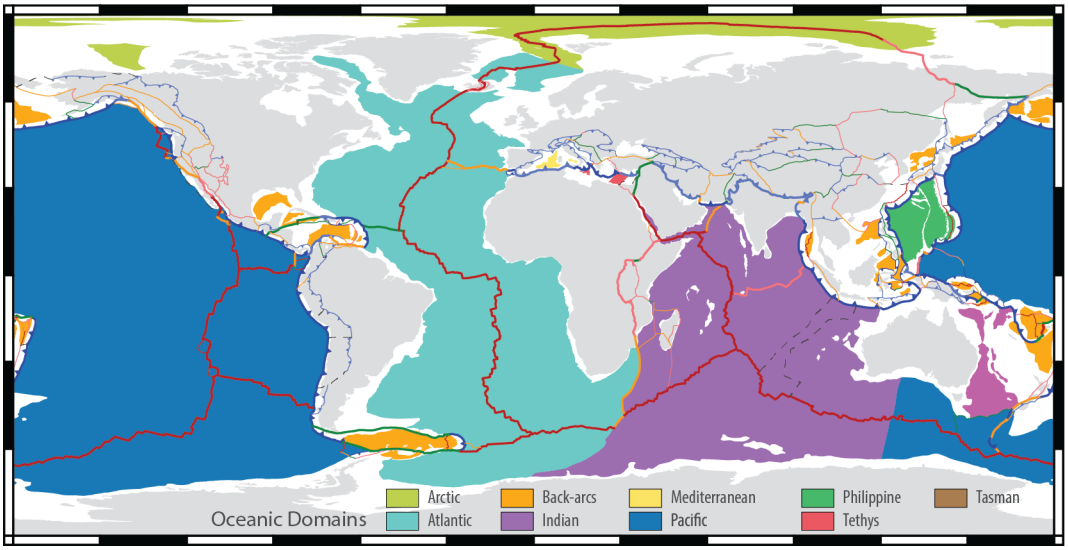

Figure 5: A hypothetical model of mantle chemical domains that source oceanic crust. At present these models are largely untested, but will be refined in future versions using global geochemical datasets.

plate compared to the rest of the Pacific (Hickey-Vargas et al., 2006).

3.2. Global Geologic Province Model

The initial province model was produced by creating a collage of overlapping geological maps from the published literature that varied from the regional to continental scale (Table 4). Many of the images were georeferenced in GIS software and vectorized using polygon tools, while others were used as a visual reference. Province names are assigned based on commonly published terms, generally taken from the reference maps themselves (Table 4).

Table 3: Geological and geophysical models used to develop province model.

Region	Data type	Description	Resolution	Reference
global	topography	ETOPO1	1 arcmin	Amante and Eakins (2009)
global	composite gravity	GGM2012	2 arc-min	Balmino et al. (2011)
global	composite magnetics	EMAG2_V3	2 arc-min	Meyer and Saltus (2016)
global	composite magnetics	WDMAMv2	5 km	Lesur et al. (2016)
global	seafloor age		2 arc-min	Seton et al. (2020)
global	volcanic centers			Global Volcanism Program (2013)
global	crustal thickness		1 degree	Szwillus et al. (2019)
global	active faults	GEM GAF-DB	various	Styron and Pagani (2020)
global	digital lithology	GLiM	0.5 degrees	Hartmann and Moosdorf (2012b), Hartmann and Moosdorf (2012a)
global	igneous dates	global geochemical database		Gard et al. (2019a)
global	metamorphic dates	metamorphic P–T database		Brown and Johnson (2018), updated
global	metamorphic dates	DateView		Eglington (2004)
Africa	surface geology and geologic provinces	USGS WEP[a]	1:5,000,000	Persits et al. (1997a)
Arabian Peninsula	surface geology and geologic provinces	USGS WEP[a]	1:2,000,000	Pollastro et al. (1999)
South Asia (India)	surface geology and geologic provinces	USGS WEP[a]	1:5,000,000	Wandrey and Law (1998)
South America	surface geology and geologic provinces	USGS WEP[a]	1:7,500,000	Schenk et al. (1999)
South America	surface geology	CGMW[b]	1:5,000,000	Gómez-Tapias et al. (2019)
Former Soviet Union	surface geology and geologic provinces	USGS WEP[a]	1:7,500,000	Persits et al. (1997b)
China, Southeast Asia, and Australia	surface geology and geologic provinces	USGS WEP[a]	1:7,500,000	Steinshouer et al. (1999)
Iran	surface geology and geologic provinces	USGS WEP[a]	1:2,500,000	Pollastro et al. (1997)
Europe	surface geology and geologic provinces	USGS WEP[a]	1:3,000,000	Pawlewicz et al. (1997)
North America	surface geology provinces	USGS	1:7,500,000	Garrity and Soller (2009)
Australia	magnetic anomaly		250 m	Australia (2004)
Australia	gravity anomaly		830 m	Wynne and Bacchin (2009)

Table 3: continued.

Region	Data type	Description	Resolution	Reference
Antarctica	bedrock topography	BEDMAP2	1 km	Fretwell et al. (2013)
Antarctica	free-air and Bouguer gravity anomalies	ANTGG	10 km	Scheinert et al. (2016)
Antarctica	shear wave tomography	AN1	4 arcmin	An et al. (2015)
Antarctica	magnetic anomaly	ADMAP2	7 km	Golynsky et al. (2018)
Antarctica	mantle gravity anomaly		5 km	Baranov et al. (2017)
Antarctica	crustal thickness	gravity and seismic based	1 degree	Baranov et al. (2017)
Antarctica	crustal thickness	satellite gravity based	0.25 degrees	Llubes et al. (2018)
Antarctica	crustal thickness	seismic methods	4 arcmin	An et al. (2015)
India	Bouguer gravity map		3 arc-min	Geological Survey of India (2006)

[a]United States Geological Survey (USGS) World Energy Project (WEP).
[b]Commission for the Geological Map of the World (CGMW)

Table 4: Published province models used to construct the initial global model.

Region	Reference
	Global
large igneous provinces	Johansson et al. (2018)
modern passive margins	Berndt et al. (2019)
	Africa
Africa	Begg et al. (2009), Hinsbergen et al. (2011)
West Africa	Ennih and Liégeois (2008)
Sahara Metacraton	Liégeois et al. (2013); Şengör et al. (2020)
Mozambique Belt	Chaúque et al. (2019), Goscombe et al. (2020)
Central Africa	Jelsma et al. (2018)
Southern Africa	McCourt et al. (2013), Hanson (2003)
Madagascar	Collins et al. (2003)
	Antarctica
Antarctica	Harley et al. (2013), Stål et al. (2019)
East Antarctica	Golynsky (2007), Harley and Kelly (2007), Elliot et al. (2015), Leitchenkov et al. (2016), Pierce et al. (2014), Pant and Dasgupta (2017), Mulder et al. (2019), Ruppel et al. (2020), Flowerdew et al. (2013), Aitken et al. (2014), Maritati et al. (2016), Maritati et al. (2019), Wang et al. (2020), Ebbing et al. (2021), Jacobs et al. (2015), Dunkley et al. (2020)
West Antarctica	Jordan et al. (2020)
	Asia
Siberian Craton	Tretiakova et al. (2017)
West Siberian Basin	Cherepanova et al. (2013)
Russia, far east	Isbell et al. (2016)
Central Asian Orogenic Belt	Xiao et al. (2015), Janoušek et al. (2018), Ivanov et al. (2014), Windley et al. (2007), Buslov et al. (2001)
North China Craton	Liu et al. (2017)
South China Craton	Wang et al. (2013)
Tian Shan Belts	Charvet et al. (2011)
Tibetan plateau	wei Zhou and Murphy (2005), Blayney et al. (2019)
southeast Asia	Mitchell et al. (2012), Burrett et al. (2014), Zhang et al. (2019), Morley and Searle (2017), Dew et al. (2021)
	Australia and Zealandia
Australia	Foster and Goscombe (2013), Pilia et al. (2015), Abdullah and Rosenbaum (2018)
Zealandia	Stagg et al. (2002), Gallais et al. (2019)
New Zealand	Mortimer (2004)
	Europe
Baltic Shield	Bogdanova et al. (2015), Zhao et al. (2002)
Mediterranean Europe	Schmid et al. (2020)
western Europe	Topuz et al. (2020)
	India and Middle East

Table 4: continued.

Region	Reference
Arabian-Nubian Shield	Johnson (2014)
Iran	Naimi-Ghassabian et al. (2018)
Pakistan	Kazmi and Rana (1982)
India	French et al. (2008)
Sri Lanka	Cooray (1994)
	North America
United States and Canada	Whitmeyer and Karlstrom (2007), Hasterok and Chapman (2007), Lund et al. (2015), Ontario Geological Survey (2011), Berman et al. (2013b), Fyffe et al. (2012), Bjorkman (2017), Linde et al. (2017)
Greenland	White et al. (2016)
Alaska and Canadian Cordillera	Colpron and Nelson (2011)
Mexico	Sedlock et al. (1993)
Caribbean and Gulf of Mexico	Allen et al. (2019); Davison et al. (2020)
	South America
South America	Ibañez-Mejia et al. (2011), Chew et al. (2008), Egydio-Silva et al. (2018)
western South America	Ramos and Aleman (2000), Eude et al. (2015), Charrier et al. (2014)

Each boundary was then adjusted for seamless fits in the global model using a combination of geologic maps, active fault databases, geochronology, topography, and geophysical anomalies/models such as gravity, magnetics, and crustal thickness (Table 3). Magnetic anomalies were the most useful geological dataset for developing the province model as the magnitude and visual character is often distinctive within a province (Figure 6). We used two global magnetic anomaly models to aid with locating province boundaries. Both are constructed from a combination of airborne and shiptrack magnetics. Because the airborne and ship track data are recorded at different altitudes and line spacing, this leads to variations in resolution and gaps filled with very low-resolution satellite observations. Where the resolution is low, it is more difficult to precisely position the province boundaries (Figure 6), , requiring more emphasis be placed on the other datasets listed in Table 3.

Topography is helpful for identifying the boundaries of many provinces as fault and shear zones are often expressed topographically. Topographic features are most helpful in active terranes, but many ancient terranes can also be delineated by the changes in morphology when the faults/shear zones are no longer immediately apparent. The relatively high resolution of ETOPO1 ($\sim$1.85 km at the equator) makes the positioning of boundaries reasonably precise.

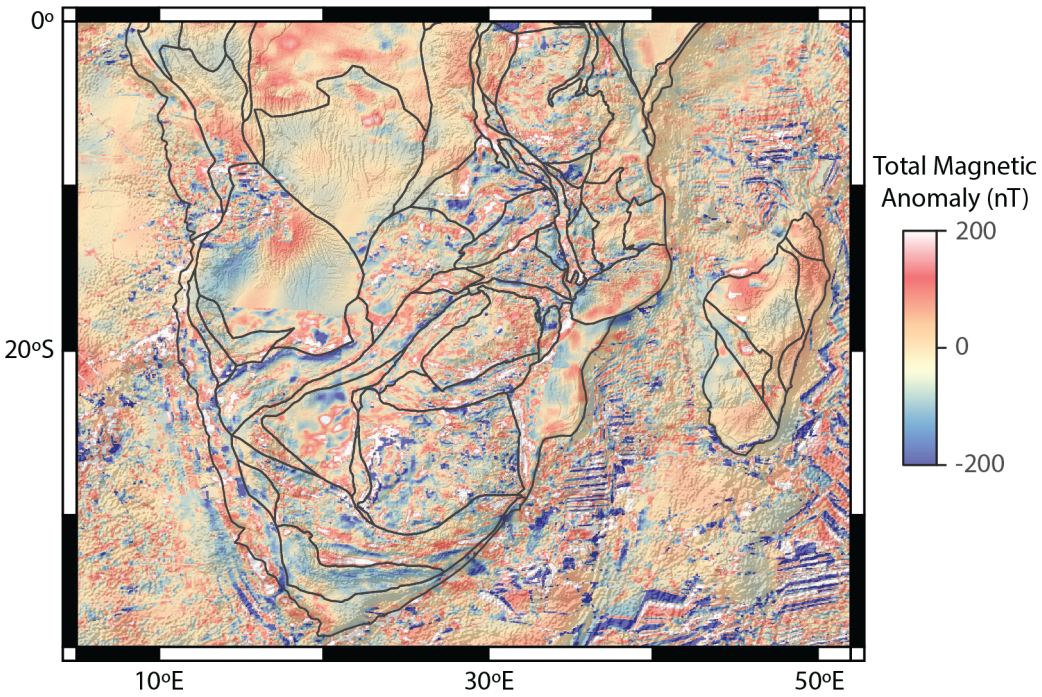

Figure 6: Magnetic anomaly map of southern Africa overlaying topographic relief. The WDMAM_V2 magnetic model has a pixel size of 1.5 minutes, which is approximately 2.8 km at the equator. The model is created from shiptrack, airborne and satellite datasets resulting in variable resolution that is evident in this image and affects the accuracy of province boundaries.

When there is a clear topographic expression at the boundary between provinces, the uncertainties are probably on the order of 3 to 5 pixels (∼5 to 10 km).

We incorporate a number of attributes ascribed to the province polygons including a province name, province group, tectonic province type, and last significant orogeny (Table 1). The province names are generally The data standards used to define these additional attributes are described below.

3.2.1. Province Type

A geologic terrane captures a set of geologic units that describe a coherent block of crust with a shared geologic history, which can include tectonic setting, magmatic history, and/or metamorphic evolution. While a terrane is less fundamental than a geologic unit or suite, there are often similarities in the physical architecture and chemistry of terranes created in similar tectonic settings (e.g., Ducea et al., 2015; Ueki et al., 2018). However, there are also differences between terranes of similar types that can be uniquely expressed in the architecture, composition, and thermal history (e.g., Furman, 2007; Dilek and Furnes, 2014; Profeta et al., 2015).

To facilitate the analysis of terranes, we include a basic province type attribute with the

shapefile. The province definitions are based on the terrane type that covers the majority of a polygon. The focus of the geologic province model is on basement terranes, hence large igneous provinces (LIPs) are not included in this model as they are superimposed on the basement, and basins have been removed except where the character of the underlying basement is unknown (Figure 7). A good model for LIPs currently exists (Johansson et al., 2018) so there is no need to recreate one as a separate layer as part of this project. A reasonable resolution (5-arc-minute) sediment thickness model by Straume et al. (2019) covers the ocean basins. Australia is covered by a high-resolution, 15-arc-second basin model (Geognostics, 2021). A 30-arc-second sediment thickness model by Pelletier et al. (2016) covers all continents except Antarctica, but only provides values for regions with less than 50 m of sediment thickness. The only available global basin thickness model has a relatively low resolution of $1° \times 1°$ (Laske and Masters, 1997).

Most of the terrane definitions we have chosen distinct characteristics within a modern plate tectonic setting:

craton, predominantly Archean core, contains granite-greenstone belts and other undifferentiated terranes with relatively small area;

shield, similar to a craton, predominantly Meso- to Paleoproterozoic lithosphere, undifferentiated;

passive margin, sediment accumulation built on thinned continental crust facing a tectonically inactive continent–ocean margin;

accretionary complex, active/subduction margin consisting of sedimentary wedges built on oceanic or continental crust;

basin, intracontinental sedimentary cover built on preexisting continental crust with uncertain or unknown basement provenance;

foredeep basin, thick intracontinental sedimentary basin created during continent-continent collision, basement uncertain;

orogenic belt, fold and thrust belts created during accretionary, collisional and intracontinental settings that may incorporate a variety of preexisting terrane types, often commingled,

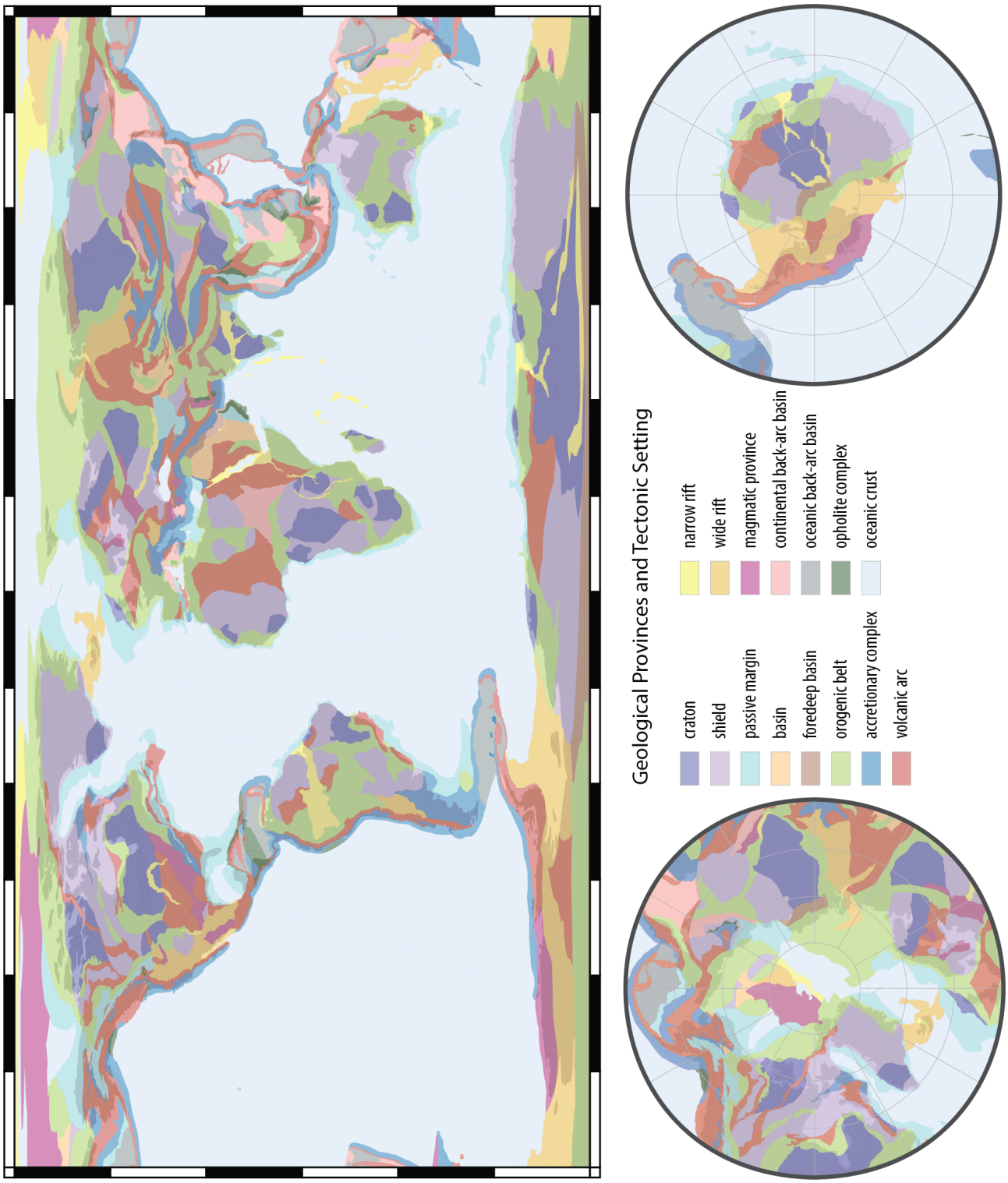

Figure 7: A global model of geological provinces with similar tectonic and compositional histories. Provinces are colored by their dominant tectonic setting. Though the setting may change with time, the provinces are defined by the environment which dominates the majority of rocks found within.

295 making them difficult to differentiate at the regional scale;

296 **narrow rift,** focused extensional terrane with continental basement;

297 **wide rift,** distributed extensional terrane with continental basement;

298 **volcanic arc,** predominantly magmatic arc crust related to subduction, but may contain crust
299 predating the arc and/or interspersed accretionary material in island arcs and in seaward
300 migrating arcs due to retreating trenches;

301 **continental back-arc basin,** a hyper-extended basin either transitional continental or oceanic
302 crust created as a result of upper plate extension in response to subduction rollback;

303 **oceanic back-arc basin,** a back-arc basin where seafloor spreading has been sustained, cre-
304 ating enriched basaltic compositions relative to mid-ocean ridge basalt;

305 **ophiolite complex,** obducted oceanic crust of some variety, excluding volcanic arc-type, but
306 including supra-subduction zone oceanic crust;

307 **magmatic province,** a large intraplate magmatic terrane not clearly associated with subduc-
308 tion or extension processes; and

309 **oceanic crust,** typical oceanic crust not created in a back-arc setting.

310 *3.2.2. Last Orogeny*

311 The most recent (last) high-temperature orogenic event to affect a province often has an en-
312 during influence on the present day thermal and physical state of the lithosphere and therefore,
313 its future potential to deform, metamorphose and melt (e.g., Sandiford et al., 2001; Fossen
314 et al., 2017; Hyndman, 2019). Here we define the last orogeny as the most recent regional
315 high-temperature thermotectonic event, excluding regions that may have experienced plume-
316 related activity. The most recent thermotectonic event is generally correlated with elevated
317 surface heat flow (Lucazeau, 2019), and lithospheric buoyancy (Fischer, 2002), depending on
318 its thermal intensity, it may reset high-temperature thermochronometers (Wan et al., 2011).

319 Orogenic systems often span a few hundred million years and comprise multiple, smaller
320 orogenic events that exhibit significant regional variability (e.g., Ge et al., 2014; de Gromard
321 et al., 2019). For example, orogenic activity may propagate along a system over time as

exhibited by protracted continent–continent collision as in the Alpine Himalayan Belt (Kuhnt et al., 2004; Dilek, 2006; Ustaszewski et al., 2010; Hu et al., 2016; Symeou et al., 2018; An et al., 2021), hence the last orogeny descriptor is not as finely resolved in age as the activity in any given region. Instead, we use the last orogeny term to represent long-lived tectonic/geodynamic systems. These descriptors are often related to consumption of ocean basins ± continental collision; though they can also apply to an intraplate orogeny. In the Phanerozoic, the divisions are generally well-defined, but in the Precambrian, the connection between orogenic systems and now-isolated provinces may be less certain (e.g., Li et al., 2008). In these cases, the names refer to periods of orogenic activity rather than discrete systems. While this somewhat blurs the meaning of the term, we prefer it over several colloquial orogenic names. It also represents a research opportunity for improving models of orogenies and more accurately capture multiple distinct systems that may overlap in age.

The last orogeny model is built from reviews and large-scale studies of orogenic systems and plate reconstructions, assigning a single orogeny to each province polygon (Figure 8). We then validate the orogeny model against databases of igneous and metamorphic dates. Recently, Condie et al. (2021)attempted to quantify orogens and link them to other global processes by using the 'number of orogens' as a measurable quantity. We suggest that this is too arbitrary a parameter and instead we have attempted an 'orogenic province' approach where we suggest linking orogens and orogenies based on their interpreted tectonic/geodynamic system. To take the modern Earth as an example, this approach then links the active circum-Pacific orogens into one orogenic province, but separates them from the Alpine-Himalayan system. Understandably, this gets more subjective in deep time, but it provides a framework for building geodynamic models and presents hypotheses that can be robustly tested by new observations.

In the Phanerozoic, the divisions are generally well-defined, but in the Precambrian, the connection between orogenic systems and now-isolated provinces is often less certain (e.g. Li et al., 2008). We have used the emerging full-plate tectonic reconstructions of Merdith et al. (2021) and Cao et al. (in prep.) to guide us here (Figure 9). While in many cases we believe these were coherent systems, the names may refer to periods of orogenic activity rather than discrete systems (e.g., Siberian Orogeny as defined below). While this somewhat blurs the meaning of the term, we prefer it over several discrete orogenies with colloquial names. It

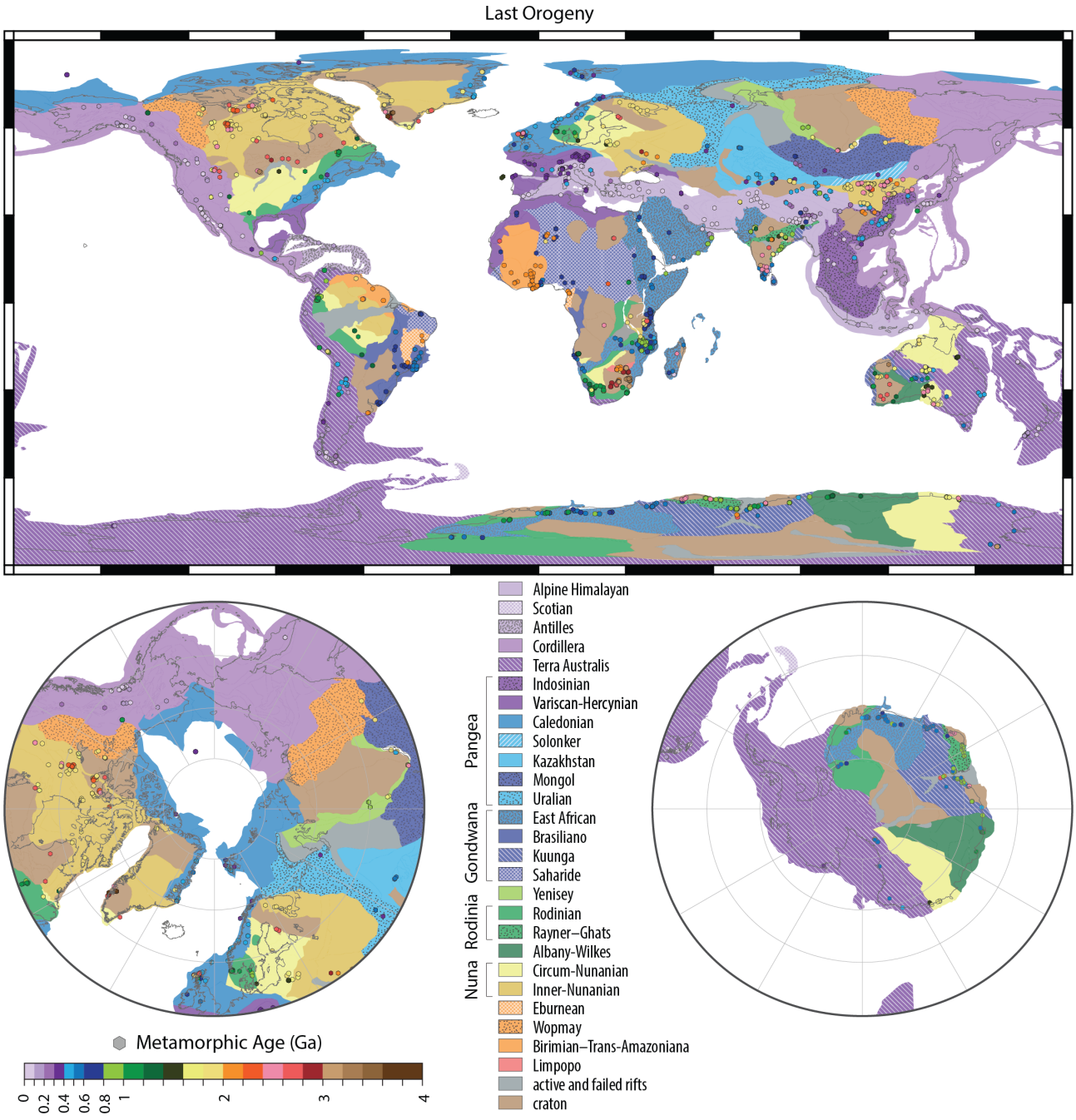

Figure 8: A map of the last orogenic event to affect a province. The colors are approximately related to the age of the orogenic event. The points show locations of observed and estimated metamorphic ages (Brown and Johnson (2018), updated; Eglington (2004)). Classification of the Phanerozoic orogens follows a systems approach as discussed in the main text.

also represents a research opportunity for improving models of orogenies and more accurately capture multiple distinct systems that may overlap in age. We define each of the orogens below.

3.2.2.1. Active Orogens

. The Alpine-Himalayan Orogeny includes the collision between several plates with Eurasia, which began ca. 65 Ma. The orogeny was initially driven by the subduction of the Tethys Ocean beneath Eurasia but has continued even as the ocean has closed in many regions. The continent–continent collisions with Eurasia were heterogeneous in time, beginning with the collision of Apulia with Europe ca. 65 Ma (Ustaszewski et al., 2010), India with Tibet ca. 61–59 Ma (earliest suggested timing; Hu et al., 2016; An et al., 2021), Australia with Indonesia ca. 25 Ma (Kuhnt et al., 2004), and Arabia with Iran ca. 13 Ma (Dilek, 2006; Symeou et al., 2018).

The Scotian Orogeny began with the initiation of subduction along the Antarctic and South American Plate margins ca. 80 Ma and continues to the present day beneath the Sandwich Islands (Eagles, 2016; van de Lagemaat et al., 2021). The Scotian Orogeny (Figure 8 and 9a), like the Antilles Orogeny (below), is geodynamically governed by a retreating subduction zone consuming the southwest Atlantic, which has created the Scotia Plate and Sandwich Microplate in its wake.

The Antilles Orogeny is a young (ca. 118 Ma to present), active orogenic system in the Caribbean that began in the mid-Cretaceous and created the Caribbean Plate as a result of rapid trench retreat (García Casco et al., 2006). The orogen is responsible for the creation of three separate arc systems: the Greater Antilles, Lesser Antilles and Aves Ridge (Figure 8 García Casco et al., 2006; Neill et al., 2011; Allen et al., 2019).

The Pacific Orogeny is defined by a set of circum-Pacific subduction zones associated with the destruction of the Pacific, Philippine Sea, Cocos and Nazca Plates beneath the South American, North American, Eurasian, and Australian Plates (Figure 9a to c). In the modern lexicon, this system is often referred to as the Cordilleran Orogeny (Dickinson, 2004); however, this is too simplistic as the Cordilleran Orogeny either merged with or grew out of the Terra Australis Orogeny (Muttoni et al., 2003), which is defined by the subduction of the Panthalassic Ocean beneath Gondwana (Cawood, 2005). We have kept these two orogens separate to preserve the association of Terra Australis with Gondwana, but acknowledge there is little reason to

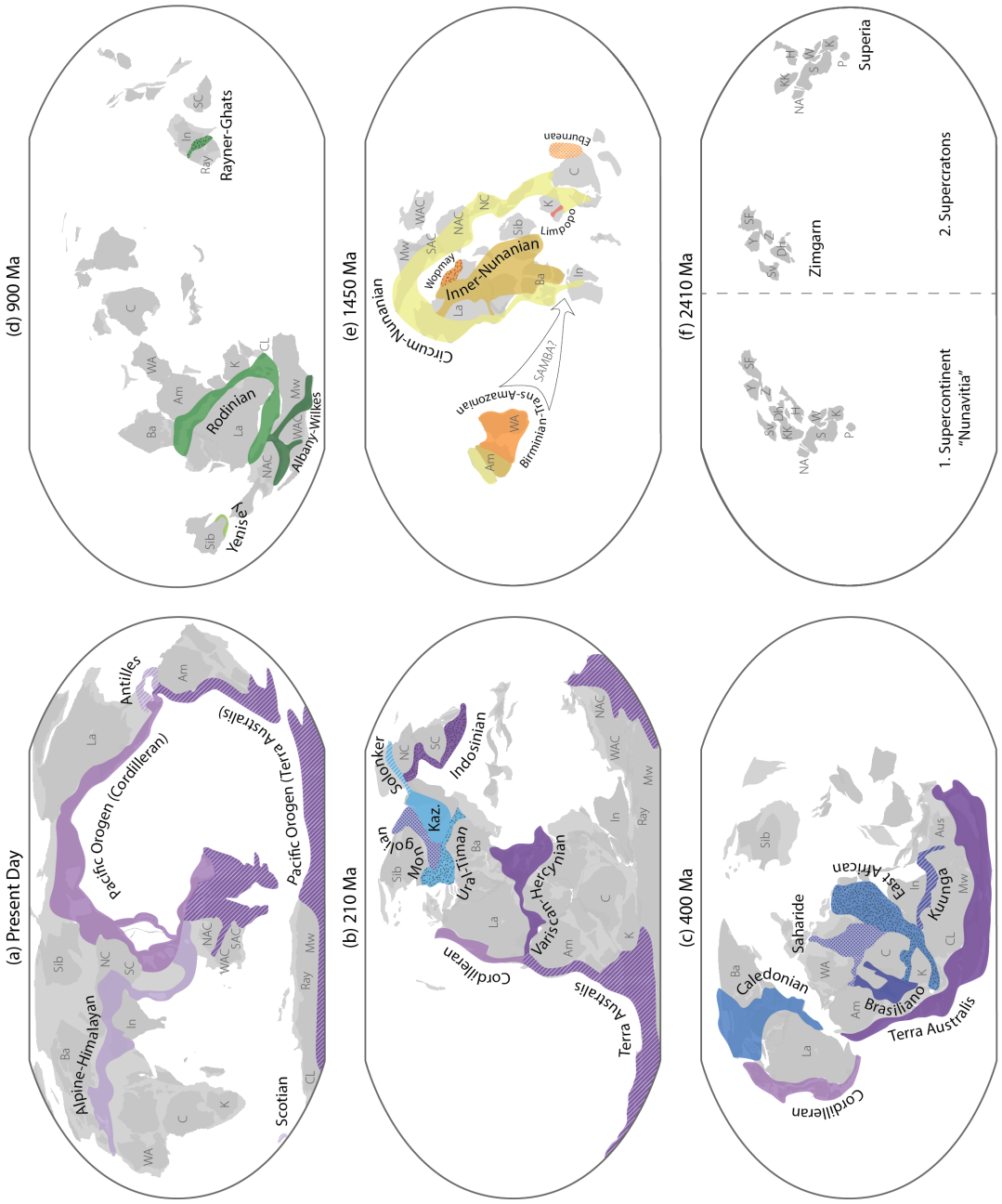

Figure 9: Reconstructions of orogenic systems at key dates. (a) Present-day shows the five active orogens. (b) Post-Pangea assembly, 210 Ma, keeping the position of Antarctica fixed. (c) Post-Gondwana assembly, 400 Ma, keeping the position of Amazonia fixed. (d) Post-Rodinia assembly, keeping Amazonia fixed. (e) Post-Nuna/Columbia assembly, 1450 Ma. Arrow indicates the alternate location of Amazonia and the West African Craton in the SAMBA reconstuctions (see Section 3.2.2.3 for discussion). (f) Supercontinent model for Nunavutia at 2410 Ma on the left and supercratons model on the right. Reconstructions (a-d) from Merdith et al. (2021), (e) from Cao et al. (in prep.), and (f) from Li et al. (2021) with terranes that were connected at 2.3 Ga: Grünehogna Craton with the Kaapvaal Craton, Penokean Orogen, North Atlantic Craton and the Nain Province with the Superior Craton; Napier Complex with the East Dharwar Craton; and the Mantiquera Province with the Saõ Francisco Craton. Abbreviations are as follows: Ba, Baltica; C, Congo Craton; CL, Coats Land; Dh, Dharwar Craton, H, Hearne Province; In, India; K, Kaapvaal/Kalahari Craton; KK, Kola-Karelia; La, Laurentia; Mw, Mawson Craton; NA, North Atlantic Craton; NAC, North Australian Craton; NC, North China; P, Pilbara Craton; Ray, Rayner Complex; S, Superior; SAC, South Australian Craton; SC, South China; SF, Saõ Francisco Craton, Sib, Siberia; Sv, Slave Craton; VU, Volgo-Ukranian Shield; W, Wyoming; WA, West Africa; WAC, West Australian Craton; Y, Yilgarn Craton; and Z, Zimbabwe Craton.

distinguish them geodynamically.

The Terra Australis Orogeny began ca. 530 to 520 Ma in response to subduction of the Pacific along the Gondwana margin (Figure 9c; Cawood, 2005; Chew et al., 2007; Paulsen et al., 2020), which continues through to the present day (Glen et al., 2016). The orogen includes a series of alternating subduction-related back-arc extensional and collisional events that built eastern Australia, Zealandia, and much of the Transantarctic Mountains (Fergusson and Henderson, 2015). Because the Terra Australis Orogen involved phases of significant extension (Gaina et al., 1998; Abdullah and Rosenbaum, 2018; Jessop et al., 2019), parts of the orogen are no longer active and/or have been separated by seafloor spreading (i.e., Delamerian, Thompson and New England orogens of Australia, Patagonia in South America, Ross Orogen in Antarctica, and the Cape Fold Belt in South Africa). Some authors consider parts of the Terra Australis Orogen to be part of the Cordilleran (Ross Orogen in Antarctica and Southern Alpine Orogen in New Zealand, Tagami and Hasebe, 1999; Dickinson, 2004) or the Alpine-Himalayan Belt (Zealandia, Lister et al., 2001). However, we associate these regions with the Terra Australis Orogeny due to (1) their former common Gondwana association and (2) the orogenic system largely predates both the Alpine-Himalayan and Cordilleran Orogenies. In the eastern South Pacific, South America is moving westward over the young oceanic lithosphere (Schepers et al., 2017). The modern Andes are ca. 66 Ma old (Capitanio et al., 2011), reaching their current heights ca. 14 Ma (Evenstar et al., 2015); however, some estimates suggest subduction formed a volcanic arc in South America by 530 Ma (Chew et al., 2007).

The Cordilleran Orogeny from Canada to Mexico is long-lived, starting in the late Devonian (ca. 370 Ma) with the collision of the Antler Orogeny and subsequently the Sonoma Orogeny in the Triassic along the western North American margin (Figure 9c; Dickinson, 2004). At the end of the Sonoma Orogeny, a continental magmatic arc system extended along the western North American boundary (Dickinson, 2004), some of the remnants of which are still active today in the Cascades, Trans-Mexican Volcanic Belt and Middle America Arc. Subduction has all but ceased along the Canada to Mexico margin as a transform margin developed ca. 50 Ma (Queen Charlotte Fault predecessor, Rusmore et al., 2010) and ca. 28 Ma (San Andreas Fault, Atwater and Stock, 1998) leading to gravitationally relaxation of the orogen (Liu and Shen, 1998). In the western Pacific, subduction zones are generally in retreat, causing significant upper-plate exten-

sion in the back-arcs (Vaes et al., 2019). We also include the Verkhoyansk-Kolyma Orogeny of far east Russia in our Cordilleran classification (Figure 8), which experienced intracontinental deformation during the mid-Cretaceous in response to compressional forces applied by relative Siberian and Alaskan convergence, but is no longer active (Oxman, 2003; Filatova and Khain, 2008). The eastern half of the North China Craton also experienced widespread volcanism in the Mesozoic and Cenozoic related to Pacific subduction (Wu et al., 2019). While there is no metamorphic evidence for resetting of high-temperature thermochronometers, there is ample evidence for significant modification of the lithosphere (Kusky et al., 2007; Yang et al., 2018; Li et al., 2019; Dong et al., 2021).

3.2.2.2. Neoproterozoic to Mesozoic Orogens

. The Indosinian Orogeny, ca. 310 to 200 Ma, resulted from the closure of the Paleo-Tethys and Paleo-Pacific oceans in the late Paleozoic and early Mesozoic and led to the formation of much of East Asia (Lepvrier et al., 2004; Morley et al., 2013; Arboit et al., 2016; Gao et al., 2017; Dew et al., 2021). Specifically, the orogeny involves the collision of South China with North China, Indochina with South China, and the Sibumasu Terrane with Indochina and the intervening Sukhothai arc terrane (Arboit et al., 2016; Gao et al., 2017; Dew et al., 2021). It is responsible for the accretion and amalgamation of much of East Asia (Figure 9b).

The Variscan-Hercynian Orogeny is defined by the closure of the Rheic Ocean ca. 290 Ma (Matte, 2001; Nance et al., 2012). The orogeny spans the period from ca. 360 to 280 Ma (Edel et al., 2014; Žák et al., 2014) and extended from north and western Mexico to Florida in North America, the Iberian Peninsula to the Tornquist zone in Europe and included parts of north and west Africa (Figure 9b; Catalán et al., 2021). The orogeny concluded with the collision of Gondwana with the Carolina Arcs, Meguma, Amorica and Avalonian terranes with Laurussia (Stampfli et al., 2013). In Europe, the orogeny involved several additional microcontinents that comprise western Europe (i.e., Iberia and Cadomia). Further east, the orogen merges into the early Alpine-Himalayan Orogen and the late Central Asian Orogenic Belt and Indosinian orogens with the closure of the various strands of the Paleotethys and Paleo-Asian Oceans (Sengör and Natal'in, 1996; Robertson et al., 2004; Xiao et al., 2015; Gardiner et al., 2016).

The Caledonian Orogeny comprises a series of orogenic events spanning the period ca. 540 to 350 Ma resulting from the closure of the Iapetus Ocean (Figure 9c; McKerrow et al., 2000; Weller

et al., 2021). The orogen is typically associated with deformation from northeastern Greenland, Svalbard and western Baltica, extending through the British Isles and continuing south in the Appalachian Mountains (Weller et al., 2021). In eastern North America and Baltica, this orogeny ended with the collision of Avalonia with Laurussia (Nance et al., 2012). We have also included the Arctic Innuitian (Ellesmerian) Orogeny in our Caledonian Orogeny definition due to its proximity in space and time to the Caledonian system sensu stricto (Barnes et al., 2020), though the Innuitian occurred near the end of the Caledonian and is nearly orthogonal in strike. While portions of the Innuitian Orogeny were overprinted in the early Tertiary by the Eurekan Orogeny, this intracontinental deformation was relatively minor and is difficult to distinguish from the earlier Innuitian Orogeny (Gion et al., 2017, and references therein).

The Central Asian Orogenic Belt (CAOB; Windley et al., 2007) has been divided into the three separate orogenic systems following the model presented by Xiao et al. (2015), which involves subduction and eventual closure of distinct regions of the Paleo-Asian Ocean from the Tonian until the Triassic. The larger system is divided into (1) the Kazakhstan tectonic collage and orocline; (2) the Mongolia tectonic collage; and (3) the Tarim-North China system, which we refer to as the Solonker Orogeny (Figures 8 and 9b), that overlaps in age with the more southern Indosinian Orogeny (Xiao et al., 2015; Song et al., 2018). Accretion of the Kazakhstan and Mongolian tectonic collages continued through the Neoproterozoic and Paleozoic and were terminated by the Solonker Orogeny at ca. 270 to 235 Ma that marks the final closure of the Paleo-Asian Ocean (Eizenhöfer et al., 2014; Song et al., 2018, 2021). The CAOB was subsequently reactivated during the Meso-Cenozoic in response to distant events related to the progressive consumption of the Tethys and Mongol-Okhotsk Oceans (e.g., Glorie and Grave, 2016). The Bureja-Jziamusy Terrane also experienced deformation as part of the Solonker Orogen, but was subsequently overprinted by Cordilleran deformation as recently as ca. 95 to 90 Ma (Derbeko, 2013).

The Uralian-Timan Orogeny is the result of several subduction-related magmatic periods spanning the period ca. 610 to 250 Ma (Figure 9b Fershtater, 2012; Pease, 2021). Oceanic arc volcanics associated with the subduction of the Paleo-Asian orogen are recorded in the Pechora arc (ca. 560 Dovzhikova et al., 2004) and blueschists and eclogites in the Urals (ca. 530 Willner et al., 2019). The latter set of magmatic events is related to the subduction and closure of the

Paleo-Asian ocean and collision with the Kazakhstan Orocline (Xiao et al., 2015). The Uralian Orogeny extends into the Taimyr Fold belt where compression continued to 220 Ma, after the orogen had ceased elsewhere (Torsvik and Andersen, 2002).

The Neoproterozoic to Cambrian Gondwana-forming orogenies are a set of generally contemporaneous orogens—though they span nearly 700 Ma (1200 to 500 Ma)—culminating in the amalgamation of Gondwana (Figure 9c; Collins and Pisarevsky, 2005; Meert and Lieberman, 2008; da Silva Schmitt et al., 2018; Goscombe et al., 2020; Şengör et al., 2020; Collins et al., 2021b). We have separated these orogenies into the East African, Saharide, Kuunga, and Brasiliano orogenies in much the same way as the Central Asian Orogenic belt was separated into distinct systems. The East African Orogen (Stern, 1994; Collins and Windley, 2002; Johnson et al., 2011; Fritz et al., 2013; Collins et al., 2021b) runs through Arabia, eastern Africa, Madagascar, southern India and into the Lützow-Holm Bay area of Antarctica. Whereas, we have located the Kuunga Orogen (Meert and Voo, 1997) as being the orogen that separated Neoproterozoic India from Australia/Mawson (Collins and Pisarevsky, 2005), running through NE India, SW Australia and into Antarctica. This is broadly the trace of the Pinjarra Orogen of Fitzsimons (2003) and Prydz-Denman-Darling Orogen of Collins and Pisarevsky (2005), but may include the Mirny Fault (Daczko et al., 2018) and Gamburtsev suture (Ferraccioli et al., 2011) as Neoproterozoic plate boundaries between Indo-Antarctica and Australo-Antarctica (Mulder et al., 2019). Şengör et al. (2020) recently suggested the Tuareg Shield, Arabian-Nubian Shield, and portions of the Saharan Metacraton constitute a single volcanic arc system that was segmented and recombined in a fashion very similar to the Kazakhstan and Mongolian oroclines. We tentatively accept this model for the Tuareg Shield and Saharan Metacraton, but include the younger Arabian Nubian Shield in the East African Orogen (Figure 8), whilst appreciating a likely continuity of orogenesis from one to the other (Blades et al., 2021; Collins et al., 2021a). Our use of Brasiliano Orogen encompasses all the South American Gondwana-forming orogens, as well as orogens along the west coast of Africa that correlate with them (including the West Congo Orogen, the Rokelides, the Gariep Belt and the Kaoko Belt).

In the early Neoproterozoic, ca. 880 to 500 Ma, a small subduction-related orogen occurred along the present-day eastern and southern margin of the Siberian Craton (Vernikovsky et al., 2003; Kuzmichev and Sklyarov, 2016), which we refer to as the Yenisey Orogeny (Figures 8 and

9). The orogeny coincided with the accretion of the Angara terrane at ca. 870 Ma, (Vernikovsky et al., 2007; Gladkochub et al., 2010). Numerous A-type magmatic dates, ca. 880 to 720 Ma, are interpreted as part of a back-arc basin system (Kozlov et al., 2012; Kuzmichev and Sklyarov, 2016) and is consistent with metamorphism recorded during this interval (Gladkochub et al., 2010). The system transitioned to seafloor spreading creating the Isakovka Terrane, an arc ophiolite, ca. 700 to 635 Ma (Vernikovsky et al., 2003; Kuzmichev and Sklyarov, 2016), which later accreted to the continent associated with a 500 to 470 Ma high-temperature metamorphic event in the middle of the orogen (Gladkochub et al., 2010, and references therein).

3.2.2.3. Paleo- to Mesoproterozoic Orogens

. Today, the Mesoproterozoic and Paleoproterozoic orogens are fragmented and scattered across multiple continents (Figure 8), and in many places, reworked by more recent events (Phillips et al., 2009). This dispersion and tectonic overprinting obscures the orogenic systems with time and makes it more difficult to associate terranes with individual orogens. As a result, we recognise that our orogenic-systems approach becomes more subjective. To retain an orogenic-systems approach as much as possible, we have used paleomagnetic-based (e.g., Condie et al., 2021) and full-plate tectonic (Merdith et al., 2021; Cao et al., in prep.) reconstructions (Figure 9d to f), while recognising an inevitable shift to a more temporal-based scheme for the pre-Neoproterozoic.

The late Mesoproterozoic to Tonian orogenies include the orogens that assembled Rodinia (Figure 9d), which are now widely dispersed across the globe (Figure 8; Li et al., 2008). Many studies refer to orogenesis during the period 1.3 to 0.9 Ga as Grenvillian-aged (e.g., Tohver et al., 2006; Sheppard et al., 2007; Goodge et al., 2010; Chattopadhyay et al., 2015). However, the conflation of orogen names to mean stretches of time has caused considerable confusion. For example, the term 'Pan-African' has been used to mean any orogen that occurred between ca. 800 and 400 Ma (Kröner, 1980), whereas orogens of this age form a number of discrete orogenic systems (see discussion of Gondwana above). Similarly with the term 'Grenvillian' (e.g., Krannendonk and Kirkland, 2013). Fitzsimons (2000) pointed out that the late Mesoproterozoic to Tonian orogens that appear to surround Antarctica, in fact, fall into discrete time brackets that relate to three different orogenic systems. Using the reconstruction by Merdith et al. (2021) as a guide, we have separated the orogens of this period into the Rodinian, Rayner-Ghats, and

Albany-Wilkes Orogenies as separate systems active between 1.3 to 0.9 Ga.

The Rayner-Ghats Orogeny, ca. 1.1-0.9 Ga, has been interpreted as a distinct orogen outside of Rodinia in recent global plate models (Figure 9d; Merdith et al., 2021). This orogen includes the Rayner Complex in Antarctica (Halpin et al., 2013; Liu et al., 2014; Morrissey et al., 2015), conjugate terranes in India (the Eastern Ghats; Korhonen et al., 2011) and the Central Indian Tectonic Zone (Bhowmik, 2019).

The 1.3 to 1.0 Ga Rodinian Orogeny (Figures 8 and 9d) includes the Grenville and Llano provinces in North America (Whitmeyer and Karlstrom, 2007; Johansson et al., 2022), which, during Rodinia assembly, we link with the 1.1 to 1.0 Ga Namaqua-Natal Belt in southern Africa, the Maud Belt and Coats Land Block in Antarctica, and possibly the eastern South Tasman Rise (Mulder et al., 2018). We also include the ca. 1.1 to 0.9 Ga Laurentia-Australia transform as part of the Rodinian Orogeny that Mulder et al. (2018) connects to Rodinian subduction zones. In South America, the Rondonia-Juruena Province and its continuation underneath the Llanos Basin had a long-lived history of deformation spanning ca. 1.32 to 0.96 Ga (Tohver et al., 2006) with late magmatic activity in the Sunsás Orogen (1.17 to 1.08 Ga; Santos et al., 2008; Nedel et al., 2020; Johansson et al., 2022).

The Albany-Wilkes Orogeny, ca. 1.38 to 1.13 Ga, resulted from the collision of the West Australian Craton with the North and South Australian Cratons and the Mawson Craton of Antarctica (Figure 9d; Maritati et al., 2019; Pawley et al., 2020). Mulder et al. (2018) suggests that the Albany-Wilkes Orogen is likely a continuation of the Grenville-Maud system (Rodinian in our lexicon). However, the Albany-Fraser and Wilkes Orogenies may have started on the same broad margin of Nuna/Columbia during break-up through to the assembly of Rodinia (Pisarevsky et al., 2003, 2014; Yang et al., 2020; Kirscher et al., 2020). Most of the Rodinian deformation occurs on the opposite side of Laurentia from East Antarctica/Australia and starts at a later time; hence we consider the Albany-Wilkes to be a separate system. Recent dating of 1.38 to 1.275 Ga metamorphism in the Rudall Province and Western Musgraves, respectively (the Parnngurr and Mount West Orogenies; Howard et al., 2015; Payne et al., 2021) extends the early Albany-Fraser orogenesis north and documents collision between the West Australian Craton and the combined South and North Australian Cratons. However, in places these were subsequently overprinted during the Miles (ca. 650 to 625 Ma) and Paterson-Petermann (ca.

580 to 530 Ma) orogenies and thus related to the Kuunga Orogeny (Figure 9c). Two metamorphic events have been dated in the Albany Fraser Orogen, ca. 1.345 to 1.260 Ga and 1.215 to 1.140 Ga, resulting from the geometry of the collision between the West Australian Cratons and the rest of Proterozoic Australia, with post-Parnngurr orogenic rotation and collision of the West and South Australian Cratons (Clark et al., 2000). The Albany-Fraser Orogen, Coompana and Madura provinces of Australia (e.g., Kirkland et al., 2017; Spaggiari et al., 2018; Pawley et al., 2020) have been linked to their Antarctic conjugates from detrital zircon spectra in offshore sediments and onshore geophysical characteristics (Maritati et al., 2019). The Wilkes Orogen records amphibolite facies metamorphism at ca. 1.305 Ga and granulite facies overprinting associated with charnockite intrusions, ca. 1.20 to 1.16 Ga (Morrissey et al., 2017). The system also includes the 1.380 to 1.275 Ga Parnngurr and Mount West Orogenies (Payne et al., 2021), an intracontinental contractional orogeny between the Yilgarn and Pilbara Cratons. Tectonothermal events are also present in the central Australian Arunta Block (ca. 1.13 Ga; Scrimgeour et al., 2005; Morrissey et al., 2011; Wong et al., 2015) and in the Western Australian Capricorn Orogen between the Yilgarn and Pilbara cratons (the 1.321–1.171 Ga Mutherbukin Tectonic Event and the 1.026–0.954 Ma Edmundian Orogeny), which occur as intracontinental far-field orogenesis to the amalgamation of Proterozoic Australia. It is unclear how far the orogen extends into Antarctica due to the extensive ice cover.

Between ca. 2.1 and 1.45 Ga two major orogenic systems are associated with Nuna (Figure 9e Pisarevsky et al., 2014; Condie et al., 2021; Cao et al., in prep.): the Inner-Nunanian Orogeny (ca. 2.1 to 1.7 Ga), which formed the core of the supercontinent; and the accretionary Circum-Nunanian Orogeny (ca. 1.85 to 1.45 Ga) that is driven by a subduction girdle surrounding the core. There are several reconstructions for Nuna (Bispo-Santos et al., 2008; Elming et al., 2009; Johansson, 2009; Zhang et al., 2012; Pisarevsky et al., 2014; D'Agrella-Filho and Cordani, 2016; Meert and Santosh, 2017; Cawood et al., 2020; Elming et al., 2021; Cao et al., in prep.), and while most are sufficiently similar to yield little difference in the last orogeny designation, there are competing models for the likely participation of Amazonia that will affect our model. In the SAMBA models, first proposed by Johansson (2009), Amazonia (Central Amazonian and Ventuari-Tapajós Belts) is contiguous with the Baltic Shield, ca. 2.1 to 1.8 Ga, both which experienced significant intrusive magmatism during the Nunanian Oro-

genies (e.g., Almeida et al., 2007; Bogdanova et al., 2015; Juliani et al., 2021). In the alternative configuration by Pisarevsky et al. (2014), Amazonia and the West African Craton form a lesser continent separate from Nuna (Figure 9e Cao et al., in prep.), deforming as part of a separate accretionary margin. We have included the Amazonian Belts as part of the Nunanian Orogenies (Figure 8 and 9e), but acknowledge that they may have evolved as a separate system.

The Inner-Nunanian Orogeny, ca. 2.1 to 1.76 Ga, was a major global event related to the closure of the Manikewan Ocean and assembly of the Nuna/Columbia supercontinent (Corrigan et al., 2009; Weller et al., 2021). In North America, the Superior Craton collided with the Reindeer Zone and Sask Craton, in a collision that has been compared to India colliding with southern Asia (St-Onge et al., 2006; Darbyshire et al., 2017; Weller and St-Onge, 2017). On the opposing side of the Reindeer Zone, the core of the orogen, contains a number of terranes, grouped into the Hearne and Rae Cratons, which are sutured together by the Snowbird Tectonic Zone (Thiessen et al., 2018). Deformation extended across to the Taltson-Thelon Arc (ca. 1.87 to 1.84 Ga) between the Rae and Slave Cratons (Chacko et al., 2000; Whalen et al., 2018). Baltica also experienced widespread orogenic activity as part of the Inner-Nunanian system that is recorded in igneous and metamorphic activity that affected the Kola Block (e.g., MIkkola et al., 2018; Daly et al., 2001; Tuisku and Huhma, 2006; Makkonen et al., 2020), which at the time, the present-day northern margin of the Kola Peninsula was adjacent to the eastern margin of northern Greenland (Evans and Mitchell, 2011). Several reconstructions place the southern margin of the Siberian Craton against the northern Margin of Laurentia at this time (Condie and Rosen, 1994; Sears and Price, 2003) and Baltica to its east (Evans and Mitchell, 2011). However, more recent models suggest it collided post 1.9 to 1.84 Ga after the Anabar and Aldan terranes had accreted to the eastern margin of the Siberian Craton based on geochronology of mafic dike swarms, and post-collisional granitoids (Donskaya et al., 2009; Ernst et al., 2016). The Inner-Nunanian Orogeny also saw the amalgamation of Volgo-Uralia and Sarmatia, ca. 2.1 to 2.0 Ga (Savko et al., 2015; Baltybaev et al., 2017), and the subsequent collision with Baltica at ca. 1.82 to 1.80 Ga (Bogdanova et al., 2015). This collision is distinguished from the Circum-Nunanian belts in Baltica that run orthogonal to the Volgo-Sarmatia collision. This collision is distinguished from the Circum-Nunanian belts in Baltica that run orthogonal to the Volgo-Sarmatia collision. The spatial complexity of the Inner-Nunanian Orogeny may

result from multiple systems just as the inner Gondwana orogenies, but uncertainties in the geographic positions of many key crustal elements make it difficult to divide further at present.

The next few paragraphs discuss the Circum-Nunanian Orogeny and some of the variations in configurations. Some of these variations are slight while others are quite dramatic, but despite these differences the orogens all appear to occur along the exterior of Nuna's core as terranes were accreted. Thus regardless of the accuracy of the geologic connections between terranes, the last orogeny classification remains the same.

Wyoming was likely the first accretionary terrane added to Laurentia during the Circum-Nunanian Orogeny, colliding with the Medicine Hat Terrane causing deformation in the Great Falls Tectonic Zone (ca. 1.86 to 1.73 Ga; Gifford et al., 2018). Also during the first phase of the Circum-Nunanian Orogeny, ca. 1.85 to 1.75 Ga, the Penokean Orogeny was a small deformation event on the southern margin of the Superior craton recorded in metamorphism and accompanying magmatism (Holm et al., 2007; Vallini et al., 2007; Klier, 2019; Zi et al., 2021). On the southern margin of Laurentia, a series of exotic terranes, Yavapai (ca., 1.80 to 1.70 Ga), Mazatzal (1.70 to 1.65 Ga), and Granite-Rhyolite terranes (1.50 to 1.45 Ga), were accreted over the course of approximately 300 Ma (Karlstrom et al., 2001; Whitmeyer and Karlstrom, 2007; Amato et al., 2008; Mako et al., 2015). The Yavapai and Mazatzal terranes include juvenile arcs, ophiolites and metasediments that were accreted ca. 1.71 to 1.68 Ga and 1.646 to 1.633 Ga during the Yavapai and Mazatzal Orogenies, respectively (Whitmeyer and Karlstrom, 2007; Amato et al., 2008). The ca. 1.49–1.45 Ga Picuris Orogeny occurred during a rare period of orogenic preservation between supercontinent cycles and is relatively limited geographically to southern Laurentia which included parts of Precambrian Australia at the time. The orogeny is identified in the southwestern United States where it deforms older crust and appears not to have juvenile magmatism associated with it (Daniel et al., 2013; Mako et al., 2015; Aronoff et al., 2016). The orogen extends into the northeastern United States (Medaris et al., 2021), where it is progressively overprinted by the Grenvillian Orogeny in the east. On the present-day eastern margin of Greenland, several exotic terranes were accreted to the Kola-Karelia Craton, including Bergslagen-Livonia (ca. 1.89 and 1.84 Ga) and Amberland (ca. 1.84 and 1.83 Ga; Bogdanova et al., 2015).

In Australia, extensive plate-margin orogenesis (ca. 1.82 to 1.55 Ga), similar to that inter-

preted for SW Laurentia, occurs throughout the South Australian Craton (Kimban and Kararan orogenies; Hand et al., 2007) and North Australian Craton (Yambah-Strangways-Leibig orogenies). These likely formed a continuous accretionary system (Payne et al., 2009; Betts et al., 2008; Betts and Giles, 2006). Extensive intracontinental orogenesis within Western Australia is marked by the 1.82 to 1.77 Ga Capricorn Orogeny (Johnson et al., 2013) and the 1.68 to 1.62 Ga Mangaroon Orogeny (Sheppard et al., 2005). The Isan Orogeny (including the Chewings and Olary orogenies) spanned the Paleo-Mesoproterozoic boundary (ca. 1.65-1.55 Ga). The effects of this orogeny dominate the eastern entirety of pre-Phanerozoic Australia (Morrissey et al., 2011; Tiddy et al., 2020; Volante et al., 2020), and extend into the Gawler Craton in southern Australia (Cutts et al., 2011) and into the central North Australian craton (Anderson et al., 2013). This orogeny is envisaged to have occurred as a consequence of collision between Paleoproterozoic Australia (then consisting of the North Australia Craton and the South Australian Craton with the North China Craton and a large piece of East Antarctica) and Laurentia (Pourteau et al., 2018), and is recorded by the Racklan Orogeny in NW Laurentia (Furlanetto et al., 2013). Orogenic activity coeval with younger Picuris Orogeny are found in the Gawler Craton of Australia (Hall et al., 2018; Morrissey et al., 2019), and in the Mount Isa region of NE Australia (Cave et al., 2022).

In Antarctica, ca. 1.7 Ga orogenesis recorded along the coast of the Mawson Craton (Peucat et al., 1999), as well as in the central Transantarctic Mountains (Goodge et al., 2001; Brown et al., 2021), although the extent of this orogenic activity into the interior of Antarctica is unknown, it appears to be an extension of deformation in the Gawler Craton. There is some ambiguity in the connections between Australia, Antarctica and western Laurentia (Wingate et al., 2002), however, the connection of these three bodies is established from paleomagnetics and geologic observations (aforementioned Nuna reconstructions; Whitmeyer and Karlstrom, 2007). The difficulty in precisely resolving the connections results from reworking of western North America during the Cordilleran Orogeny and the uncertainties in paleomagnetic poles.

The accretionary orogenesis at this time on both the Dharwar-Bastar Cratons (South India) and the Bundelkhand Craton (northern India) is recorded in the Krishna Orogeny of the Ongole Domain (1.68-1.60 Ma; Henderson et al., 2014) and in the Central Indian Tectonic Zone (Bhowmik, 2019), respectively. The two halves of Peninsula India were likely separate conti-

682 nents before the Neoproterozoic. Paleomagnetic reconstructions have placed Southern India
683 conjugate to Antarctica or NE Australia (Zhang et al., 2012); however, more recent models
684 place the Indian continent adjacent to Baltica (Pisarevsky et al., 2003; Cawood et al., 2020).
685 Regardless, the Eastern Ghats appear to have been part of the active accretionary margin of
686 Nuna from 1.85 to 1.60 Ga or possibly as late as 1.45 Ga based on dating of tectonomagmatic
687 activity and an accreted ophiolite terrane in the Krishna Province (Dasgupta et al., 2013).

688 Prior to 1.95 Ga, the North China Craton was a set of microcontinents separated by ocean
689 basins that closed during the same period as both major Nunanian orogenies, completing by
690 1.85 Ga (Zhao et al., 2012), which is recorded in magmatism and widespread metamorphism
691 (e.g., Yin et al., 2014; Cai et al., 2015; Wu et al., 2016; Liu et al., 2017). However, the location of
692 the North China Craton has been subject to extensive debate, with various hypothesis ranging
693 from the northern margin of Siberia (Halls et al., 2000), paired with the Kola-Karelia Craton
694 and (Wilde et al., 2002), positioned between Baltica and Amazonia (Pesonen et al., 2012), or
695 joined with India outboard of the Nuna accretionary margin (Zhao et al., 2011). However,
696 we prefer more recent models that suggest a long-lived connection with the North Australian
697 Craton on the basis of more extensive paleomagnetic and geologic correlations (Wang et al.,
698 2019; Nixon et al., 2022; Zhang et al., 2022). Much of the North China Craton has similar
699 ages to the Inner-Nunanian Orogen, about half the craton experience widespread magmatism
700 as part of the Cordilleran Orogeny (Wu et al., 2019).

701 Most models for Nuna do not include the Kalahari Craton; however, the two models that
702 do, place it in opposite hemispheres (Djeutchou et al., 2021; Cao et al., in prep.). A recent
703 paleomagnetic reconstruction by Djeutchou et al. (2021) suggests the Zimbabwe Craton (the
704 northern part of the Paleoproterozoic Kalahari Craton) was juxtaposed against the southern
705 margin of the Superior Craton at 1.88 Ga. Additionally, their model calls for a pair of sub-
706 duction zones along the south and western margins of the Kaapvaal Craton (the southern part
707 of the Kalahari Craton), reworking the Magondi and Kheis Belts and accreting the Rehoboth
708 Block at this time (Kleinhanns et al., 2013). However, such placement would leave little time for
709 the Kalahari Cratons to rift away from Superior, prior to the arrival of the Mazatzal Orogeny
710 ca. 1650 Ma along a margin that experienced the accretion of at least three major terranes ca.
711 1850 to 1450 Ma (Yavapai, Mazatzal and the Granite-Rhyolite terranes). The paleomagnetic

712 data and timing dates of deformed terranes are also consistent with a collision between Congo-
713 Tanzanian Craton with the south African cratons, which is consistent with ca. 2.0 Ga, resulting
714 in exhumation of eclogites in the Ubendian-Usagaran Belts (Collins et al., 2004; Tamblyn et al.,
715 2021). Regardless, both interpretations place these deformed and accretionary terranes within
716 the Circum-Nunanian Orogeny.

717 The Wopmay Orogeny, ca. 1.95 to 1.84 Ga, was a small subduction-related event on the
718 western margin of the present-day Slave Craton in northern Canada (Figure 8 Bowring and
719 Podosek, 1989). East-dipping subduction on the western margin accreted three separate arc
720 terranes, Great Bear, Hottah, and Fort Simpson, to the craton at ca. 1.88 Ga in the short-lived
721 Calderian Orogeny (Hildebrand et al., 2009; Cook, 2011).

722 The Eburnean Orogeny records the collision between the Saõ Francisco Craton and the
723 Gabon Belt on the eastern Congo Craton margin, (ca. 2.12 to 2.0 Ga; Weber et al., 2016).
724 The orogeny is recorded in a set of tectonomagmatic events (Doumbia et al., 1998; Barbosa
725 et al., 2008; Peucat et al., 2011; Loose and Schenk, 2018; de Carvalho Filgueiras et al., 2020).
726 Although the Eburnean Orogeny was accretionary at the margins of Nuna (Figure 8e), it was
727 geographically isolated and earlier than the majority of Circum-Nunanian orogenesis.

728 Early models of the Limpopo Orogeny suggested it was active between 2.7 and 2.65 Ga
729 as the result of the collision between the Kaapvaal and Zimbabwe Cratons (Barton and van
730 Reenen, 1992), which is based on the age of granitoids contained within the thrust sheets.
731 However, metamorphic ages and more recent interpretations suggest it was active ca. 2.0 Ga
732 (Yin et al., 2019). The Limpopo Orogeny was probably intracontinental due to a lack of arc or
733 accretionary sediments of appropriate age (Yin et al., 2019).

734 The Birimian–Trans-Amazonian Orogeny occurred during the early stages or just prior to
735 the assembly of Nuna and may have been multiple spatially discrete events between ca 2.3 and
736 1.9 Ga. During this period, the West African Craton records considerable tectonomagmatic
737 activity in sedimentary deposits (Grenholm, 2019; Grenholm et al., 2019) as it collided with
738 the present-day northeastern Amazonian Craton (Grenholm, 2019). Both magmatic and meta-
739 morphic events are recorded in Amazonia during this period (De Roever et al., 2003; Savko
740 et al., 2015; Baltybaev et al., 2017; Klaver et al., 2015; da Rosa-Costa et al., 2008).

741 In the early Paleoproterozoic (ca. 2.5 to 2.3 Ga), a purported drop in magmatism corre-

sponded with several cratonic regions that experienced high-temperature, often contractional, metamorphic events (Pehrsson et al., 2013, 2014). Pehrsson et al. (2013) hypothesized these events are related to a formation of a supercontinent (Nunavutia), however, a recent paleomagnetic reconstruction suggested two separate supercratons were also consistent with pole determinations and patterns of dike swarms (Figure 9f; Liu et al., 2021). The reconstructions of the Siderian are based on paleomagnetic poles from 11 terranes (Liu et al., 2021; Salminen et al., 2021); however, less than one-quarter of blocks with igneous dates older than 2.3 Ga (Figure 10) are included in the reconstructions. Igneous activity in the interval 2.5 to 2.3 Ga is nearly ubiquitous across Archean terranes with the exception of regions covered by ice, sediments, and or Phanerozoic large igneous provinces. As a result, the classification as a super-continent/craton may be premature without the reconstructed positions of additional Archean terranes. Metamorphic dates in this time interval are sparse (Figure 10), but the metamorphic database is incomplete, so it is difficult to make clear inferences at this point. We refer to the regions with significant 2.4 Ga tectonothermal activity collectively as the Siderian Metamorphic Event, referring to the geologic time period rather than a coherent orogen due to the present uncertainty in reconstructions. The ca. 2.4 Ga affected terranes are now scattered across all seven continents and many have been reworked (Figure 9f and 10). Some of the terranes where the Siderian Metamorphic Event has been documented include the Mawson Craton (Duclaux et al., 2008), the Sask Craton (Chiarenzelli et al., 1998), Arrowsmith Orogen in Northern Canada (Hartlaub et al., 2007; Schultz et al., 2007; Berman et al., 2013a), the East Dharwar in India (Clark et al., 2009; Li et al., 2018), and the Sleaford Complex in south Australia (Halpin and Reid, 2016) and the North China Craton (Liu et al., 2017).

4. Model Evaluation

4.1. Ocean–Continent Boundary

Not counting for topographic relief, we estimate 57.7% of the Earth's surface is covered by oceanic crust and 42.3% is covered by continental crust (Figure 4). The seafloor age model by Seton et al. (2020) covers a slightly smaller proportion of the Earth's surface with seafloor ages, 57.4%. However, there are a few significant differences between the models.

In general, the edges of the seafloor age model by Seton et al. (2020) are easily correlated with high bathymetric gradients and deep water. However, there are a few regions where lo-

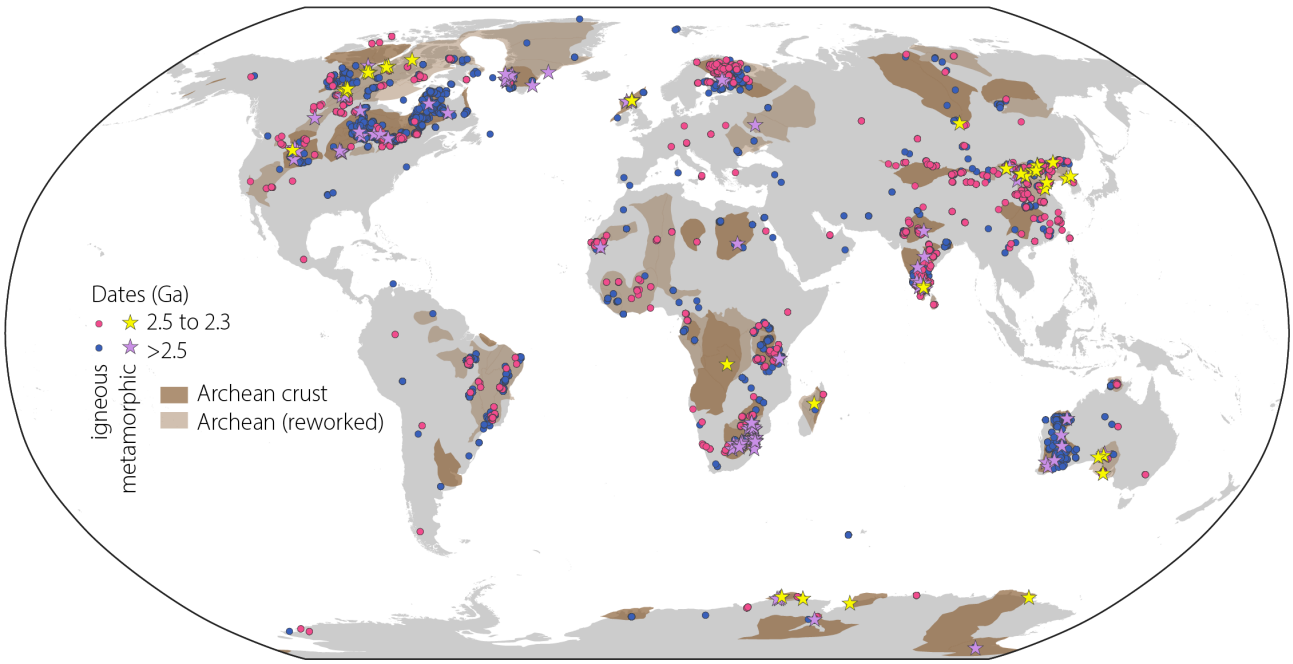

Figure 10: Regions with crust >2.3 Ga with superimposed locations of dated igneous and metamorphic activity. The observed dates are divided into the period 2.5 to 2.3 Ga, and older than 2.5 Ga. Reworked Archean crust is displayed in a lighter shade. Province boundaries from Figure 7 and a few additional Archean basement provinces in North America by Lund et al. (2015). Igneous ages extracted from Gard et al. (2019a) and Puetz (2018); metamorphic ages from DateView (Eglington, 2004) and the expanded metamorphic database by Brown and Johnson (2018).

cations differ significantly between their model and our ocean–continent boundary. Some of the differences may be due to the quality of magnetic data near the continents where remnant magnetization may be reset by high temperatures beneath insulating sediments or where magnetic data is of insufficient quality and/or density to resolve seafloor ages. A few of the larger differences include the Greenland-Iceland-Faroe Ridge (GIFR), Blake Plateau, Gulf of Mexico, and some microcontinents.

Perhaps the most obvious difference between our model and Seton et al. (2020) is the inclusion of the GIFR as a region of continental crust. In a recent comprehensive paper by Foulger et al. (2020), the authors make a compelling case that the GIFR is a peculiar region with variably extended continental crust rather than the product of anomalous oceanic volcanism. The nearby Jan Mayen microcontinent has been recognized as a microcontinents for decades (Peron-Pinvidic et al., 2012, and references therein), lending credence to the model. The total thickness of the crust approaches 40 km thick beneath the Iceland microcontinent—a value more typical of continental than oceanic crust. The symmetric, linear magnetic anomalies characteristic of seafloor spreading are muddled in this region, possibly indicating a complex history of rifting and volcanism. The upper crust in the region exhibits seismic properties and

788 layer thicknesses typical of oceanic crust (3–10 km), but the middle and lower crustal seismic
789 velocities and densities are better explained by continental material (Foulger et al., 2020).
790 Therefore, we favor their interpretation in our model.

791 There are a number of other microcontinents that we have included in our model that are
792 not found in the Seton et al. (2020) model. We have included the Hovgaard Ridge and the East
793 Greenland Ridge in the Arctic Ocean (Funck et al., 2016). Several microcontinents lie in the
794 Indian Ocean including the Mascarene Plateau, Chagos–Laccadive Ridge, Gulden Draak, and
795 Batavia Knoll (Torsvik et al., 2013; Gardner et al., 2015; Halpin et al., 2017), which are formerly
796 pieces of Madagascar and India, respectively. We have also included the Bollons Seamount east
797 of the Campbell Plateau in the Pacific (Davy, 2006).

798 The Blake Plateau on the Atlantic side of Florida sits at a bathymetric depth of ∼1000 m
799 and is underlain by transitional crust (Dillon et al., 1988). In the Gulf of Mexico, the ocean–
800 continent transition is obscured by sedimentary cover making magnetic data the most useful for
801 identifying the boundary, but the global models are relatively low resolution. However, there
802 are industry magnetic datasets that we do not have access to that yield a much clearer view of
803 the Gulf of Mexico.

804 In the future, incorporation of seismic reflection profiles taken across the ocean–continent
805 transition and improvements in the magnetic datasets may warrant alterations to the ocean–
806 continent boundary.

807 *4.2. Plate Boundaries*

808 There are significant differences in the lengths of plate boundaries by type (Table 5). The
809 total length of all major plate boundaries is nearly five times the Earth's circumference. Among
810 major boundaries, the total length of divergent boundaries is significantly greater than con-
811 vergent boundaries. The mid-ocean ridge system and associated transforms is ∼1.7 times the
812 length of subduction zones. Transform boundaries account for the least length of major bound-
813 aries, but this does not include the transforms between mid-ocean ridge segments.

814 Including minor deformation zone and microplate boundaries more than doubles the total
815 length of boundaries (Table 5). The latter number may be a bit misleading as the minor bound-
816 aries generally bracket the deformation, while in reality multiple structures may accommodate

Table 5: Lengths of plate boundaries. Major and minor boundaries are identified in Figure 2.

Boundary Type	Major (km)	Minor (km)
spreading center	87,001	12,680
extensional zone	13,702	40,134
subduction zone	52,966	9,688
thrust	17,614	65,077
dextral transform	15,476	41,723
sinistral transform	13,276	24,099
inferred	0	19,177

the motion. Among minor boundaries, convergent and transform boundaries are longer than divergent boundaries. Also in contrast to major boundaries, spreading ridges and subduction zones are less common than extensional zones and thrusts.

4.3. Plate Model

4.3.1. Comparison with Bird (2003)

The major differences between the Bird (2003) plate model and our model are the microplates and deformation zones (Figure 1a). Most major plate boundaries are very similar to Bird (2003) with some refinement. The Bird (2003) model contains 52 polygons, whereas ours contains 121 regions comprising rigid plates, microplates and deformation zones. Most of these added regions are located in the Alpine–Himalayan Belt and the North American Cordillera. These changes are driven by a significant improvement in the number and quality of land-based GPS coverage; however, several of our additions have long been recognized as plate boundary zones (e.g., Gordon, 1998; Lowman and Yates, 2002; Kreemer et al., 2014). Many of these regions have also been previously identified as microplates (case studies in Table 2). In total, we estimate 16% of the Earth's surface is covered by microplates and deformation zones, divided roughly equally between them whereas the Bird model only includes 6%.

The southern Somali–African boundary has changed considerably with respect to the Bird (2003) model. The Bird (2003) model connects several discrete regions of seismicity in southern Mozambique and central South Africa. However, GPS motions suggest there is little deformation on either side of this boundary (Kreemer et al., 2014). From GPS data, the boundary appears to be further east, near the southern Mozambique coast (Stamps et al., 2021).

Another region of significant refinement relative to Bird's model among the microplates and deformation zones of the Philippines and eastern Indonesia. Our model more closely follows

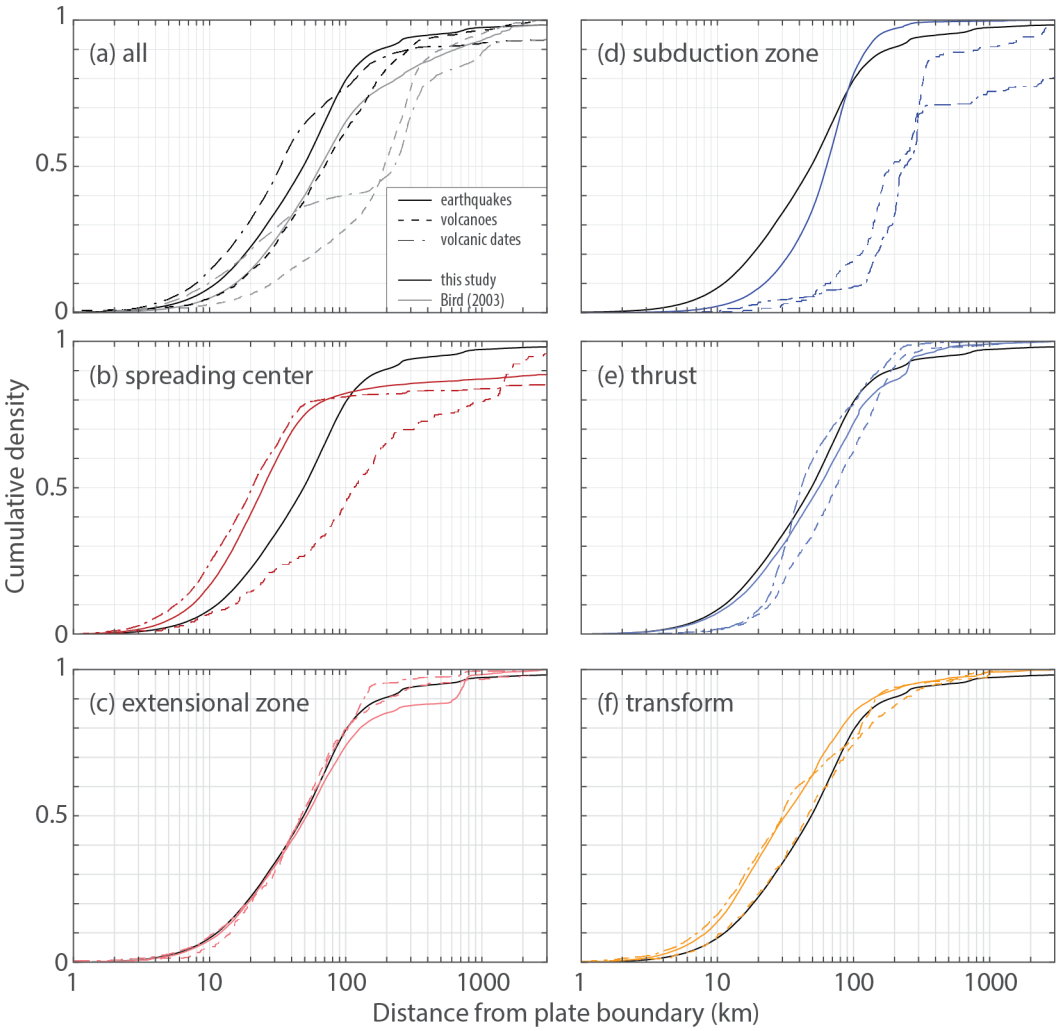

Figure 11: Cumulative distributions of earthquakes and volcanoes by distance to plate boundaries. Each subplot contains CDFs from three datasets: (solid) earthquakes from the ANSS catalog, magnitude 3.0 to 5.5, 1990 to 2020 and magnitude 5.5+, 1970 to 2020 (ANSS, 2020); (dashed) Quaternary volcanoes (Global Volcanism Program, 2013); and (dashed-dotted) dates of volcanic samples limited to Quaternary samples Gard et al. (2019a) with duplicate sample locations removed to limit oversampling. (a) Computed using all data in each respective dataset, black lines using our model and grey lines using Bird (2003). (b-f) Computed for listed plate boundary types as classified in Figure 2. The black line on each plot is earthquakes from all plate boundaries as a reference.

several boundaries identified by Zahirovic et al. (2014), which shows better correlations with seismicity and active fault models (ANSS, 2020; Styron and Pagani, 2020).

In our plate model, ~80% of earthquakes occur within 100 km of a plate boundary and ~91% within 200 km (Figure 11a). Approximately 73% of earthquakes occur within deformation zones and microplates. For the Bird (2003) model, these percentages are significantly lower. Less than 27% of earthquakes lie within Bird's microplates and 65% of earthquakes lie within 100 km of plate boundaries. Therefore, we suggest our new model provides a more accurate representation of the actively deforming crustal regions.

The pattern of distance of earthquakes from plate boundaries varies depending on the type

of plate boundary. Earthquakes are centered close to spreading centers (Figure 11b), but are more diffuse around transforms (Figure 11f), which occurs because transform plate motion is frequently accommodated by multiple faults rather than a single structure (e.g., Pacific–North American boundary in California, Hauksson et al., 2013; DeMets et al., 2014). In contrast to spreading centers and transforms that identify the centers of deformation, extensional zones and thrusts identify the boundaries of internal deformation so it makes sense that earthquakes are distributed at a greater distance from these boundaries (Figure 11c, e). Subduction zone earthquakes are distributions furthest from their associated plate boundaries (Figure 11d). The more rapid increase in cumulative density of subduction zone earthquakes could be due to our limiting earthquakes to 30 km depth and/or the earthquakes extend far enough into the deformation zone that the opposite boundary becomes the closest (Figure 2).

4.3.2. Comparison with Tomography and Volcanism

Our plate boundary model correlates well with slow seismic velocity slices from 40 to 90 km depth, with 70 km displaying the most similarity to the plate boundary zones (Figure 12). Greater than 90 km depth, the mantle beneath the oceans has significantly larger negative velocity anomalies. Greater than approximately 125 km depth, some of the continental plate boundary zones begin to lose their negative velocity anomalies. The correlation between plate boundary zones and shallow mantle shear wave velocity anomalies are the result of thinner and warmer lithosphere in actively deforming regions with respect to cold, thick, rigid plate interiors.

Only a few plate boundaries and deformation zones are not clearly associated with negative seismic velocity anomalies. The Cordilleran Frontal Thrust, Lesser Antilles Arc and the Lwandle Plate have positive seismic anomalies. Oceanic intraplate deformation zones do not show clear correlations with negative tomographic anomalies. For example, the Capricorn region between the Indian and Australian Plates, the Macquarie Microplate, and the boundary between North and South America are not clearly delineated by tomography.

Volcanoes also show high correlation with the plate boundary zones as ~80% lie within deformation zones and microplates (Figure 12). Like earthquakes, there are differences between the distribution of distance from plate boundaries by type (Figure 11). Volcanoes are furthest from subduction zones, with the majority ranging between 130 to 330 km. For transforms

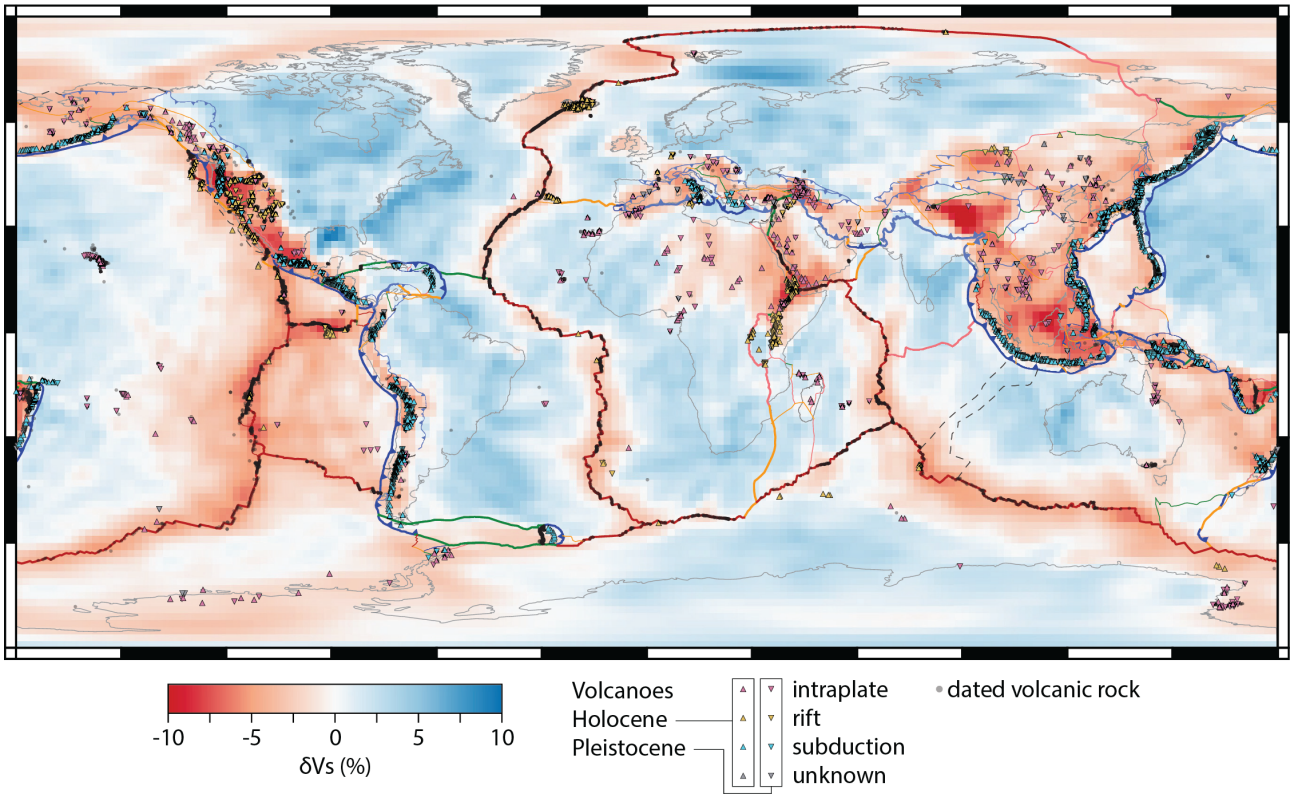

Figure 12: Shear wave tomography at 70 km depth demonstrates a high spatial correlation between negative velocity perturbations and plate boundaries and deformation zones. The shear wave velocity model is by Debayle et al. (2016). Nearly 80% of recently active, Quaternary volcanoes lie within microplates and deformation zones. Volcano locations from Global Volcanism Program (2013). Pleistocene and younger volcanics from Gard et al. (2019a); originally from EarthChem.org affiliated databases.

and extension zones, >75% lie within 100 km of the boundary. The distribution of volcanoes from spreading centers is more complex because most of the volcanoes identified near these environments are seamounts associated with hotspots rather than flows at ridges. If a full accounting of flows could be made along ridges, it is likely the distribution would indicate most are much closer to the drawn boundaries Rubin (2016). We try to account for this by using dates from a global geochemical dataset (Gard et al., 2019a, and Figure 12), which results in a similar distribution of distances as the volcanic eruption database (Figure 11). The only exception is the distribution of dates from recent volcanic samples, which fall considerably closer to spreading centers than the eruption database similar to earthquakes (Figure 11b).

The correlation between volcanoes and seismic velocities may imply partial melt is common beneath most plate boundary zones. However, there are a few that have minimal volcanism but high seismicity, including Tibet and the Tien Shan Mountains. The Amur, Yangtze and Okhotsk regions also have very little volcanism outside the volcanic arcs on their margins. These regions also have little seismicity in their interiors.

There are a few regions with negative seismic anomalies and/or recently active volcanic centers that do not correspond with plate boundaries. Several of these regions are hotspots associated with mantle plumes (e.g., Hawaii, Reunion, Cape Verde). These regions do not have clear negative velocity anomalies at 70 km depth within the scale of the tomography model (Figure 12). There is a negative shear wave anomaly in the Arctic without volcanics, which may be related to prior rifting and the Eureka Orogeny (Darbyshire, 2005). The Saharan Metacraton has both low shear velocities and volcanism, but little seismicity. There are currently no GPS data from western Egypt, Chad, Sudan or Libya above the seismic anomaly, but GPS data in Nigeria do not indicate active deformation above the negative velocity region. The West Antarctic Rift contains both volcanoes and a negative shear wave anomaly related to renewed extension in the Cenozoic (Winberry and Anandakrishnan, 2004; Gupta et al., 2009; O'Donnell et al., 2019). While there is active volcanism associated with the Marie Byrd and Erebus hotspots, seafloor magnetic anomalies suggest the rift was active as recently as 11 Ma (Granot and Dyment, 2018) and minimal seismicity suggests the region is inactive at present.

4.3.3. Uncertain Plate Boundaries

Many oceanic deformation zones and microplates have relatively uncertain boundaries due to a lack of GPS constraints, significant seismicity and/or distinctive bathymetric features akin to boundaries. The Azores deformation zone, for example, has a well-defined boundary along the northern margin by seismicity. GPS data on individual islands suggest internal deformation (Fernandes et al., 2006; Marques et al., 2013), but the southern boundary is not clear from seismicity. Our best estimate places the southern boundary on the East Azores Fracture Zone due to its clear topographic expression.

The Capricorn Plate is a region of diffuse extension between the Indian and Australian Plates. The region is large, nearly the same size as the Indian Plate, but the eastern and southeastern boundaries are very uncertain (Figure 13). Magnetic anomaly maps of the plate are sparse on the southern boundary (i.e., Wharton Basin). Bathymetry is complicated by several features including the Ninetyeast Ridge, Diamantina Escarpment, Roo Rise, Vening Meinesz Seamounts, and the Raitt Rise. Earthquakes, while indicating extension, are not of sufficient density to clearly delineate the boundaries (Figure 13). Furthermore, the Indian and Australian Plates have relatively high rates of diffuse intraplate seismicity, without clear clustering indicative of rigid plates boundaries.

The eastern, western, and northern boundary of the Lwandle Microplate are poorly constrained. Most authors have drawn the northern boundary as an extension of the Quasama Seismic Axis on the southern end of the Rovuma Microplate to Madagascar and then traversing Madagascar along a constant line of latitude before running along the eastern margin of the island (e.g., Saria et al., 2014). However, there is little to no observed seismicity to constrain this model. A more recent model suggests the northern boundary is constrained by a dextral transform that runs along the Comoros archipelago which is consistent with seismicity and GPS velocities in northern Madagascar (King et al., 2017; Famin et al., 2020; Stamps et al., 2018, 2021). For this reason, we prefer the northernmost boundary in our model, and have separated the northern Lwandle region into the Comoros deformation zone.

The boundary between the oceanic portion of the North and South American Plates east of the Lesser Antilles Trench is poorly defined by limited diffuse seismicity. In fact, the low level of seismicity is similar to many intraplate regions not considered deformation zones. The lack

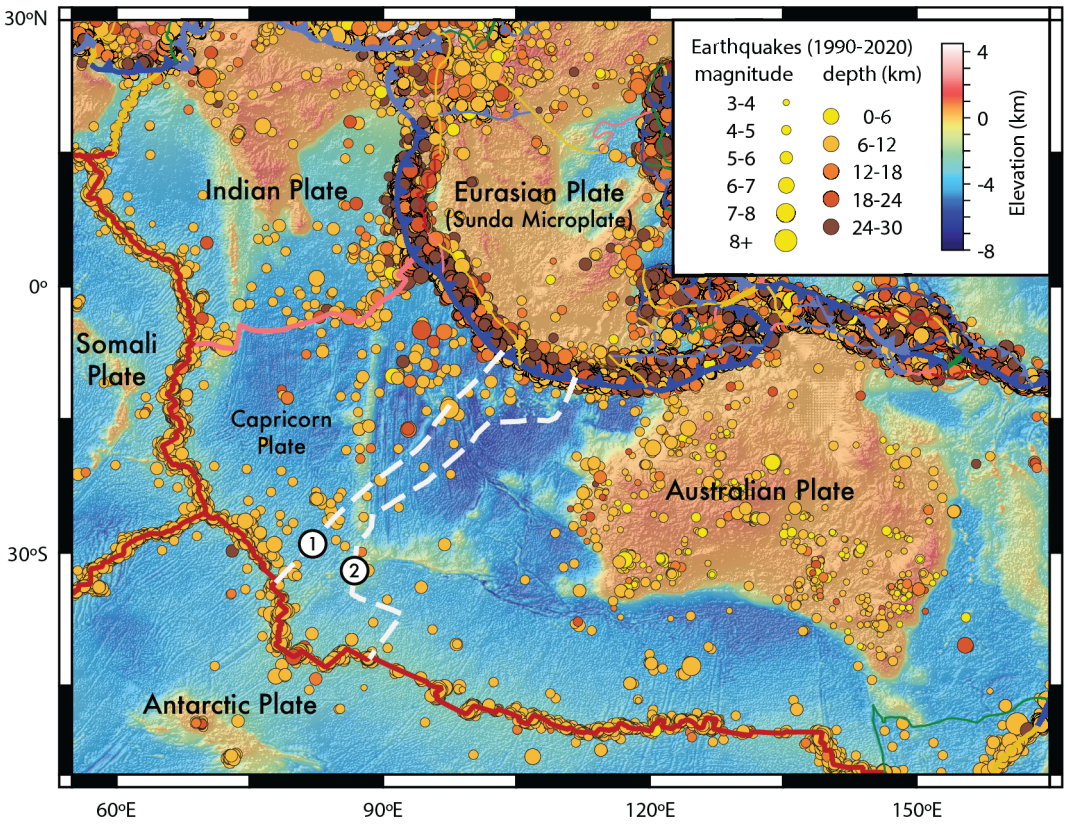

Figure 13: Models of the Capricorn Plate and associated Mid-Indian deformation zone. The white boundaries are a couple of the proposed southern boundaries: 1, (Rathnayake et al., 2019); 2, (Royer and Gordon, 1997).

of GPS stations in both regions makes it difficult to define the edges of the deformation zone reliably. Given the lack of a clear diffuse region, we draw the boundary as the most prominent feature, the Fifteen-Twenty Fracture Zone, which is consistent with prior interpretations (Roest and Collette, 1986; Dixon and Mao, 1997).

4.4. Geologic Province Model

The geological province model includes 918 polygons, of which 790 (86%) are continental. Most continental terranes are linear belts with areas that range between 10^4 and 10^6 km^2. The median province area is 175,000 km^2, but varies between different continental regions from 10^5 and 3×10^5 km^2 (Figure 14a). The distribution of province sizes is largest in South America and Africa. Part of the reason may be due to the inability to pick out smaller terranes beneath thick sedimentary cover and relatively few studies with high resolution geophysical data. It is also due to the number of composite type terranes such as cratons, shields and orogens that are built from ophiolites, accretionary complexes, and volcanic arcs (Figure 14b). However, some provinces are naturally larger due to the processes involved in their formation (i.e., passive margins and wide rifts).

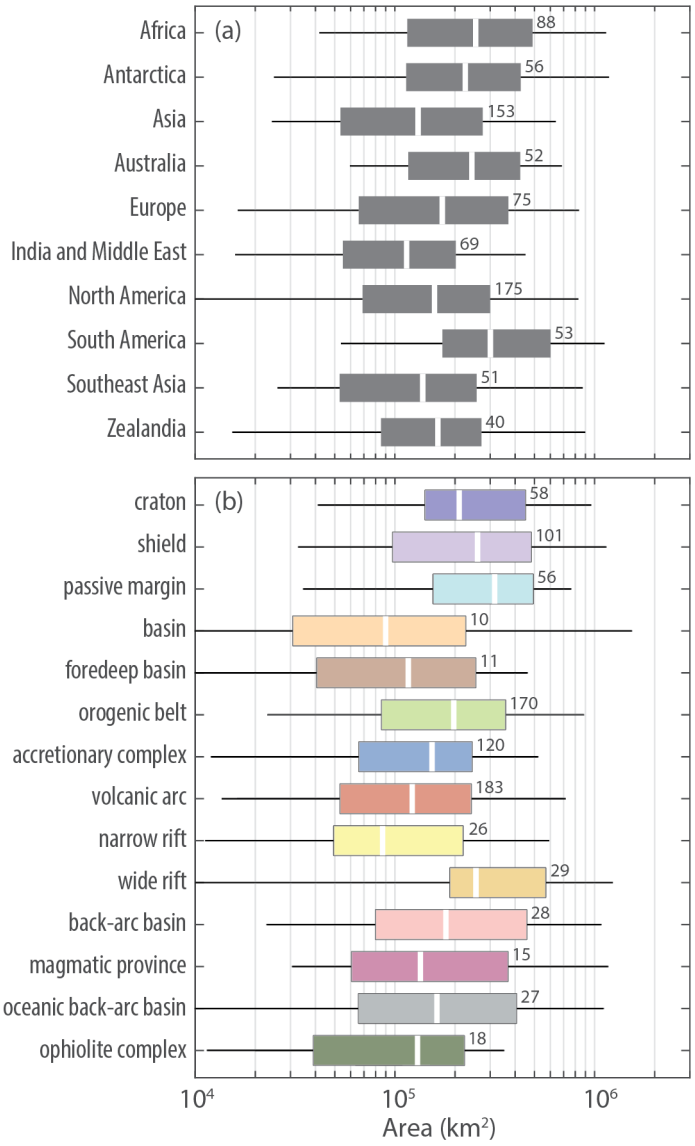

Figure 14: Area of geological provinces for (a) continental regions and by (b) province type. The white bar indicates the median, box enclose the 0.25 to 0.75 quantiles and whiskers extend to the 0.05 and 0.95 quantiles. The number beside the boxes indicates the number of provinces for each region.

The most common province types are orogenic belts, volcanic arcs and accretionary complexes (Figure 14b). There are many fewer extended terranes, however, passive margins are generally rifted margins with thick sediment on top. Many ancient rifts are incorporated into orogenic belts. Where orogenic belts have been separated into their individual constituents, there is often an accretionary complex and associated arc. However, in many cases only a volcanic arc is identified, which may be because the related accretionary complex is commingled with the volcanic arc and difficult to separate or was destroyed during orogenesis.

4.4.1. Comparison with Matthews et al. (2016) and Merdith et al. (2021)

The model by Matthews et al. (2016) was constructed to model plate motions over the past 400 Ma. Given their model timeframe, continental provinces that moved relative to one another prior to 400 Ma are not typically subdivided. As a result, our model contains a significantly greater number of terrane divisions. Many of the divisions in the Matthews et al. (2016) model are also simpler than ours. This simplicity requires fewer polygon vertices, which may make computation of plate rotations more rapid, but it compromises accuracy of filtering geologic data for analysis.

The Merdith et al. (2021) model extends the Matthews et al. (2016) plate motions back to 1000 Ma, which required the addition of many more province boundaries. The models for southern Africa, the northwest Cordillera, and the Mongol Orocline are similar to ours. However, there are significant differences in the number of provinces in Australia, Antarctica, eastern Europe and the Superior Craton. Many of these differences occur where we include a finer resolution of terrane boundaries with tectonic histories that converge prior to 1000 Ma. In light of the agreement with previous reconstruction polygons, the model presented in this study could be used in the future for plate reconstructions into the Archean.

4.4.2. Last Orogeny

To ensure that our orogenic model is reasonable (Figures 8 and 9), we have computed kernel density estimates (KDE) for both magmatic crystallization dates and metamorphic dates for each orogen (Figure 15). The dates are mostly derived from U–Pb, ^{2}07Pb–^{2}06Pb, and U–Th–Pb analyses of zircon and monazite. The zircon dates can provide constraints for both igneous and metamorphic events whereas most monazite dates record metamorphic events in the datasets we used (Eglington, 2004; Puetz, 2018; Brown and Johnson, 2018; Gard et al., 2019a). Other

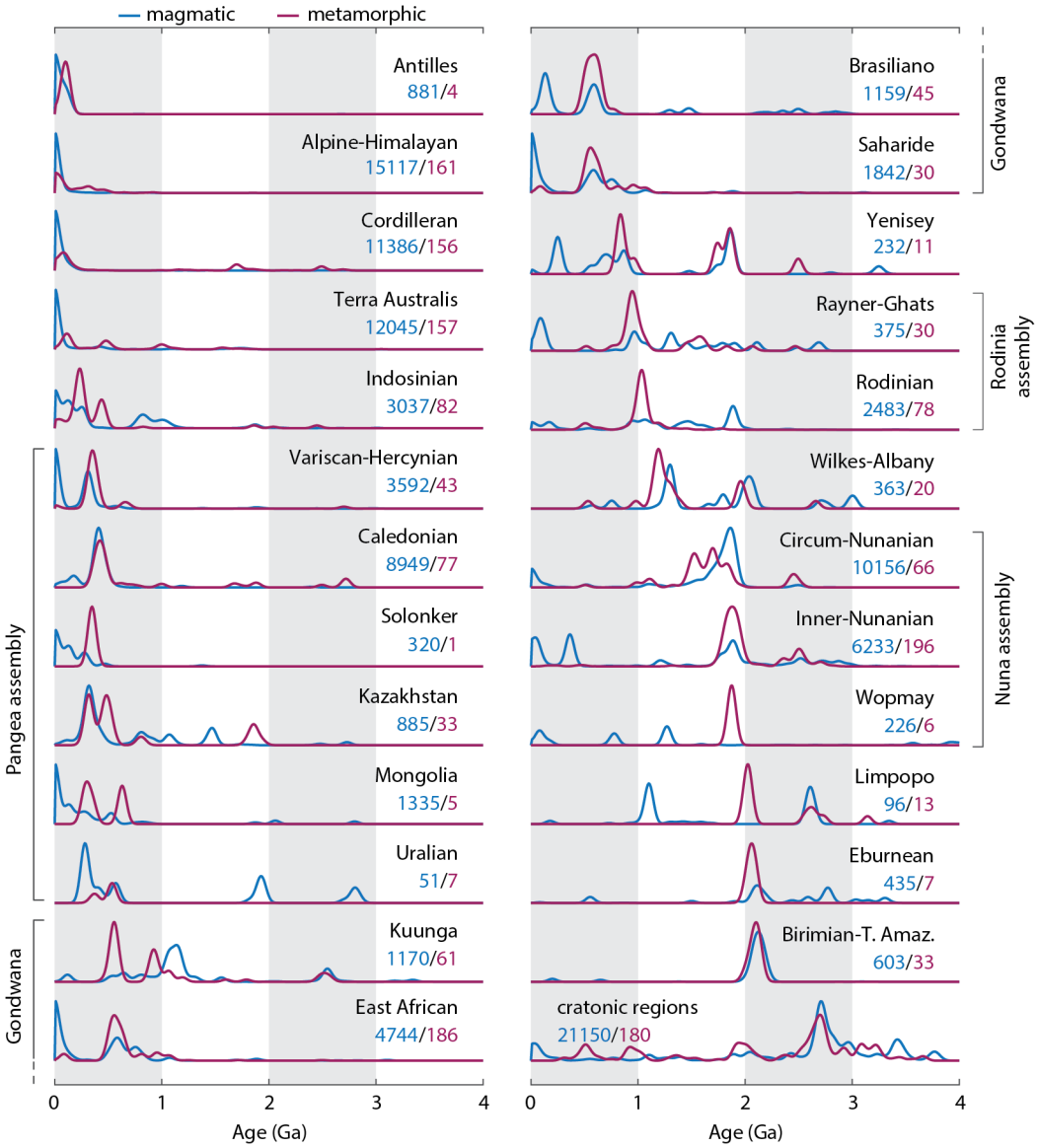

Figure 15: Kernel density estimates for magmatic crystallization dates (blue, Gard et al. (2019a)) and metamorphic dates (violet, Brown and Johnson (2018) updated; Eglington (2004)). A list of metamorphic dates are given in the Supplemental Material. No dates for the Scotian Orogeny are available in the database.

isotopic dating systems (e.g., ^{4}0Ar–^{3}9Ar, K–Ar, and Rb–Sr) may record lower closure temperatures and can correspond to less significant heating events and are therefore generally excluded from the dataset except where the dates match the regional higher temperature metamorphism or in younger systems where U–Th–Pb lose precision.

The largest age peak for metamorphic KDEs always falls within the range of dates attributed to an orogen as discussed in Section 3.2.2. It is important to note that these dates were not used to define the orogen, but undoubtedly many of these orogen models are based in part on geochronology. In Figure 8, one can see the spatial correspondence between metamorphic dates and our orogen interpretation. In a few cases, there are smaller-magnitude metamorphic date peaks that record P-T conditions of previous orogenic events. For example, in the Canadian

Cordillera Frontal Thrust Belt a few dates are associated with the Wyoming Craton (ca. 1780 Ma; Cheney et al., 2004b,a) and not the more recent Cordilleran deformation (Figure 8). These older metamorphic events are still evident because Cordilleran deformation reaches relatively shallow levels in these regions and has not reset the isotopic systems associated with the older events.

Very few orogens have significant age peaks younger than the assigned orogen. The exceptions include the Rodinian Orogeny which in some cases includes some Gondwana-associated dates, particularly in Antarctica, and the Circum-Nunanian terranes, which include some Rodinia-associated overprinting (Figure 15)—specifically in North America where metamorphic conditions are poorly sampled (Figure 8). These discrepancies between the orogenic model and observed metamorphic conditions may indicate some refinement of the province model may be necessary.

The magmatic dates are noisier, often indicating several episodes of magmatism, which attests to the multi-generational history to the growth of many provinces (Figure 15). There are a surprising number of provinces which have magmatic peaks near the present day that lie in generally much older orogens. In the East African Orogen, the younger ages are associated with the East African Rift. In the Saharides and Trans Hudson Orogen, these younger magmatic ages are the result of Cenozoic intraplate magmatism, which does not appear to be associated with active tectonics. In many regions with younger volcanism, the geodynamic process that has created the melts does not appear to have reset metamorphic conditions or alternatively the depths at which metamorphism has occurred have not yet been exhumed.

While magmatic dates appear to be less reliable for identifying the last orogen event, there is often a peak in the KDE that corresponds with the metamorphic peak. The Limpopo Orogen is a clear exception where no magmatic peak is observed during the orogenic event. The missing magmatic peak at ca. 2.0 Ga is the reason the Limpopo orogen was originally interpreted as a ca. 2.7 Ga event, rather than a younger intracontinental orogen (Barton and van Reenen, 1992; Yin et al., 2019). The only other orogen with missing magmatic dates is the Wopmay Orogen in northwest Canada, however, this orogen is poorly exposed so there are very few data from the terranes that comprise it.

The KDEs for the cratonic regions display significant magmatic and metamorphic activity

prior to 2.5 Ga, with a few minor metamorphic and igneous peaks. Many of these small younger (<2.5 Ga) metamorphic peaks do not appear to correspond with magmatism, which may indicate minor degrees of intracratonic deformation as orogens occur around them. We suggest this observation is consistent with a persistent mechanically strong lithosphere able to resist deformation in most cases. The young magmatic peak within cratonic regions is common across most orogens. As most of these regions are intraplate several questions arise regarding the lack of widespread intraplate volcanism in the past. Are intraplate volcanics easily eroded and therefore poorly preserved? If not, is there a sampling bias, i.e., petrologists and geochemists vastly oversample present-day intraplate volcanism, or are they generally too small and distributed in the past to easily recognize and thus ignored?

4.4.3. Uncertain Province Boundaries

Perhaps the poorest geologically characterized region is Antarctica due to the lack of outcrops. Most geological province information about Antarctica comes from regions near the coast typically combined with constraints from conjugate terranes on now-distant continents (e.g., Boger, 2011; Flowerdew et al., 2013; Goodge et al., 2017; Maritati et al., 2019; Ruppel et al., 2020). Due to the nature of these peripheral constraints, province boundaries are more uncertain into the subglacial interior and are typically guided by geophysical fields such as gravity and magnetics following linear trends (Aitken et al., 2014; Maritati et al., 2016). Because of the uncertainties, it has resulted in a myriad of province models that can change significantly as additional geological data are added and higher resolution geophysical models are produced. Very few models include interior provinces that do not reach the coast because of the lack of geological control (cf., Ferraccioli et al., 2011), however new multivariate approaches to mapping lithospheric boundaries suggest significant interior complexity characterizes East Antarctica (Stål et al., 2019).

Our Antarctic province model is derived from several geophysical constraints (Table 3). As with other continents, magnetic anomalies are often the best constraint on province boundaries in the upper crust (Figure 16a). Geochronology is important for defining provinces and identifying boundaries in areas of outcrop, which are mostly concentrated near the coast. The PetroChron Antarctica database is a compilation of geochronology and other geological data of Antarctica (Sanchez et al., 2021), that will surely continue to improve our insights into the pre-

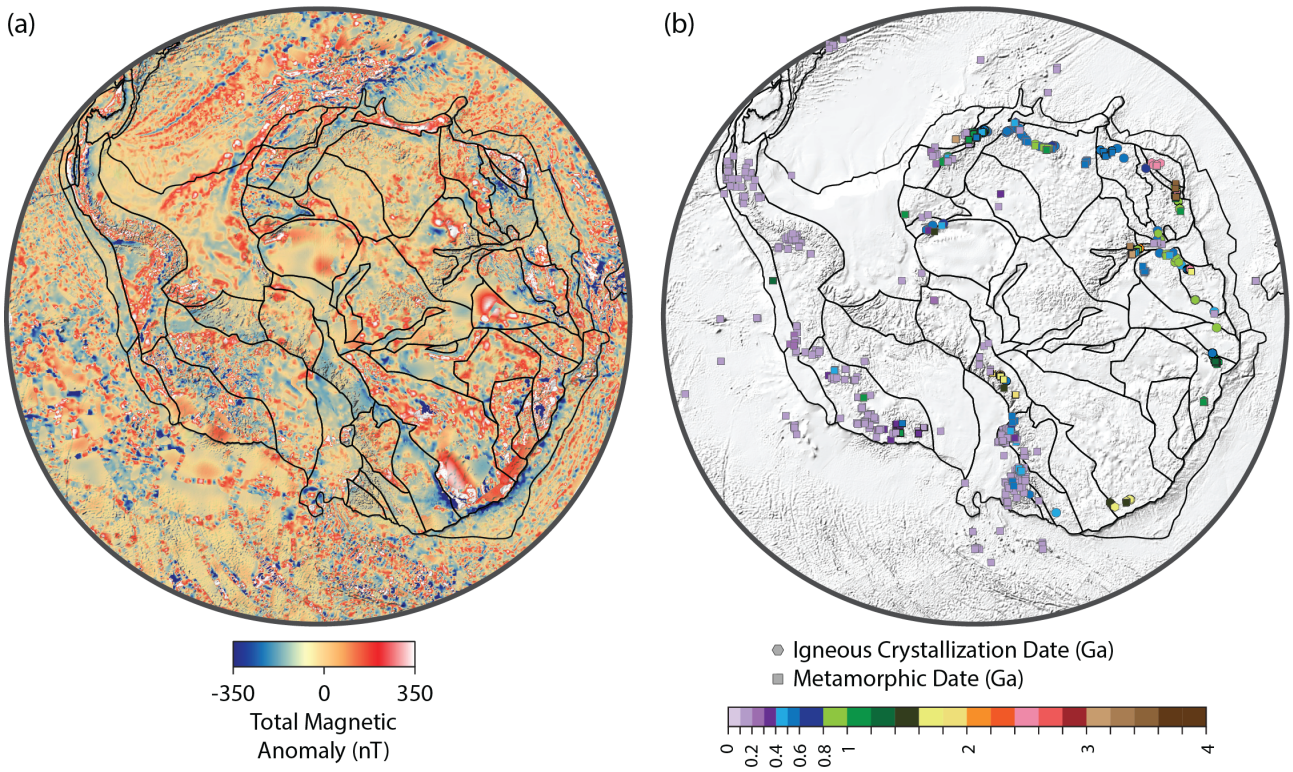

Figure 16: Magnetic (a) and geochronologic (b) constraints on the Antarctic province model. Magnetic data from ADMAP2 (Golynsky et al., 2018) and EMAG2_V3 (Meyer and Saltus, 2016) to fill gaps. Igneous crystallization dates from Gard et al. (2019a) and Puetz (2018) and metamorphic dates from Brown and Johnson (2018), updated, and DateView, (Eglington, 2004).

cise positioning of Antarctic province boundaries. Our model includes a few interior provinces that we interpret as cratonic or shield terranes due to the lithospheric characteristics, though they are relatively large. These terranes are ringed by orogens at the edges of the continent, similar to many other continental shields (e.g., Kaapvaal, Congo, and Siberian Cratons).

Most other poorly resolved regions include those covered by thick sedimentary cover: Patagonia, Parana Basin, Saudi Arabian Platform, North Africa, and West Siberian Basin. In these regions the provinces tend to be much larger than the average and there are multiple interpretations for their divisions. These models are difficult to independently assess because the geophysical data in many of these regions is relatively poor. For example, the Saharan Metacraton and Tuareg Shield have considerably different interpretations for their evolution. The Tuareg Shield is constructed of a set of imbricated arc terranes. Most models show little to no association with the Saharan Metacraton, which is interpreted as a set of Archean cores with reworked subcontinental lithosphere (Liégeois et al., 2013; Sobh et al., 2020). This interpretation is based on thermophysical modeling using multiple geophysical data, but the data are relatively low resolution. An alternative explanation developed using geochronological

and geochemical data suggests the Tuareg Shield, Arabian–Nubian Shield and portions of the Saharan Metacraton were a single volcanic arc system that was broken in multiple segments, reorganized and then accreted to the core of the metacraton, deforming it in the process in the Neoproterozoic (Liégeois, 2018; Şengör et al., 2020; Blades et al., 2021).

4.5. Future Improvements

There are a number of improvements that can be made to the province definitions in future versions. Higher resolution geologic maps could be incorporated that have better lithological data and finer age resolution in the Precambrian, especially the Archean. Likewise, higher resolution magnetic data will be very useful for improving terrane boundaries, especially when the resolution is ∼10 km pixel spacing. Most global geophysical datasets are available at too low a resolution to precisely resolve many terrane boundaries.

Province types that do not provide information about the tectonic construction of the crust (basin, shield, and craton), should be replaced in future versions. Doing so may require improved geologic models of Precambrian regions, which may require the addition of new tectonic settings that are unique to the early Earth such as granite-greenstone belts. Likewise, orogenic belts could also be deconstructed into the types of terranes that build them, i.e., separating out arcs and accretionary margins could help improve models of crustal growth and composition.

Although we currently only ascribe the last orogenic event to provinces, many regions have experienced multiple orogenic events throughout their history. Adding this history to the attribute tables would provide a more complete view of an individual province's chronological history, which could be paired with information about the changing tectonic environments. Such a model would require a more sophisticated analysis of global geochemical and geochronological data. This process would be tedious to perform on a province by province scale so an automated approach will be warranted and could include recent machine-learning based approaches to predicting tectonic environments (e.g., Tang et al., 2020; Tetley et al., 2020). These improvements would place valuable constraints on plate reconstruction models.

Constructing the province models can include a community-driven approach that is updated by individuals or small groups with expertise in specific regions. To that end, we have set up a GitHub project page where individuals can download the shapefiles, update them, and upload their changes along with a description, references, and rationale for the changes. The

changes can then be evaluated and incorporated into the model if deemed credible. Thus, one would not need to wait for a formally published reference before using the improved maps (https://github.com/dhasterok/global_tectonics).

5. Summary

We have produced a set of plate and geologic province maps that can be used to improve spatial analysis of geoscientific data. The plate model boundaries are validated against earthquake locations, active fault traces, and GPS motions and shows good correlation with shear wave velocities at 70 km depth and active volcanism. The geological province model is constructed from a collage of published models and refined using a wide-variety geophysical and geological data. The most useful data were found to be aeromagnetic anomalies when the models are high resolution. The province model has not been independently validated at this point, but relies on the accuracy of the original studies. However, the last orogeny is validated using metamorphic and igneous dates. The plate and province polygons are drawn so that the boundaries are seamless between the files and additionally include an ocean–continent boundary and a plate boundary type.

The maps are available in a shapefile format that can be easily interpreted by many modern computer languages and have advantages over raster maps for geographically selecting data for various types of analysis. The maps can also be used as a data standard for prescribing spatial metadata in global databases. Because the models are available on GitHub, the geologic community can submit updates and fixes to improve their accuracy.

Data Availability

Plate and province models produced in this study are available at the GitHub repository, https://github.com/dhasterok/global_tectonics. The models can be found in shapefile format suitable for GIS programs, KML for programs such as GoogleEarth, and GMT format for Generic Mapping Tools. The models are also available in the global tectonics library on Zenodo, http://doi.org/10.5281/zenodo.5093930, which includes additional global geophysical and geochronological datasets that are useful for research and educational applications.

Acknowledgements

The authors would like to thank Sabin Zahirovic for suggestions related to earlier versions of the plate and province model. Xianzhi Cao was kind enough to share his new plate reconstruction and Yebo Liu provided GPlates files for the Siderian period.

Funding

This work was partially funded by the Australian Government through the Australian Research Council's Discovery Projects funding scheme (project DP180104074) to DH, JH, and MH. JH's contributions were also partly funded by the Australian Research Council Special Research Initiative for Antarctic Gateway Partnership (SR140300001). SG is supported by an Australian Research Council Future Fellowship (FT210100906). The views expressed herein are those of the authors and are not necessarily those of the Australian Government or Australian Research Council. MG was supported by an Australian Government Research Training Program Scholarship.

References

Abdullah, R., Rosenbaum, G., 2018. Devonian crustal stretching in the northern Tasmanides (Australia) and implications for oroclinal bending. Journal of Geophysical Research: Solid Earth doi:10.1029/2018jb015724.

Aitken, A.R.A., Young, D.A., Ferraccioli, F., Betts, P.G., Greenbaum, J.S., Richter, T.G., Roberts, J.L., Blankenship, D.D., Siegert, M.J., 2014. The subglacial geology of Wilkes Land, East Antarctica. Geophysical Research Letters 41, 2390–2400. doi:10.1002/2014gl059405.

Allen, R., Collier, J., Stewart, A., Henstock, T., Goes, S., and, A.R., 2019. The role of arc migration in the development of the Lesser Antilles: A new tectonic model for the Cenozoic evolution of the eastern Caribbean. Geology 47, 891–895. doi:10.1130/g46708.1.

Almeida, M.E., Macambira, M.J., Oliveira, E.C., 2007. Geochemistry and zircon geochronology of the I-type high-K calc-alkaline and S-type granitoid rocks from southeastern Roraima, Brazil: Orosirian collisional magmatism evidence (1.97–1.96Ga) in central portion of Guyana Shield. Precambrian Research 155, 69–97. doi:10.1016/j.precamres.2007.01.004.

Amante, C., Eakins, B., 2009. ETOPO1 1 Arc-Minute Global Relief Model: Procedures, Data Sources and Analysis. Technical Memorandum NESDIS NGDC-24. NOAA. doi:10.7289/V5C8276M.

Amato, J.M., Boullion, A.O., Serna, A.M., Sanders, A.E., Farmer, G.L., Gehrels, G.E., Wooden, J.L., 2008. Evolution of the Mazatzal province and the timing of the Mazatzal orogeny: Insights from U-Pb geochronology and geochemistry of igneous and metasedimentary rocks in southern New Mexico. Geological Society of America Bulletin 120, 328–346. doi:10.1130/b26200.1.

An, M., Wiens, D.A., Zhao, Y., Feng, M., Nyblade, A.A., Kanao, M., Li, Y., Maggi, A., Lévêque, J.J., 2015. S -velocity model and inferred Moho topography beneath the Antarctic Plate from Rayleigh waves. Journal of Geophysical Research: Solid Earth 120, 359–383. doi:10.1002/2014jb011332.

An, W., Hu, X., Garzanti, E., Wang, J.G., Liu, Q., 2021. New precise dating of the India-Asia collision in the Tibetan Himalaya at 61 Ma. Geophysical Research Letters 48. doi:10.1029/2020gl090641.

Anderson, J., Kelsey, D., Hand, M., Collins, W., 2013. Conductively driven, high-thermal gradient metamorphism in the Anmatjira Range, Arunta region, central Australia. Journal of Metamorphic Petrology 31, 1003–1026. doi:10.1111/jmg.12054.

ANSS, 2020. Comprehensive earthquake catalog (comcat), https://earthquake.usgs.gov/earthquakes/search/, downloaded 26 dec. 2020.

Arboit, F., Collins, A.S., Morley, C.K., King, R., Amrouch, K., 2016. Detrital zircon analysis of the southwest Indochina terrane, central Thailand: Unravelling the Indosinian orogeny. Geological Society of America Bulletin 128, 1024–1043. doi:10.1130/b31411.1.

Aronoff, R.F., Andronicos, C.L., Vervoort, J.D., Hunter, R.A., 2016. Redefining the metamorphic history of the oldest rocks in the southern rocky mountains. Geological Society of America Bulletin 128, 1207–1227. doi:10.1130/b31455.1.

Artemieva, I., 2006. Global $1^\circ \times 1^\circ$ thermal model TC1 for the continental lithosphere: implications for lithosphere secular evolution. Tectonophysics 416, 245–277. doi:10.1016/j.tecto.2005.11.022.

Artemieva, I.M., 2019. Lithosphere structure in Europe from thermal isostasy. Earth-Science Reviews 188, 454–468. doi:10.1016/j.earscirev.2018.11.004.

Atwater, T., Stock, J., 1998. Pacific-North America Plate tectonics of the Neogene southwestern United States: An update. International Geology Review 40, 375–402. doi:10.1080/00206819809465216.

Australia, G., 2004. Magnetic Anomaly Map of Australia. Technical Report Fourth Edition. Geoscience Australia. Canberra. doi:10.4225/25/56258E723A032.

Balmino, G., Vales, N., Bonvalot, S., Briais, A., 2011. Spherical harmonic modelling to ultra-high degree of bouguer and isostatic anomalies. Journal of Geodesy 86, 499–520. doi:10.1007/s00190-011-0533-4.

Baltybaev, S., Yurchenko, A., Lobach-Zhuchenko, S., Balagansky, V., Galankina, O., Morozov, M., Bogomolov, E., 2017. Conditions of metamorphism of garnet-bearing aluminous gneisses in the Orekhov–Pavlograd zone of the Ukrainian Shield. Russian Geology and Geophysics 58, 1333–1348. doi:10.1016/j.rgg.2017.11.002.

Baranov, A., Tenzer, R., Bagherbandi, M., 2017. Combined gravimetric–seismic crustal model for Antarctica. Surveys in Geophysics 39, 23–56. doi:10.1007/s10712-017-9423-5.

Barbosa, J., Peucat, J., Martin, H., Dasilva, F., Demoraes, A., Correagomes, L., Sabate, P., Marinho, M., Fanning, C., 2008. Petrogenesis of the late-orogenic Bravo granite and surrounding high-grade country rocks in the Palaeoproterozoic orogen of Itabuna-Salvador-Curaçá block, Bahia, Brazil. Precambrian Research 167, 35–52. doi:10.1016/j.precamres.2008.06.002.

Barnes, C.J., Walczak, K., Janots, E., Schneider, D., Majka, J., 2020. Timing of Paleozoic Exhumation and Deformation of the High-Pressure Vestgötabreen Complex at the Motalafjella Nunatak, Svalbard. Minerals 10, 125. doi:10.3390/min10020125.

Barton, J., van Reenen, D., 1992. When was the Limpopo Orogeny? Precambrian Research 55, 7–16. doi:10.1016/0301-9268(92)90010-l.

Battaglia, M., Murray, M.H., Serpelloni, E., Bürgmann, R., 2004. The Adriatic region: An independent microplate within the Africa-Eurasia collision zone. Geophysical Research Letters 31, L09605. doi:10.1029/2004gl019723.

Begg, G., Griffin, W., Natapov, L., O'Reilly, S.Y., Grand, S., O'Neill, C., Hronsky, J., Djomani, Y.P., Swain, C., Deen, T., Bowden, P., 2009. The lithospheric architecture of Africa: Seismic tomography, mantle petrology, and tectonic evolution. Geosphere 5, 23–50. URL: https://doi.org/10.1130%2Fges00179.1, doi:10.1130/GES00179.1.

Berman, R., Pehrsson, S., Davis, W., Ryan, J., Qui, H., Ashton, K., 2013a. The Arrowsmith orogeny: Geochronological and thermobarometric constraints on its extent and tectonic setting in the Rae craton, with implications for pre-Nuna supercontinent reconstruction. Precambrian Research 232, 44–69. doi:10.1016/j.precamres.2012.10.015.

Berman, R., Sanborn-Barrie, M., Rayner, N., Whalen, J., 2013b. The tectonometamorphic evolution of Southampton Island, Nunavut: Insight from petrologic modeling and in situ SHRIMP geochronology of multiple episodes of monazite growth. Precambrian Research 232, 140–166. doi:10.1016/j.precamres.2012.08.011.

Berndt, C., Planke, S., Teagle, D., Huismans, R., Torsvik, T., Frieling, J., Jones, M.T., Jerram, D.A., Tegner, C., Faleide, J.I., Coxall, H., Hong, W.L., 2019. Northeast Atlantic breakup volcanism and consequences for Paleogene climate change – MagellanPlus Workshop report. Scientific Drilling 26, 69–85. doi:10.5194/sd-26-69-2019.

Betts, P., Giles, D., 2006. The 1800–1100Ma tectonic evolution of Australia. Precambrian Research 144, 92–125. doi:10.1016/j.precamres.2005.11.006.

Betts, P., Giles, D., Schaefer, B., 2008. Comparing 1800–1600Ma accretionary and basin processes in Australia and Laurentia: Possible geographic connections in Columbia. Precambrian Research 166, 81–92. doi:10.1016/j.precamres.2007.03.007.

Bhowmik, S.K., 2019. The current status of orogenesis in the Central Indian Tectonic Zone: A view from its southern margin. Geological Journal 54, 2912–2934. doi:10.1002/gj.3456.

Bird, P., 2003. An updated digital model of plate boundaries. Geochemistry, Geophysics, Geosystems 4. doi:10.1029/2001gc000252.

Bispo-Santos, F., D'Agrella-Filho, M.S., Pacca, I.I., Janikian, L., Trindade, R.I., Elming, S.A., Silva, J.A., Barros, M.A., Pinho, F.E., 2008. Columbia revisited: Paleomagnetic results from the 1790Ma colider volcanics (SW Amazonian Craton, Brazil). Precambrian Research 164, 40–49. doi:10.1016/j.precamres.2008.03.004.

Bjorkman, K.E., 2017. 40 crust-mantle evolution of the Western Superior Craton: implications for Archaean granite-greenstone petrogenesis and geodynamics. Ph.D. thesis. University of Western Australia. doi:10.4225/23/5A39C88A2F559.

Blades, M.L., Collins, A.S., Foden, J., Payne, J.L., Stüwe, K., Abu-Alam, T., Makroum, F., Hassan, M., 2021. Age and hafnium isotope evolution of Sudanese Butana and Chad illuminates the Stenian to Ediacaran evolution of the south and east Sahara. Precambrian Research 362, 106323. doi:10.1016/j.precamres.2021.106323.

Blayney, T., Dupont-Nivet, G., Najman, Y., Proust, J.N., Meijer, N., Roperch, P., Sobel, E.R., Millar, I., Guo, Z., 2019. Tectonic evolution of the Pamir recorded in the western Tarim Basin (China): Sedimentologic and magnetostratigraphic analyses of the Aertashi section. Tectonics 38, 492–515. doi:10.1029/2018tc005146.

Bogdanova, S., Gorbatschev, R., Skridlaite, G., Soesoo, A., Taran, L., Kurlovich, D., 2015. Trans-Baltic Palaeoproterozoic correlations towards the reconstruction of supercontinent Columbia/Nuna. Precambrian Research 259, 5–33. doi:10.1016/j.precamres.2014.11.023.

Boger, S.D., 2011. Antarctica — Before and after Gondwana. Gondwana Research 19, 335–371. doi:10.1016/j.gr.2010.09.003.

Bowring, S.A., Podosek, F.A., 1989. Nd isotopic evidence from Wopmay Orogen for 2.0–2.4 Ga crust in western North America. Earth and Planetary Science Letters 94, 217–230. doi:10.1016/0012-821x(89)90141-6.

Brandl, P.A., Regelous, M., Beier, C., Haase, K.M., 2013. High mantle temperatures following rifting caused by continental insulation. Nature Geoscience 6, 391–394. URL: https://doi.org/10.1038%2Fngeo1758, doi:10.1038/ngeo1758.

Breton, E.L., Handy, M.R., Molli, G., Ustaszewski, K., 2017. Post-20 Ma motion of the Adriatic Plate: New constraints from surrounding orogens and implications for crust-mantle decoupling. Tectonics 36, 3135–3154. doi:10.1002/2016tc004443.

Brown, D.A., Morrissey, L.J., Goodge, J.W., Hand, M., 2021. Absence of evidence for Palaeoproterozoic eclogite-facies metamorphism in East Antarctica: no record of subduction orogenesis during Nuna development. Scientific Reports 11. doi:10.1038/s41598-021-86184-4.

Brown, M., Johnson, T., 2018. Secular change in metamorphism and the onset of global plate tectonics. American Mineralogist 103, 181–196. doi:10.2138/am-2018-6166.

Bruhn, R., Sauber, J.M., Cotton, M.M., Pavlis, T.L., Burgess, E.W., Ruppert, N.A., Forster, R., 2012. Plate margin deformation and active tectonics along the northern edge of the Yakutat Terrane in the Saint Elias Orogen, Alaska, and Yukon, Canada. Geosphere 8, 1384–1407. doi:10.1130/ges00807.1.

Burrett, C., Zaw, K., Meffre, S., Lai, C.K., Khositanont, S., Chaodumrong, P., Udchachon, M., Ekins, S., Halpin, J., 2014. The configuration of Greater Gondwana–Evidence from LA ICPMS, U–Pb geochronology of detrital zircons from the Palaeozoic and Mesozoic of Southeast Asia and China. Gondwana Research 26, 31–51. doi:10.1016/j.gr.2013.05.020.

Buslov, M.M., Saphonova, I.Y., Watanabe, T., Obut, O.T., Fujiwara, Y., Iwata, K., Semakov, N.N., Sugai, Y., Smirnova, L.V., Kazansky, A.Y., 2001. Evolution of the Paleo-Asian Ocean (Altai-Sayan Region, Central Asia) and collision of possible Gondwana-derived terranes with the southern marginal part of the Siberian continent. Geosciences Journal 5, 203–224. doi:10.1007/bf02910304.

Cai, J., Liu, F., Liu, P., Liu, C., Wang, F., Shi, J., 2015. Silica-undersaturated spinel granulites in the Daqingshan complex of the Khondalite Belt, North China Craton: Petrology and quantitative P–T–X constraints. Precambrian Research 266, 119–136. doi:10.1016/j.precamres.2015.05.005.

Cao, X., Flamet, N., Collins, A., Pisarevksy, S., Müller, D., Hasterok, D., in prep. Earth's tectonic and plate boundary evolution over 1.8 billion years. Earth Science Reviews .

Capitanio, F.A., Faccenna, C., Zlotnik, S., Stegman, D.R., 2011. Subduction dynamics and the origin of Andean orogeny and the Bolivian orocline. Nature 480, 83–86. doi:10.1038/nature10596.

de Carvalho Filgueiras, B., de Oliveira, C.G., de Sousa, I.M.C., Cordeiro, P., 2020. Further evidence of Rhyacian arc magmatism in the basement of the Brasília Belt, western São Francisco pericraton. Journal of South American Earth Sciences 103, 102739. doi:10.1016/j.jsames.2020.102739.

Catalán, J.R.M., Schulmann, K., Ghienne, J.F., 2021. The Mid-Variscan Allochthon: Keys from correlation, partial retrodeformation and plate-tectonic reconstruction to unlock the geometry of a non-cylindrical belt. Earth-Science Reviews 220, 103700. doi:10.1016/j.earscirev.2021.103700.

Cave, B., Perkins, W., Lilly, R., 2022. Linking uplift and mineralisation at the Mount Novit Zn-Pb-Ag Deposit, Northern Australia: Evidence from geology, U–Pb geochronology and sphalerite geochemistry. Geoscience Frontiers 13, 101347. doi:10.1016/j.gsf.2021.101347.

Cawood, P.A., 2005. Terra Australis Orogen: Rodinia breakup and development of the Pacific and Iapetus margins of Gondwana during the Neoproterozoic and Paleozoic. Earth-Science Reviews 69, 249–279. doi:10.1016/j.earscirev.2004.09.001.

Cawood, P.A., Wang, W., Zhao, T., Xu, Y., Mulder, J.A., Pisarevsky, S.A., Zhang, L., Gan, C., He, H., Liu, H., Qi, L., Wang, Y., Yao, J., Zhao, G., Zhou, M.F., Zi, J.W., 2020. Deconstructing South China and consequences for reconstructing Nuna and Rodinia. Earth-Science Reviews 204, 103169. doi:10.1016/j.earscirev.2020.103169.

Chacko, T., De, S.K., Creaser, R.A., Muehlenbachs, K., 2000. Tectonic setting of the Taltson magmatic zone at 1.9–2.0 Ga: a granitoid-based perspective. Canadian Journal of Earth Sciences 37, 1597–1609. doi:10.1139/e00-029.

Charrier, R., Ramos, V.A., Tapia, F., Sagripanti, L., 2014. Tectono-stratigraphic evolution of the Andean Orogen between 31 and 37°S (Chile and Western Argentina). Geological Society, London, Special Publications 399, 13–61. doi:10.1144/sp399.20.

Charvet, J., Shu, L., Laurent-Charvet, S., Wang, B., Faure, M., Cluzel, D., Chen, Y., Jong, K.D., 2011. Palaeozoic tectonic evolution of the Tianshan belt, NW China. Science China Earth Sciences 54, 166–184. doi:10.1007/s11430-010-4138-1.

Chattopadhyay, S., Upadhyay, D., Nanda, J.K., Mezger, K., Pruseth, K.L., Berndt, J., 2015. Proto-India was a part of Rodinia: Evidence from Grenville-age suturing of the Eastern Ghats Province with the Paleoarchean Singhbhum Craton. Precambrian Research 266, 506–529. doi:10.1016/j.precamres.2015.05.030.

Chaúque, F., Cordani, U., Jamal, D., 2019. Geochronological systematics for the Chimoio-Macossa frontal nappe in central Mozambique: Implications for the tectonic evolution of the southern part of the Mozambique belt. Journal of African Earth Sciences 150, 47–67. doi:10.1016/j.jafrearsci.2018.10.013.

Cheney, J.T., Brady, J.B., Tierney, K.A., DeGraff, K.A., Mohlman, H.K., Frisch, J.D., Hatch, C.E., Steiner, M.L., Carmichael, S.K., Fisher, R.G., Tuit, C.B., Steffen, K.J., Cady, P., Lowell, J., Archuleta, L.L., Hirst, J., Wegmann, K.W., Monteleone, B., 2004a. Proterozoic metamorphism of the Tobacco Root Mountains, Montana, in: Precambrian Geology of the Tobacco Root Mountains, Montana. Geological Society of America, pp. 105–129. doi:10.1130/0-8137-2377-9.105.

Cheney, J.T., Webb, A.A.G., Coath, C.D., McKeegan, K.D., 2004b. In situ ion microprobe $^{207}Pb/^{206}Pb$ dating of monazite from Precambrian metamorphic suites, Tobacco Root Mountains, Montana, in: Precambrian Geology of the Tobacco Root Mountains, Montana. Geological Society of America, pp. 151–179. doi:10.1130/0-8137-2377-9.151.

Cherepanova, Y., Artemieva, I.M., Thybo, H., Chemia, Z., 2013. Crustal structure of the Siberian craton and the West Siberian basin: An appraisal of existing seismic data. Tectonophysics 609, 154–183. doi:10.1016/j.tecto.2013.05.004.

Chew, D., Magna, T., Kirkland, C., Miskovic, A., Cardona, A., Spikings, R., Schaltegger, U., 2008. Detrital zircon fingerprint of the Proto-Andes: Evidence for a Neoproterozoic active margin? Precambrian Research 167, 186–200. doi:10.1016/j.precamres.2008.08.002.

Chew, D.M., Schaltegger, U., Kosler, J., Whitehouse, M.J., Gutjahr, M., Spikings, R.A., Miskovic, A., 2007. U-Pb geochronologic evidence for the evolution of the Gondwanan margin of the north-central Andes. Geological Society of America Bulletin 119, 697–711. doi:10.1130/b26080.1.

Chiarenzelli, J., Aspler, L., Villeneuve, M., Lewry, J., 1998. Early Proterozoic evolution of the Saskatchewan Craton and its allochthonous cover, Trans-Hudson Orogen. The Journal of Geology 106, 247–268. doi:10.1086/516020.

Clark, C., Collins, A.S., Timms, N.E., Kinny, P.D., Chetty, T., Santosh, M., 2009. SHRIMP U–Pb age constraints on magmatism and high-grade metamorphism in the Salem Block, southern India. Gondwana Research 16, 27–36. doi:10.1016/j.gr.2008.11.001.

Clark, D., Hensen, B., Kinny, P., 2000. Geochronological constraints for a two-stage history of the Albany–Fraser Orogen, Western Australia. Precambrian Research 102, 155–183. doi:10.1016/s0301-9268(00)00063-2.

Collins, A.S., Blades, M.L., Merdith, A.S., 2021a. The Arabian–Nubian Shield within the Neoproterozoic plate tectonic circuit, in: The Geology of the Arabian-Nubian Shield. Springer International Publishing, pp. 195–202. doi:10.1007/978-3-030-72995-0_8.

Collins, A.S., Blades, M.L., Merdith, A.S., Foden, J.D., 2021b. Closure of the Proterozoic Mozambique Ocean was instigated by a late Tonian plate reorganization event. Communications Earth & Environment 2. doi:10.1038/s43247-021-00149-z.

Collins, A.S., Fitzsimons, I.C.W., Hulscher, B., Razakamanana, T., 2003. Structure of the eastern margin of the East African Orogen in central Madagascar. Precambrian Research 123, 111–133. doi:10.1016/s0301-9268(03)00064-0.

Collins, A.S., Pisarevsky, S.A., 2005. Amalgamating eastern Gondwana: The evolution of the Circum-Indian Orogens. Earth-Science Reviews 71, 229–270. doi:10.1016/j.earscirev.2005.02.004.

Collins, A.S., Reddy, S.M., Buchan, C., Mruma, A., 2004. Temporal constraints on Palaeoproterozoic eclogite formation and exhumation (Usagaran Orogen, Tanzania). Earth and Planetary Science Letters 224, 175–192. doi:10.1016/j.epsl.2004.04.027.

Collins, A.S., Windley, B.F., 2002. The tectonic evolution of central and northern Madagascar and its place in the final assembly of Gondwana. The Journal of Geology 110, 325–339. doi:10.1086/339535.

Colpron, M., Nelson, J., 2011. A Digital Atlas of Terranes for the Northern Cordillera. Technical Report. Yukon Geological Survey. Whitehorse, Canada. Accessed 11 November, 2017.

Condie, K.C., Pisarevsky, S.A., Puetz, S.J., 2021. LIPs, orogens and supercontinents: The ongoing saga. Gondwana Research 96, 105–121. doi:10.1016/j.gr.2021.05.002.

Condie, K.C., Rosen, O.M., 1994. Laurentia-Siberia connection revisited. Geology 22, 168. doi:10.1130/0091-7613(1994)022<0168:lscr>2.3.co;2.

Cook, F.A., 2011. Multiple arc development in the Paleoproterozoic Wopmay Orogen, Northwest Canada, in: Frontiers in Earth Sciences. Springer Berlin Heidelberg, pp. 403–427. doi:10.1007/978-3-540-88558-0_14.

Cooray, P., 1994. The Precambrian of Sri Lanka: a historical review. Precambrian Research 66, 3–18. doi:10.1016/0301-9268(94)90041-8.

Corrigan, D., Pehrsson, S., Wodicka, N., de Kemp, E., 2009. The Palaeoproterozoic Trans-Hudson Orogen: a prototype of modern accretionary processes. Geological Society, London, Special Publications 327, 457–479. doi:10.1144/sp327.19.

Cutts, K., Hand, M., Kelsey, D., 2011. Evidence for early Mesoproterozoic (ca. 1590Ma) ultrahigh-temperature metamorphism in southern Australia. Lithos 124, 1–16. doi:10.1016/j.lithos.2010.10.014.

Daczko, N.R., Halpin, J.A., Fitzsimons, I.C.W., Whittaker, J.M., 2018. A cryptic Gondwana-forming orogen located in Antarctica. Scientific Reports 8. doi:10.1038/s41598-018-26530-1.

D'Agrella-Filho, M.S., Cordani, U.G., 2016. The Paleomagnetic Record of the São Francisco-Congo Craton, in: São Francisco Craton, Eastern Brazil. Springer International Publishing, pp. 305–320. doi:10.1007/978-3-319-01715-0_16.

Daly, J., Balagansky, V., Timmerman, M., Whitehouse, M., de Jong, K., Guise, P., Bogdanova, S., Gorbatschev, R., Bridgwater, D., 2001. Ion microprobe U-Pb zircon geochronology and isotopic evidence for a trans-crustal suture in the Lapland–Kola Orogen, northern Fennoscandian Shield. Precambrian Research 105, 289–314. doi:10.1016/s0301-9268(00)00116-9.

Daniel, C.G., Pfeifer, L.S., Jones, J.V., McFarlane, C.M., 2013. Detrital zircon evidence for non-Laurentian provenance, Mesoproterozoic (ca. 1490-1450 Ma) deposition and orogenesis in a reconstructed orogenic belt, northern New Mexico, USA: Defining the Picuris orogeny. Geological Society of America Bulletin 125, 1423–1441. doi:10.1130/b30804.1.

Darbyshire, F.A., 2005. Upper mantle structure of Arctic Canada from Rayleigh wave dispersion. Tectonophysics 405, 1–23. doi:10.1016/j.tecto.2005.02.013.

Darbyshire, F.A., Bastow, I.D., Petrescu, L., Gilligan, A., Thompson, D.A., 2017. A tale of two orogens: Crustal processes in the Proterozoic Trans-Hudson and Grenville Orogens, eastern Canada. Tectonics 36, 1633–1659. doi:10.1002/2017tc004479.

Dasgupta, S., Bose, S., Das, K., 2013. Tectonic evolution of the Eastern Ghats Belt, India. Precambrian Research 227, 247–258. doi:10.1016/j.precamres.2012.04.005.

Davison, I., Pindell, J., Hull, J., 2020. The Basins, Orogens and Evolution of the southern Gulf of Mexico and northern Caribbean. Geological Society, London, Special Publications , SP504–2020–218doi:10.1144/sp504-2020-218.

Davy, B., 2006. Bollons Seamount and early New Zealand-Antarctic seafloor spreading. Geochemistry, Geophysics, Geosystems 7, Q06021. doi:10.1029/2005gc001191.

De Roever, E., Lafon, J.M., Delor, C., Cocherie, A., Rossi, P., Guerrrot, C., Potrel, A., 2003. The Bakhuis ultrahigh-temperature granulite belt (Suriname): I. Petrological and geochronological evidence for a counterclockwise P–T path at 2.07–2.05 Ga. Géol. France 2-3-4, 175–205.

Debayle, E., Dubuffet, F., Durand, S., 2016. An automatically updated S-wave model of the upper mantle and the depth extent of azimuthal anisotropy. Geophysical Research Letters 43, 674–682. doi:10.1002/2015gl067329.

Debayle, E., Dubuffet, F., Durand, S., 2019. Data Services Products: 3D2018_08Sv, a global Sv wave upper mantle model updated until August 2018. Technical Report. Incorporated Research Institutions for Seismology (IRIS). doi:10.17611/DP/EMC3D201808S.

DeMets, C., Gordon, R.G., Argus, D.F., 2010. Geologically current plate motions. Geophysical Journal International 181, 1–80. doi:10.1111/j.1365-246x.2009.04491.x.

DeMets, C., Márquez-Azúa, B., Cabral-Cano, E., 2014. A new GPS velocity field for the Pacific Plate – Part 2: implications for fault slip rates in western California. Geophysical Journal International 199, 1900–1909. doi:10.1093/gji/ggu347.

DeMets, C., Wiggins-Grandison, M., 2007. Deformation of Jamaica and motion of the Gonâve microplate from GPS and seismic data. Geophysical Journal International 168, 362–378. doi:10.1111/j.1365-246x.2006.03236.x.

Derbeko, I., 2013. The region of matching of Central-Asian Mobile Belt and Pacific Mobile Belt. International Journal of Geosciences 04, 605–610. doi:10.4236/ijg.2013.43055.

Dew, R.E., Collins, A.S., Morley, C.K., King, R.C., Evans, N.J., Glorie, S., 2021. Coupled detrital zircon U–Pb and Hf analysis of the Sibumasu Terrane: From Gondwana to northwest Thailand. Journal of Asian Earth Sciences 211, 104709. doi:10.1016/j.jseaes.2021.104709.

Dickinson, W.R., 2004. Evolution of the North American Cordillera. Annual Review of Earth and Planetary Sciences 32, 13–45. doi:10.1146/annurev.earth.32.101802.120257.

Dilek, Y., 2006. Collision tectonics of the Mediterranean region: Causes and consequences, in: Postcollisional Tectonics and Magmatism in the Mediterranean Region and Asia. Geological Society of America, pp. 1–13. doi:10.1130/2006.2409(01).

Dilek, Y., Furnes, H., 2014. Ophiolites and their origins. Elements 10, 93–100. doi:10.2113/gselements.10.2.93.

Dillon, W.P., Schlee, J.S., Klitgord, K.D., 1988. The development of the continental margin of eastern North America—conjugate continental margin to West Africa. Journal of African Earth Sciences (and the Middle East) 7, 361–367. doi:10.1016/0899-5362(88)90080-2.

Dixon, T.H., Mao, A., 1997. A GPS estimate of relative motion between North and South America. Geophysical Research Letters 24, 535–538. doi:10.1029/97gl00284.

Dixon, T.H., Miller, M., Farina, F., Wang, H., Johnson, D., 2000. Present-day motion of the Sierra Nevada block and some tectonic implications for the Basin and Range province, North American Cordillera. Tectonics 19, 1–24. doi:10.1029/1998tc001088.

Djeutchou, C., de Kock, M.O., Wabo, H., Gaitán, C.E., Söderlund, U., Gumsley, A.P., 2021. Late Paleoproterozoic mafic magmatism and the Kalahari craton during Columbia assembly. Geology 49, 1375–1380. doi:10.1130/g48811.1.

Dong, X., Yang, D., Niu, F., Liu, S., Tong, P., 2021. Adjoint traveltime tomography unravels a scenario of horizontal mantle flow beneath the North China craton. Scientific Reports 11. doi:10.1038/s41598-021-92048-8.

Donskaya, T., Gladkochub, D., Pisarevsky, S., Poller, U., Mazukabzov, A., Bayanova, T., 2009. Discovery of Archaean crust within the Akitkan orogenic belt of the Siberian craton: New insight into its architecture and history. Precambrian Research 170, 61–72. doi:10.1016/j.precamres.2008.12.003.

Doumbia, S., Pouclet, A., Kouamelan, A., Peucat, J., Vidal, M., Delor, C., 1998. Petrogenesis of juvenile-type Birimian (Paleoproterozoic) granitoids in Central Côte-d'Ivoire, West Africa: geochemistry and geochronology. Precambrian Research 87, 33–63. doi:10.1016/s0301-9268(97)00201-5.

Dovzhikova, E., Pease, V., Remizov, D., 2004. Neoproterozoic island are magmatism beneath the pechora basin, NW russia. GFF 126, 353–362. doi:10.1080/11035890401264353.

Ducea, M.N., Saleeby, J.B., Bergantz, G., 2015. The architecture, chemistry, and evolution of continental magmatic arcs. Annual Review of Earth and Planetary Sciences 43, 299–331. doi:10.1146/annurev-earth-060614-105049.

Duclaux, G., Rolland, Y., Ruffet, G., Ménot, R.P., Guillot, S., Peucat, J.J., Fanning, M., Rey, P., Pêcher, A., 2008. Superimposed Neoarchaean and Paleoproterozoic tectonics in the Terre Adélie Craton (East Antarctica): Evidence from Th–U–Pb ages on monazite and 40Ar/39Ar ages. Precambrian Research 167, 316–338. doi:10.1016/j.precamres.2008.09.009.

Dunkley, D.J., Hokada, T., Shiraishi, K., Hiroi, Y., Nogi, Y., Motoyoshi, Y., 2020. Geological subdivision of the lützow–holm complex in east antarctica: From the neoarchean to the neoproterozoic. Polar Science 26, 100606. doi:10.1016/j.polar.2020.100606.

Eagles, G., 2016. Tectonic reconstructions of the southernmost Andes and the Scotia Sea during the opening of the Drake Passage, in: Geodynamic Evolution of the Southernmost Andes. Springer International Publishing, pp. 75–108. doi:10.1007/978-3-319-39727-6_4.

Eagles, G., Gloaguen, R., Ebinger, C., 2002. Kinematics of the Danakil microplate. Earth and Planetary Science Letters 203, 607–620. doi:10.1016/s0012-821x(02)00916-0.

Ebbing, J., Dilixiati, Y., Haas, P., Ferraccioli, F., Scheiber-Enslin, S., 2021. East Antarctica magnetically linked to its ancient neighbours in Gondwana. Scientific Reports 11. doi:10.1038/s41598-021-84834-1.

Edel, J.B., Casini, L., Oggiano, G., Rossi, P., Schulmann, K., 2014. Early Permian 90° clockwise rotation of the Maures–Estérel–Corsica–Sardinia block confirmed by new palaeomagnetic data and followed by a Triassic 60° clockwise rotation. Geological Society, London, Special Publications 405, 333–361. doi:10.1144/sp405.10.

Eglington, B.M., 2004. DateView: a windows geochronology database. Computers & Geosciences 30, 847–858. doi:10.1016/j.cageo.2004.06.002.

Egydio-Silva, M., Vauchez, A., Fossen, H., Cavalcante, G.C.G., Xavier, B.C., 2018. Connecting the Araçuaí and Ribeira belts (SE – Brazil): Progressive transition from contractional to transpressive strain regime during the Brasiliano orogeny. Journal of South American Earth Sciences 86, 127–139. doi:10.1016/j.jsames.2018.06.005.

Eizenhöfer, P.R., Zhao, G., Zhang, J., Sun, M., 2014. Final closure of the Paleo-Asian Ocean along the Solonker Suture Zone: Constraints from geochronological and geochemical data of Permian volcanic and sedimentary rocks. Tectonics 33, 441–463. doi:10.1002/2013tc003357.

Elliot, D.H., Fanning, C.M., Hulett, S.R., 2015. Age provinces in the Antarctic craton: Evidence from detrital zircons in Permian strata from the Beardmore Glacier region, Antarctica. Gondwana Research 28, 152–164. doi:10.1016/j.gr.2014.03.013.

Elliott, J., Freymueller, J.T., 2020. A block model of present-day kinematics of Alaska and Western Canada. Journal of Geophysical Research: Solid Earth 125. doi:10.1029/2019jb018378.

Elming, S.Å., D'Agrella-Filho, M.S., Page, L.M., Tohver, E., Trindade, R.I.F., Pacca, I.I.G., Geraldes, M.C., Teixeira, W., 2009. A palaeomagnetic and $^{40}Ar/^{39}Ar$ study of late Precambrian sills in the SW part of the Amazonian craton: Amazonia in the Rodinia reconstruction. Geophysical Journal International 178, 106–122. doi:10.1111/j.1365-246x.2009.04149.x.

Elming, S.Å., Salminen, J., Pesonen, L.J., 2021. Paleo-Mesoproterozoic Nuna supercycle, in: Ancient Supercontinents and the Paleogeography of Earth. Elsevier, pp. 499–548. doi:10.1016/b978-0-12-818533-9.00001-1.

Ennih, N., Liégeois, J.P., 2008. The boundaries of the West African craton, with special reference to the basement of the Moroccan metacratonic Anti-Atlas belt. Geological Society, London, Special Publications 297, 1–17. doi:10.1144/sp297.1.

Ernst, R.E., Hamilton, M.A., Söderlund, U., Hanes, J.A., Gladkochub, D.P., Okrugin, A.V., Kolotilina, T., Mekhonoshin, A.S., Bleeker, W., LeCheminant, A.N., Buchan, K.L., Chamberlain, K.R., Didenko, A.N., 2016. Long-lived connection between southern Siberia and northern Laurentia in the Proterozoic. Nature Geoscience 9, 464–469. doi:10.1038/ngeo2700.

Eude, A., Roddaz, M., Brichau, S., Brusset, S., Calderon, Y., Baby, P., Soula, J.C., 2015. Controls on timing of exhumation and deformation in the northern Peruvian eastern Andean wedge as inferred from low-temperature thermochronology and balanced cross section. Tectonics 34, 715–730. doi:10.1002/2014tc003641.

Evenstar, L.A., Stuart, F.M., Hartley, A.J., Tattitch, B., 2015. Slow Cenozoic uplift of the western Andean Cordillera indicated by cosmogenic 3 He in alluvial boulders from the Pacific Planation Surface. Geophysical Research Letters 42, 8448–8455. doi:10.1002/2015gl065959.

Famin, V., Michon, L., Bourhane, A., 2020. The Comoros Archipelago: a right-lateral transform boundary between the Somalia and Lwandle plates. Tectonophysics 789, 228539. doi:10.1016/j.tecto.2020.228539.

Fergusson, C., Henderson, R., 2015. Early Palaeozoic continental growth in the Tasmanides of northeast Gondwana and its implications for Rodinia assembly and rifting. Gondwana Research 28, 933–953. doi:10.1016/j.gr.2015.04.001.

Fernandes, R., Bastos, L., Miranda, J., Lourenço, N., Ambrosius, B., Noomen, R., Simons, W., 2006. Defining the plate boundaries in the Azores region. Journal of Volcanology and Geothermal Research 156, 1–9. doi:10.1016/j.jvolgeores.2006.03.019.

Ferraccioli, F., Finn, C.A., Jordan, T.A., Bell, R.E., Anderson, L.M., Damaske, D., 2011. East Antarctic rifting triggers uplift of the Gamburtsev Mountains. Nature 479, 388–392. doi:10.1038/nature10566.

Fershtater, G.B., 2012. The main features of the Uralian Paleozoic magmatism and the epioceanic nature of the orogen. Mineralogy and Petrology 107, 39–52. doi:10.1007/s00710-012-0218-6.

Filatova, N.I., Khain, V.E., 2008. Development of the Verkhoyansk-Kolyma orogenic system as a result of interaction of adjacent continental and oceanic plates. Geotectonics 42, 258–285. doi:10.1134/s001685210804002x.

Fischer, K.M., 2002. Waning buoyancy in the crustal roots of old mountains. Nature 417, 933–936. doi:10.1038/nature00855.

Fitzsimons, I., 2000. Grenville-age basement provinces in East Antarctica: Evidence for three separate collisional orogens. Geology 28, 879. doi:10.1130/0091-7613(2000)28<879:gbpiea>2.0.co;2.

Fitzsimons, I.C.W., 2003. Proterozoic basement provinces of southern and southwestern Australia, and their correlation with Antarctica. Geological Society, London, Special Publications 206, 93–130. doi:10.1144/gsl.sp.2003.206.01.07.

Fletcher, H.J., Freymueller, J.T., 1999. New GPS constraints on the motion of the Yakutat Block. Geophysical Research Letters 26, 3029–3032. doi:10.1029/1999gl005346.

Flowerdew, M.J., Tyrrell, S., Boger, S.D., Fitzsimons, I.C.W., Harley, S.L., Mikhalsky, E.V., Vaughan, A.P.M., 2013. Pb isotopic domains from the Indian Ocean sector of Antarctica: implications for past Antarctica–India connections. Geological Society, London, Special Publications 383, 59–72. doi:10.1144/sp383.3.

Fossen, H., Cavalcante, G.C., de Almeida, R.P., 2017. Hot versus cold orogenic behavior: Comparing the Araçuaí-West Congo and the Caledonian Orogens. Tectonics 36, 2159–2178. doi:10.1002/2017tc004743.

Foster, D., Goscombe, B., 2013. Continental growth and recycling in convergent orogens with large turbidite fans on oceanic crust. Geosciences 3, 354–388. doi:10.3390/geosciences3030354.

Foulger, G.R., Doré, T., Emeleus, C.H., Franke, D., Geoffroy, L., Gernigon, L., Hey, R., Holdsworth, R.E., Hole, M., Höskuldsson, Á., Julian, B., Kusznir, N., Martinez, F., McCaffrey, K.J., Natland, J.H., Peace, A.L., Petersen, K., Schiffer, C., Stephenson, R., Stoker, M., 2020. The Iceland Microcontinent and a continental Greenland-Iceland-Faroe Ridge. Earth-Science Reviews 206, 102926. doi:10.1016/j.earscirev.2019.102926.

French, J.E., Heaman, L.M., Chacko, T., Srivastava, R.K., 2008. 1891–1883Ma Southern Bastar–Cuddapah mafic igneous events, India: A newly recognized large igneous province. Precambrian Research 160, 308–322. doi:10.1016/j.precamres.2007.08.005.

Fretwell, P., Pritchard, H.D., Vaughan, D.G., Bamber, J.L., Barrand, N.E., Bell, R., Bianchi, C., Bingham, R.G., Blankenship, D.D., Casassa, G., Catania, G., Callens, D., Conway, H., Cook, A.J., Corr, H.F.J., Damaske, D., Damm, V., Ferraccioli, F., Forsberg, R., Fujita, S., Gim, Y., Gogineni, P., Griggs, J.A., Hindmarsh, R.C.A., Holmlund, P., Holt, J.W., Jacobel, R.W., Jenkins, A., Jokat, W., Jordan, T., King, E.C., Kohler, J., Krabill, W., Riger-Kusk, M., Langley, K.A., Leitchenkov, G., Leuschen, C., Luyendyk, B.P., Matsuoka, K., Mouginot, J., Nitsche, F.O., Nogi, Y., Nost, O.A., Popov, S.V., Rignot, E., Rippin, D.M., Rivera, A., Roberts, J., Ross, N., Siegert, M.J., Smith, A.M., Steinhage, D., Studinger, M., Sun, B., Tinto, B.K., Welch, B.C., Wilson, D., Young, D.A., Xiangbin, C., Zirizzotti, A., 2013. Bedmap2: improved ice bed, surface and thickness datasets for Antarctica. The Cryosphere 7, 375–393. doi:10.5194/tc-7-375-2013.

Fritz, H., Abdelsalam, M., Ali, K., Bingen, B., Collins, A., Fowler, A., Ghebreab, W., Hauzenberger, C., Johnson, P., Kusky, T., Macey, P., Muhongo, S., Stern, R., Viola, G., 2013. Orogen styles in the East African Orogen: A review of the Neoproterozoic to Cambrian tectonic evolution. Journal of African Earth Sciences 86, 65–106. doi:10.1016/j.jafrearsci.2013.06.004.

Funck, T., Erlendsson, Ö., Geissler, W.H., Gradmann, S., Kimbell, G.S., McDermott, K., Petersen, U.K., 2016. A review of the NE Atlantic conjugate margins based on seismic refraction data. Geological Society, London, Special Publications 447, 171–205. doi:10.1144/sp447.9.

Furlanetto, F., Thorkelson, D.J., Gibson, H.D., Marshall, D.D., Rainbird, R.H., Davis, W.J., Crowley, J.L., Vervoort, J.D., 2013. Late Paleoproterozoic terrane accretion in northwestern Canada and the case for circum-Columbian orogenesis. Precambrian Research 224, 512–528. doi:10.1016/j.precamres.2012.10.010.

Furman, T., 2007. Geochemistry of East African Rift basalts: An overview. Journal of African Earth Sciences 48, 147–160. doi:10.1016/j.jafrearsci.2006.06.009.

Fyffe, L.R., Johnson, S.C., Staal, C.R.V., 2012. A review of Proterozoic to Early Paleozoic lithotectonic terranes in New Brunswick, Canada and their tectonic evolution during Penobscot, Taconic, Salinic and Acadian Orogenesis. Atlantic Geology 47, 211–248. doi:10.4138/atlgeol.2011.010.

Gaina, C., Müller, R.D., Roest, W.R., Symonds, P., 1998. The opening of the Tasman Sea: A gravity anomaly animation. Earth Interactions 2, 1–23. doi:10.1175/1087-3562(1998)002<0001:tootts>2.3.co;2.

Gallais, F., Fujie, G., Boston, B., Hackney, R., Kodaira, S., Miura, S., Nakamura, Y., Kaiho, Y., 2019. Crustal structure across the Lord Howe Rise, northern Zealandia, and rifting of the eastern Gondwana margin. Journal of Geophysical Research: Solid Earth 124, 3036–3056. doi:10.1029/2018jb016798.

Gao, P., Zheng, Y.F., Zhao, Z.F., 2017. Triassic granites in South China: A geochemical perspective on their characteristics, petrogenesis, and tectonic significance. Earth-Science Reviews 173, 266–294. doi:10.1016/j.earscirev.2017.07.016.

García Casco, A., Torres-Roldán, R., Iturralde-Vinent, M.A., Millán Trujillo, G., K. E. Nuúñez Cambra, C. Lázaro, A.R., 2006. High pressure metamorphism of eclogites in Cuba. Geologica Acta 4, 63–88. doi:10.1344/105.000000358.

Gard, M., Hasterok, D., Halpin, J., 2019a. Global whole-rock geochemical database compilation. Earth System Science Data 11, 1553–1566. doi:10.5194/essd-11-1553-2019.

Gard, M., Hasterok, D., Hand, M., Cox, G., 2019b. Variations in continental heat production from 4 Ga to the present: Evidence from geochemical data. Lithos 342-343, 391–406. doi:10.1016/j.lithos.2019.05.034.

Gardiner, N., Searle, M., Morley, C., Whitehouse, M., Spencer, C., Robb, L., 2016. The closure of Palaeo-Tethys in Eastern Myanmar and Northern Thailand: New insights from zircon U–Pb and Hf isotope data. Gondwana Research 39, 401–422. doi:10.1016/j.gr.2015.03.001.

Gardner, R.L., Daczko, N.R., Halpin, J.A., Whittaker, J.M., 2015. Discovery of a microcontinent (Gulden Draak Knoll) offshore Western Australia: Implications for East Gondwana reconstructions. Gondwana Research 28, 1019–1031. doi:10.1016/j.gr.2014.08.013.

Garrity, C.P., Soller, D.R., 2009. Database of the Geologic Map of North America: Adapted from the map by J.C. Reed, Jr. and others (2005). Digital Data Series 424. US Geological Survey. doi:10.3133/ds424.

Ge, R., Zhu, W., Wilde, S.A., He, J., Cui, X., Wang, X., Bihai, Z., 2014. Neoproterozoic to Paleozoic long-lived accretionary orogeny in the northern Tarim Craton. Tectonics 33, 302–329. doi:10.1002/2013tc003501.

Gee, D.G., Stephenson, R.A., 2006. The European lithosphere: an introduction. Geological Society, London, Memoirs 32, 1–9. doi:10.1144/gsl.mem.2006.032.01.01.

Geognostics, 2021. OZ SEEBASE® 2021 (March 2021), https://www.geognostics.com/oz-seebase-2021. Technical Report. Geognostics Australia Pty Ltd.

Geological Survey of India, 2006. Gravity Map Series of India. Technical Report. National Geophysical Research Institute and Geological Survey of India. Hyderabad, India.

Gifford, J.N., Mueller, P.A., Foster, D.A., Mogk, D.W., 2018. Extending the realm of Archean crust in the Great Falls tectonic zone: Evidence from the Little Rocky Mountains, Montana. Precambrian Research 315, 264–281. doi:10.1016/j.precamres.2018.07.021.

Gion, A.M., Williams, S.E., Müller, R.D., 2017. A reconstruction of the Eurekan Orogeny incorporating deformation constraints. Tectonics 36, 304–320. doi:10.1002/2015tc004094.

Gladkochub, D., Donskaya, T., Fedorovsky, V., Mazukabzov, A., Larionov, A., Sergeev, S., 2010. The Olkhon metamorphic terrane in the Baikal region: An Early Paleozoic collage of Neoproterozoic active margin fragments. Russian Geology and Geophysics 51, 447–460. doi:10.1016/j.rgg.2010.04.001.

Glen, R., Belousova, E., Griffin, W., 2016. Different styles of modern and ancient non-collisional orogens and implications for crustal growth: a Gondwanaland perspective. Canadian Journal of Earth Sciences 53, 1372–1415. doi:10.1139/cjes-2015-0229.

Global Volcanism Program, 2013. Volcanoes of the World, v. 4.7.3. Venzke, E (ed.). Technical Report. Smithsonian Institution. doi:10.5479/si.GVP.VOTW4-2013. downloaded 12 September 2018.

Glorie, S., Grave, J.D., 2016. Exhuming the Meso–Cenozoic Kyrgyz Tianshan and Siberian Altai-Sayan: A review based on low-temperature thermochronology. Geoscience Frontiers 7, 155–170. doi:10.1016/j.gsf.2015.04.003.

Golynsky, A.V., 2007. Magnetic anomalies in East Antarctica and surrounding regions: a window on major tectonic provinces and their boundaries, in: Cooper, A., Raymond, C. (Eds.), Antarctica: A Keystone in a Changing World – Online Proceedings of the 10th ISAES. US Geological Survey. volume 2007. doi:10.3133/of2007-1047.srp006.

Golynsky, A.V., Ferraccioli, F., Hong, J.K., Golynsky, D.A., von Frese, R.R.B., Young, D.A., Blankenship, D.D., Holt, J.W., Ivanov, S.V., Kiselev, A.V., Masolov, V.N., Eagles, G., Gohl, K., Jokat, W., Damaske, D., Finn, C., Aitken, A., Bell, R.E., Armadillo, E., Jordan, T.A., Greenbaum, J.S., Bozzo, E., Caneva, G., Forsberg, R., Ghidella, M., Galindo-Zaldivar, J., Bohoyo, F., Martos, Y.M., Nogi, Y., Quartini, E., Kim, H.R., Roberts, J.L., 2018. New magnetic anomaly map of the Antarctic. Geophysical Research Letters 45, 6437–6449. doi:10.1029/2018gl078153.

Gómez-Tapias, J., Schobbenhaus, C., Montes-Ramírez, N., 2019. Geological Map Of South America At a Scale of 1: 5M. Technical Report. Commission for the Geological Map of the World. doi:10.32685/10.143.2019.929.

Goodge, J.W., Fanning, C., Bennett, V.C., 2001. U–Pb evidence of ∼1.7 Ga crustal tectonism during the Nimrod Orogeny in the Transantarctic Mountains, Antarctica: implications for Proterozoic plate reconstructions. Precambrian Research 112, 261–288. doi:10.1016/s0301-9268(01)00193-0.

Goodge, J.W., Fanning, C.M., Brecke, D.M., Licht, K.J., Palmer, E.F., 2010. Continuation of the Laurentian Grenville Province across the Ross Sea Margin of East Antarctica. The Journal of Geology 118, 601–619. doi:10.1086/656385.

Goodge, J.W., Fanning, C.M., Fisher, C.M., Vervoort, J.D., 2017. Proterozoic crustal evolution of central East Antarctica: Age and isotopic evidence from glacial igneous clasts, and links with Australia and Laurentia. Precambrian Research 299, 151–176. doi:10.1016/j.precamres.2017.07.026.

Gordon, R., 1998. The plate tectonic approximation: Plate nonrigidity, diffuse plate boundaries, and global plate reconstructions. Annual Review of Earth and Planetary Sciences 26, 615–642. doi:10.1146/annurev.earth.26.1.615.

Goscombe, B., Foster, D.A., Gray, D., Wade, B., 2020. Assembly of central Gondwana along the Zambezi Belt: Metamorphic response and basement reactivation during the Kuunga Orogeny. Gondwana Research 80, 410–465. doi:10.1016/j.gr.2019.11.004.

Goutorbe, B., Poort, J., Lucazeau, F., Raillard, S., 2011. Global heat flow trends resolved from multiple geological and geophysical proxies. Geophys. J. Int. 187, 1405–1419. doi:10.1111/j.1365-246X.2011.05228.x.

Granot, R., Dyment, J., 2018. Late Cenozoic unification of East and West Antarctica. Nature Communications 9. doi:10.1038/s41467-018-05270-w.

Grenholm, M., 2019. The global tectonic context of the ca. 2.27-1.96 Ga Birimian Orogen – Insights from comparative studies, with implications for supercontinent cycles. Earth-Science Reviews 193, 260–298. doi:10.1016/j.earscirev.2019.04.017.

Grenholm, M., Jessell, M., Thébaud, N., 2019. A geodynamic model for the Paleoproterozoic (ca. 2.27–1.96 Ga) Birimian Orogen of the southern West African Craton – Insights into an evolving accretionary-collisional orogenic system. Earth-Science Reviews 192, 138–193. doi:10.1016/j.earscirev.2019.02.006.

de Gromard, R.Q., Kirkland, C.L., Howard, H.M., Wingate, M.T., Jourdan, F., McInnes, B.I., Danišík, M., Evans, N.J., McDonald, B.J., Smithies, R.H., 2019. When will it end? Long-lived intracontinental reactivation in central Australia. Geoscience Frontiers 10, 149–164. doi:10.1016/j.gsf.2018.09.003.

Gupta, S., Zhao, D., Rai, S., 2009. Seismic imaging of the upper mantle under the Erebus hotspot in Antarctica. Gondwana Research 16, 109–118. doi:10.1016/j.gr.2009.01.004.

Hall, J.W., Glorie, S., Reid, A.J., Boone, S.C., Collins, A.S., Gleadow, A., 2018. An apatite U–Pb thermal history map for the northern Gawler Craton, South Australia. Geoscience Frontiers 9, 1293–1308. doi:10.1016/j.gsf.2017.12.010.

Halls, H.C., Li, J., Davis, D., Hou, G., Zhang, B., Qian, X., 2000. A precisely dated Proterozoic palaeomagnetic pole from the North China craton, and its relevance to palaeocontinental reconstruction. Geophysical Journal International 143, 185–203. doi:10.1046/j.1365-246x.2000.00231.x.

Halpin, J.A., Daczko, N.R., Clarke, G.L., Murray, K.R., 2013. Basin analysis in polymetamorphic terranes: An example from east Antarctica. Precambrian Research 231, 78–97. doi:10.1016/j.precamres.2013.03.015.

Halpin, J.A., Daczko, N.R., Kobler, M.E., Whittaker, J.M., 2017. Strike-slip tectonics during the Neoproterozoic–Cambrian assembly of East Gondwana: Evidence from a newly discovered microcontinent in the Indian Ocean (Batavia Knoll). Gondwana Research 51, 137–148. doi:10.1016/j.gr.2017.08.002.

Halpin, J.A., Reid, A.J., 2016. Earliest Paleoproterozoic high-grade metamorphism and orogenesis in the Gawler Craton, South Australia: The southern cousin in the Rae family? Precambrian Research 276, 123–144. doi:10.1016/j.precamres.2016.02.001.

Hand, M., Reid, A., Jagodzinski, L., 2007. Tectonic Framework and Evolution of the Gawler Craton, Southern Australia. Economic Geology 102, 1377–1395. doi:10.2113/gsecongeo.102.8.1377.

Hanson, R.E., 2003. Proterozoic geochronology and tectonic evolution of southern Africa. Geological Society, London, Special Publications 206, 427–463. doi:10.1144/gsl.sp.2003.206.01.20.

Hardy, N., 1991. Tectonic evolution of the easternmost Panama basin: Some new data and inferences. Journal of South American Earth Sciences 4, 261–269. doi:10.1016/0895-9811(91)90035-j.

Harley, S.L., Fitzsimons, I.C.W., Zhao, Y., 2013. Antarctica and supercontinent evolution: historical perspectives, recent advances and unresolved issues. Geological Society, London, Special Publications 383, 1–34. doi:10.1144/sp383.9.

Harley, S.L., Kelly, N.M., 2007. Chapter 3.2 Ancient Antarctica: The Archaean of the East Antarctic Shield, in: Earth's Oldest Rocks. Elsevier, pp. 149–186. doi:10.1016/s0166-2635(07)15032-5.

Hartlaub, R.P., Heaman, L.M., Chacko, T., Ashton, K.E., 2007. Circa 2.3-Ga Magmatism of the Arrowsmith Orogeny, Uranium City Region, Western Churchill Craton, Canada. The Journal of Geology 115, 181–195. doi:10.1086/510641.

Hartmann, J., Moosdorf, N., 2012a. Global Lithological Map Database v1.0 (gridded to 0.5° spatial resolution), supplement to: Hartmann, Jens; Moosdorf, Nils (2012): The new global lithological map database GLiM: A representation of rock properties at the Earth surface. Geochemistry, Geophysics, Geosystems, 13, Q12004. Technical Report. doi:10.1594/PANGAEA.788537.

Hartmann, J., Moosdorf, N., 2012b. The new global lithological map database GLiM: A representation of rock properties at the Earth surface. Geochemistry, Geophysics, Geosystems 13, Q12004. doi:10.1029/2012gc004370.

Hasterok, D., Chapman, D., 2007. Continental thermal isostasy II: Applications to North America. J. Geophys. Res. 112, B06415. doi:10.1029/2006JB004664.

Hauksson, E., Kanamori, H., Stock, J., Cormier, M.H., Legg, M., 2013. Active Pacific North America Plate boundary tectonics as evidenced by seismicity in the oceanic lithosphere offshore Baja California, Mexico. Geophysical Journal International 196, 1619–1630. doi:10.1093/gji/ggt467.

He, Z.Y., Klemd, R., Yan, L.L., Lu, T.Y., Zhang, Z.M., 2018. Mesoproterozoic juvenile crust in microcontinents of the Central Asian Orogenic Belt: evidence from oxygen and hafnium isotopes in zircon10.3389/feart.2020.00363. Scientific Reports 8. doi:10.1038/s41598-018-23393-4.

Henderson, B., Collins, A.S., Payne, J., Forbes, C., Saha, D., 2014. Geologically constraining India in Columbia: The age, isotopic provenance and geochemistry of the protoliths of the Ongole Domain, Southern Eastern Ghats, India. Gondwana Research 26, 888–906. doi:10.1016/j.gr.2013.09.002.

Hickey-Vargas, R., Savov, I.P., Bizimis, M., Ishii, T., Fujioka, K., 2006. Origin of diverse geochemical signatures in igneous rocks from the West Philippine Basin: Implications for tectonic models, in: Back-Arc Spreading Systems: Geological, Biological, Chemical, and Physical Interactions. American Geophysical Union, pp. 287–303. doi:10.1029/166gm15.

Hildebrand, R.S., Hoffman, P.F., Bowring, S.A., 2009. The Calderian orogeny in Wopmay orogen (1.9 Ga), northwestern Canadian Shield. Geological Society of America Bulletin 122, 794–814. doi:10.1130/b26521.1.

Hinsbergen, D.J.J.V., Buiter, S.J.H., Torsvik, T.H., Gaina, C., Webb, S.J., 2011. The formation and evolution of Africa from the Archaean to Present: introduction. Geological Society, London, Special Publications 357, 1–8. URL: https://doi.org/10.1144%2Fsp357.1, doi:10.1144/SP357.1.

Holm, D., Schneider, D., Rose, S., Mancuso, C., McKenzie, M., Foland, K., Hodges, K., 2007. Proterozoic metamorphism and cooling in the southern Lake Superior region, North America and its bearing on crustal evolution. Precambrian Research 157, 106–126. doi:10.1016/j.precamres.2007.02.012.

Howard, H., Smithies, R., Kirkland, C., Kelsey, D., Aitken, A., Wingate, M., de Gromard, R.Q., Spaggiari, C., Maier, W., 2015. The burning heart—the Proterozoic geology and geological evolution of the west Musgrave Region, central Australia. Gondwana Res. 27, 64–94. doi:10.1016/j.gr.2014.09.001.

Hu, X., Garzanti, E., Wang, J., Huang, W., An, W., Webb, A., 2016. The timing of India-Asia collision onset – Facts, theories, controversies. Earth-Science Reviews 160, 264–299. doi:10.1016/j.earscirev.2016.07.014.

Hyndman, R.D., 2019. Origin of regional barrovian metamorphism in hot backarcs prior to orogeny deformation. Geochemistry, Geophysics, Geosystems 20, 460–469. doi:10.1029/2018gc007650.

Ibañez-Mejia, M., Ruiz, J., Valencia, V.A., Cardona, A., Gehrels, G.E., Mora, A.R., 2011. The Putumayo Orogen of Amazonia and its implications for Rodinia reconstructions: New U–Pb geochronological insights into the Proterozoic tectonic evolution of northwestern South America. Precambrian Research 191, 58–77. doi:10.1016/j.precamres.2011.09.005.

Isbell, J.L., Biakov, A.S., Vedernikov, I.L., Davydov, V.I., Gulbranson, E.L., Fedorchuk, N.D., 2016. Permian diamictites in northeastern Asia: Their significance concerning the bipolarity of the late Paleozoic ice age. Earth-Science Reviews 154, 279–300. doi:10.1016/j.earscirev.2016.01.007.

Ivanov, A.V., Demonterova, E.I., Gladkochub, D.P., Donskaya, T.V., 2014. The Tuva–Mongolia Massif and the Siberian Craton – are they the same? A comment on 'Age and provenance of the Ergunahe Group and the Wubinaobao Formation, northeastern Inner Mongolia, NE China: implications for tectonic setting of the Erguna Massif' by Zhang et al. International Geology Review 56, 954–958. doi:10.1080/00206814.2014.905999.

Jacobs, J., Elburg, M., Läufer, A., Kleinhanns, I.C., Henjes-Kunst, F., Estrada, S., Ruppel, A.S., Damaske, D., Montero, P., Bea, F., 2015. Two distinct Late Mesoproterozoic/Early Neoproterozoic basement provinces in central/eastern Dronning Maud Land, East Antarctica: The missing link, 15–21°E. Precambrian Research 265, 249–272. doi:10.1016/j.precamres.2015.05.003.

Janoušek, V., Jiang, Y., Buriánek, D., Schulmann, K., Hanžl, P., Soejono, I., Kröner, A., Altanbaatar, B., Erban, V., Lexa, O., Ganchuluun, T., Košler, J., 2018. Cambrian–Ordovician magmatism of the Ikh-Mongol Arc System exemplified by the Khantaishir Magmatic Complex (Lake Zone, south–central Mongolia). Gondwana Research 54, 122–149. doi:10.1016/j.gr.2017.10.003.

Jelsma, H.A., McCourt, S., Perritt, S.H., Armstrong, R.A., 2018. The geology and evolution of the Angolan Shield, Congo Craton, in: Regional Geology Reviews. Springer International Publishing, pp. 217–239. doi:10.1007/978-3-319-68920-3_9.

Jessop, K., Daczko, N.R., Piazolo, S., 2019. Tectonic cycles of the New England Orogen, eastern Australia: A Review. Australian Journal of Earth Sciences 66, 459–496. doi:10.1080/08120099.2018.1548378.

Johansson, Å., 2009. Baltica, Amazonia and the SAMBA connection–1000 million years of neighbourhood during the Proterozoic? Precambrian Research 175, 221–234. doi:10.1016/j.precamres.2009.09.011.

Johansson, Å., Bingen, B., Huhma, H., Waight, T., Vestergaard, R., Soesoo, A., Skridlaite, G., Krzeminska, E., Shumlyanskyy, L., Holland, M.E., Holm-Denoma, C., Teixeira, W., Faleiros, F.M., Ribeiro, B.V., Jacobs, J., Wang, C., Thomas, R.J., Macey, P.H., Kirkland, C.L., Hartnady, M.I., Eglington, B.M., Puetz, S.J., Condie, K.C., 2022. A geochronological review of magmatism along the external margin of Columbia and in the Grenville-age orogens

forming the core of Rodinia. Precambrian Research , 106463doi:10.1016/j.precamres.2021.106463.

Johansson, L., Zahirovic, S., Müller, R.D., 2018. The interplay between the eruption and weathering of large igneous provinces and the deep-time carbon cycle. Geophysical Research Letters 45, 5380–5389. doi:10.1029/2017gl076691.

Johnson, P., Andresen, A., Collins, A., Fowler, A., Fritz, H., Ghebreab, W., Kusky, T., Stern, R., 2011. Late Cryogenian–Ediacaran history of the Arabian–Nubian Shield: A review of depositional, plutonic, structural, and tectonic events in the closing stages of the northern East African Orogen. Journal of African Earth Sciences 61, 167–232. doi:10.1016/j.jafrearsci.2011.07.003.

Johnson, P.R., 2014. An expanding Arabian-Nubian Shield geochronologic and isotopic dataset: Defining limits and confirming the tectonic setting of a Neoproterozoic accretionary orogen. The Open Geology Journal 8, 3–33. URL: https://doi.org/10.2174%2F1874262901408010003, doi:10.2174/1874262901408010003.

Johnson, S.P., Thorne, A.M., Tyler, I.M., Korsch, R.J., Kennett, B.L.N., Cutten, H.N., Goodwin, J., Blay, O., Blewett, R.S., Joly, A., Dentith, M.C., Aitken, A.R.A., Holzschuh, J., Salmon, M., Reading, A., Heinson, G., Boren, G., Ross, J., Costelloe, R.D., Fomin, T., 2013. Crustal architecture of the Capricorn Orogen, Western Australia and associated metallogeny. Australian Journal of Earth Sciences 60, 681–705. doi:10.1080/08120099.2013.826735.

Jordan, T.A., Riley, T.R., Siddoway, C.S., 2020. The geological history and evolution of West Antarctica. Nature Reviews Earth & Environment 1, 117–133. doi:10.1038/s43017-019-0013-6.

Juliani, C., de Assis, R.R., Monteiro, L.V.S., Fernandes, C.M.D., da Silva Martins, J.E.Z., e Costa, J.R.C., 2021. Gold in Paleoproterozoic (2.1 to 1.77 Ga) Continental Magmatic Arcs at the Tapajós and Juruena Mineral Provinces (Amazonian Craton, Brazil): A New Frontier for the Exploration of Epithermal–Porphyry and Related Deposits. Minerals 11, 714. doi:10.3390/min11070714.

Karlstrom, K.E., Åhäll, K.I., Harlan, S.S., Williams, M.L., McLelland, J., Geissman, J.W., 2001. Long-lived (1.8–1.0 Ga) convergent orogen in southern Laurentia, its extensions to Australia and Baltica, and implications for refining Rodinia. Precambrian Research 111, 5–30. doi:10.1016/s0301-9268(01)00154-1.

Kazmi, A., Rana, R., 1982. Tectonic map of Pakistan. Technical Report. Geological Survey of Pakistan.

King, R., Floyd, M., Reilinger, R., Bendick, R., 2017. GPS velocity field (MIT 2016.0a) for the East African Rift System generated by King et al. doi:10.1594/IEDA/321764.

Kirkland, C., Smithies, R., Spaggiari, C., Wingate, M., de Gromard, R.Q., Clark, C., Gardiner, N., Belousova, E., 2017. Proterozoic crustal evolution of the Eucla basement, Australia: Implications for destruction of oceanic crust during emergence of Nuna. Lithos 278-281, 427–444. doi:10.1016/j.lithos.2017.01.029.

Kirscher, U., Mitchell, R.N., Liu, Y., Nordsvan, A.R., Cox, G.M., Pisarevsky, S.A., Wang, C., Wu, L., Murphy, J.B., Li, Z.X., 2020. Paleomagnetic constraints on the duration of the Australia-Laurentia connection in the core of the Nuna supercontinent. Geology 49, 174–179. doi:10.1130/g47823.1.

Klaver, M., de Roever, E.W., Nanne, J.A., Mason, P.R., Davies, G.R., 2015. Charnockites and UHT metamorphism in the Bakhuis Granulite Belt, western Suriname: Evidence for two separate UHT events. Precambrian Research 262, 1–19. doi:10.1016/j.precamres.2015.02.014.

Kleinhanns, I.C., Fullgraf, T., Wilsky, F., Nolte, N., Fliegel, D., Klemd, R., Hansen, B.T., 2013. U–Pb zircon ages and (isotope) geochemical signatures of the Kamanjab Inlier (NW Namibia): constraints on Palaeoproterozoic crustal evolution along the southern Congo craton. Geological Society, London, Special Publications 389, 165–195. doi:10.1144/sp389.1.

Klett, T.R., Ahlbrandt, T.S., Schmoker, J.W., Dolton, G.L., 1997. Ranking of the world's oil and gas provinces by known petroleum volumes. Open-File Report 97-463. US Geological Survey. Http://pubs.usgs.gov/of/1997/ofr-97-463/97463.html.

Klier, J.J., 2019. The Marshfield terrane : redefinition of origin through zircon geochronology and geochemistry. Master's thesis. Ball State University. Wisconsin.

Korhonen, F., Saw, A., Clark, C., Brown, M., Bhattacharya, S., 2011. New constraints on UHT metamorphism in the Eastern Ghats Province through the application of phase equilibria modelling and in situ geochronology. Gondwana Research 20, 764–781. doi:10.1016/j.gr.2011.05.006.

Kozlov, P., Likhanov, I., Reverdatto, V., Zinoviev, S., 2012. Tectonometamorphic evolution of the Garevka polymetamorphic complex (Yenisei Ridge). Russian Geology and Geophysics 53, 1133–1149. doi:10.1016/j.rgg.2012.09.002.

Kranendonk, M.J.V., Kirkland, C.L., 2013. Orogenic climax of Earth: The 1.2-1.1 Ga Grenvillian superevent. Geology 41, 735–738. doi:10.1130/g34243.1.

Kreemer, C., Blewitt, G., Klein, E.C., 2014. A geodetic plate motion and Global Strain Rate Model. Geochemistry, Geophysics, Geosystems 15, 3849–3889. doi:10.1002/2014gc005407.

Kröner, A., 1980. Pan African crustal evolution. Episodes 3, 3–8. doi:10.18814/epiiugs/1980/v3i2/001.

Kuhnt, W., Holbourn, A., Hall, R., Zuvela, M., Käse, R., 2004. Neogene history of the Indonesian throughflow, in: Continent-Ocean Interactions Within East Asian Marginal Seas. American Geophysical Union, pp. 299–320. doi:10.1029/149gm16.

Kusky, T.M., Windley, B.F., Zhai, M.G., 2007. Tectonic evolution of the North China Block: from orogen to craton to orogen. Geological Society, London, Special Publications 280, 1–34. doi:10.1144/sp280.1.

Kuzmichev, A.B., Sklyarov, E.V., 2016. The precambrian of transangaria, yenisei ridge (siberia): Neoproterozoic microcontinent, grenville-age orogen, or reworked margin of the siberian craton? Journal of Asian Earth Sciences 115, 419–441. doi:10.1016/j.jseaes.2015.10.017.

Kwékam, M., Talla, V., Fozing, E.M., Kouémo, J.T., Dunkl, I., Njonfang, E., 2020. The pan-african high-k i-type granites from batié complex, west cameroon: Age, origin, and tectonic implications. Frontiers in Earth Science 8. doi:10.3389/feart.2020.00363.

van de Lagemaat, S.H., Swart, M.L., Vaes, B., Kosters, M.E., Boschman, L.M., Burton-Johnson, A., Bijl, P.K., Spakman, W., van Hinsbergen, D.J., 2021. Subduction initiation in the Scotia Sea region and opening of the Drake Passage: When and why? Earth-Science Reviews 215, 103551. doi:10.1016/j.earscirev.2021.103551.

Langmuir, C., Bézos, A., Escrig, S., Parman, S., 2006. Chemical systematics and hydrous melting of the mantle in back-arc basins, in: Christie, D., Fisher, C., Lee, S.M., Givens, S. (Eds.), Back-Arc Spreading Systems: Geological, Biological, Chemical, and Physical Interactions. Am. Geophys. Un.. volume 166 of *Geophys. Monogr.*, pp. 87–146. doi:10.1029/166GM07.

Laske, G., Masters, G., 1997. A global digital map of sediment thickness. EOS Trans. AGU 78, F483.

Laske, G., Masters, G., Ma, Z., Pasyanos, M., 2013. Update on CRUST1.0 - A 1-degree Global Model of Earth's Crust, in: Geophys. Res. Abstracts. European Geophysical Union. volume 15, pp. EGU2013–2658.

Leitchenkov, G.L., Antonov, A.V., Luneov, P.I., Lipenkov, V.Y., 2016. Geology and environments of subglacial Lake Vostok. Philosophical Transactions of the Royal Society A: Mathematical, Physical and Engineering Sciences 374, 20140302. doi:10.1098/rsta.2014.0302.

Lepvrier, C., Maluski, H., Tich, V.V., Leyreloup, A., Thi, P.T., Vuong, N.V., 2004. The Early Triassic Indosinian orogeny in Vietnam (Truong Son Belt and Kontum Massif): implications for the geodynamic evolution of Indochina. Tectonophysics 393, 87–118. doi:10.1016/j.tecto.2004.07.030.

Lesur, V., Hamoudi, M., Choi, Y., Dyment, J., Thébault, E., 2016. Building the second version of the world digital magnetic anomaly map (WDMAM). Earth, Planets and Space 68. doi:10.1186/s40623-016-0404-6.

Li, B., Massonne, H.J., Hartmann, L.A., Zhang, J., Luo, T., 2021. Kyanite-garnet granulite from the andrelândia nappe system, brasília belt, registers two late neoproterozoic metamorphic cycles. Precambrian Research 355, 106086. doi:10.1016/j.precamres.2020.106086.

Li, J., yan Cai, W., yong Wang, K., Kim, N., lun Liu, H., Lee, G.J., Yoo, B.C., 2019. Initial decratonization of the eastern North China Craton: New constraints from geochronology, geochemistry, and Hf isotopic compositions of Mesozoic igneous rocks in the Qingchengzi district. Geological Journal 55, 3796–3820. doi:10.1002/gj.3635.

Li, S.S., Santosh, M., Palin, R.M., 2018. Metamorphism during the Archean–Paleoproterozoic Transition Associated with Microblock Amalgamation in the Dharwar Craton, India. Journal of Petrology 59, 2435–2462. doi:10.1093/petrology/egy102.

Li, Z., Bogdanova, S., Collins, A., Davidson, A., Waele, B.D., Ernst, R., Fitzsimons, I., Fuck, R., Gladkochub, D., Jacobs, J., Karlstrom, K., Lu, S., Natapov, L., Pease, V., Pisarevsky, S., Thrane, K., Vernikovsky, V., 2008. Assembly, configuration, and break-up history of Rodinia: A synthesis. Precambrian Research 160, 179–210. doi:10.1016/j.precamres.2007.04.021.

Liégeois, J.P., 2018. A new synthetic geological map of the Tuareg Shield: An overview of Its global structure and geological evolution, in: The Geology of the Arab World—An Overview. Springer International Publishing, pp. 83–107. doi:10.1007/978-3-319-96794-3_2.

Liégeois, J.P., Abdelsalam, M.G., Ennih, N., Ouabadi, A., 2013. Metacraton: Nature, genesis and behavior. Gondwana Research 23, 220–237. doi:10.1016/j.gr.2012.02.016.

Linde, G.M., Trexler, J.H., Cashman, P.H., Gehrels, G., Dickinson, W.R., 2017. Three-dimensional evolution of the early Paleozoic western Laurentian margin: New insights from detrital zircon U-Pb geochronology and Hf isotope geochemistry of the Harmony Formation of Nevada. Tectonics 36, 2347–2369. doi:10.1002/2017tc004520.

Lister, G.S., Forster, M.A., Rawling, T.J., 2001. Episodicity during orogenesis. Geological Society, London, Special Publications 184, 89–113. doi:10.1144/gsl.sp.2001.184.01.06.

Liu, F., Zhang, J., Liu, C., 2017. Archean to Paleoproterozoic Evolution of the North China Craton: Preface. Precambrian Research 303, 1–9. doi:10.1016/j.precamres.2017.11.011.

Liu, M., Shen, Y., 1998. Sierra Nevada uplift: A ductile link to mantle upwelling under the Basin and Range province. Geology 26, 299–302. doi:10.1130/0091-7613(1998)026<0299:snuadl>2.3.co;2.

Liu, X., m. Jahn, B., Zhao, Y., Liu, J., Ren, L., 2014. Geochemistry and geochronology of Mesoproterozoic basement rocks from the Eastern Amery Ice Shelf and southwestern Prydz Bay, East Antarctica: Implications for a long-lived magmatic accretion in a continental arc. American Journal of Science 314, 508–547. doi:10.2475/02.2014.03.

Liu, Y., Mitchell, R.N., Li, Z.X., Kirscher, U., Pisarevsky, S.A., Wang, C., 2021. Archean geodynamics: Ephemeral supercontinents or long-lived supercratons. Geology doi:10.1130/g48575.1.

Llubes, M., Seoane, L., Bruinsma, S., Rémy, F., 2018. Crustal thickness of Antarctica estimated using data from gravimetric satellites. Solid Earth 9, 457–467. doi:10.5194/se-9-457-2018.

Loose, D., Schenk, V., 2018. 2.09 Ga old eclogites in the Eburnian-Transamazonian orogen of southern Cameroon: Significance for Palaeoproterozoic plate tectonics. Precambrian Research 304, 1–11. doi:10.1016/j.precamres.2017.10.018.

Lowman, P., Yates, J., 2002. Digital tectonic activity map. NASA Goddard Space Flight Center, http://denali.gsfc.nasa.gov/dtam/.

Lucazeau, F., 2019. Analysis and mapping of an updated terrestrial heat flow dataset. Geochemistry, Geophysics, Geosystems doi:10.1029/2019gc008389.

Lund, K., Box, S.E., Holm-Denoma, C.S., Juan, C.A.S., Blakely, R.J., Saltus, R.W., Anderson, E.D., DeWitt, E., 2015. Basement domain map of the conterminous United States and Alaska. Data Series 898. U.S. Geological Survey. URL: https://doi.org/10.3133%2Fds898, doi:10.3133/ds898.

Makkonen, H.V., , and, P.T., 2020. Geology and crystallization conditions of the särkiniemiintrusion and related nickel-copper ore, central finland – implications for depth of emplacement of 1.88 ga nickel-bearing intrusions. Bulletin of the Geological Society of Finland 92, 111–130. doi:10.17741/bgsf/92.2.003.

Mako, C.A., Williams, M.L., Karlstrom, K.E., Doe, M.F., Powicki, D., Holland, M.E., Gehrels, G., Pecha, M., 2015. Polyphase proterozoic deformation in the four peaks area, central arizona, and relevance for the mazatzal orogeny. Geosphere 11, 1975–1995. doi:10.1130/ges01196.1.

Maritati, A., Aitken, A.R.A., Young, D.A., Roberts, J.L., Blankenship, D.D., Siegert, M.J., 2016. The tectonic development and erosion of the Knox Subglacial Sedimentary Basin, East Antarctica. Geophysical Research Letters 43, 10,728–10,737. doi:10.1002/2016gl071063.

Maritati, A., Halpin, J.A., Whittaker, J.M., Daczko, N.R., 2019. Fingerprinting Proterozoic bedrock in interior Wilkes Land, East Antarctica. Scientific Reports 9. doi:10.1038/s41598-019-46612-y.

Marques, F., Catalão, J., DeMets, C., Costa, A., Hildenbrand, A., 2013. GPS and tectonic evidence for a diffuse plate boundary at the Azores Triple Junction. Earth and Planetary Science Letters 381, 177–187. doi:10.1016/j.epsl.2013.08.051.

Matte, P., 2001. The Variscan collage and orogeny (480-290 Ma) and the tectonic definition of the Armorica microplate: a review. Terra Nova 13, 122–128. doi:10.1046/j.1365-3121.2001.00327.x.

Matthews, K.J., Maloney, K.T., Zahirovic, S., Williams, S.E., Seton, M., Müller, R.D., 2016. Global plate boundary evolution and kinematics since the late Paleozoic. Global and Planetary Change 146, 226–250. doi:10.1016/j.gloplacha.2016.10.002.

McClusky, S., Reilinger, R., Ogubazghi, G., Amleson, A., Healeb, B., Vernant, P., Sholan, J., Fisseha, S., Asfaw, L., Bendick, R., Kogan, L., 2010. Kinematics of the southern Red Sea-Afar Triple Junction and implications for plate dynamics. Geophysical Research Letters 37, L05301. doi:10.1029/2009gl041127.

McCourt, S., Armstrong, R.A., Jelsma, H., Mapeo, R.B.M., 2013. New U–Pb SHRIMP ages from the Lubango region, SW Angola: insights into the Palaeoproterozoic evolution of the Angolan Shield, southern Congo Craton, Africa. Journal of the Geological Society 170, 353–363. URL: https://doi.org/10.1144%2Fjgs2012-059, doi:10.1144/jgs2012-059.

McKerrow, W.S., MacNiocaill, C., Dewey, J.F., 2000. The Caledonian Orogeny redefined. Journal of the Geological Society 157, 1149–1154. doi:10.1144/jgs.157.6.1149.

Medaris, L.G., Singer, B.S., Jicha, B.R., Malone, D.H., Schwartz, J.J., Stewart, E.K., Lankvelt, A.V., Williams, M.L., Reiners, P.W., 2021. Early Mesoproterozoic evolution of midcontinental Laurentia: Defining the geon 14 Baraboo orogeny. Geoscience Frontiers 12, 101174. doi:10.1016/j.gsf.2021.101174.

Meert, J.G., Lieberman, B.S., 2008. The Neoproterozoic assembly of Gondwana and its relationship to the Ediacaran–Cambrian radiation. Gondwana Research 14, 5–21. doi:10.1016/j.gr.2007.06.007.

Meert, J.G., Santosh, M., 2017. The Columbia supercontinent revisited. Gondwana Research 50, 67–83. doi:10.1016/j.gr.2017.04.011.

Meert, J.G., Voo, R.V.D., 1997. The assembly of Gondwana 800-550 Ma. Journal of Geodynamics 23, 223–235. doi:10.1016/s0264-3707(96)00046-4.

Merdith, A.S., Williams, S.E., Collins, A.S., Tetley, M.G., Mulder, J.A., Blades, M.L., Young, A., Armistead, S.E., Cannon, J., Zahirovic, S., Müller, R.D., 2021. Extending full-plate tectonic models into deep time: Linking the Neoproterozoic and the Phanerozoic. Earth-Science Reviews 214, 103477. doi:10.1016/j.earscirev.2020.103477.

Meyer, B., Saltus, R., 2016. Emag2: Earth magnetic anomaly grid (2-arc-minute resolution) version 3. doi:10.7289/v5h70cvx.

MIkkola, P., Mönkäre, K., Ahven, M., Huhma, H., 2018. Geochemistry and age of the paleoproterozoic makkola suite volcanic rocks in central finland. Development of the Paleoproterozoic Svecofennian orogeny: new constraints from the southeastern boundary of the Central Finland Granitoid Complex , 85–105doi:10.30440/bt407.5.

Mitchell, A., Chung, S.L., Oo, T., Lin, T.H., Hung, C.H., 2012. Zircon U–Pb ages in Myanmar: Magmatic–metamorphic events and the closure of a neo-Tethys ocean? Journal of Asian Earth Sciences 56, 1–23. doi:10.1016/j.jseaes.2012.04.019.

Morley, C., Ampaiwan, P., Thanudamrong, S., Kuenphan, N., Warren, J., 2013. Development of the Khao Khwang Fold and Thrust Belt: Implications for the geodynamic setting of Thailand and Cambodia during the Indosinian Orogeny. Journal of Asian Earth Sciences 62, 705–719. doi:10.1016/j.jseaes.2012.11.021.

Morley, C.K., Searle, M., 2017. Chapter 5 Regional tectonics, structure and evolution of the Andaman–Nicobar Islands from ophiolite formation and obduction to collision and back-arc spreading. Geological Society, London, Memoirs 47, 51–74. doi:10.1144/m47.5.

Morrissey, L., Payne, J.L., Kelsey, D.E., Hand, M., 2011. Grenvillian-aged reworking in the North Australian Craton, central Australia: Constraints from geochronology and modelled phase equilibria. Precambrian Research 191, 141–165. doi:10.1016/j.precamres.2011.09.010.

Morrissey, L.J., Barovich, K.M., Hand, M., Howard, K.E., Payne, J.L., 2019. Magmatism and metamorphism at ca. 1.45 Ga in the northern Gawler Craton: The Australian record of rifting within Nuna (Columbia). Geoscience Frontiers 10, 175–194. doi:10.1016/j.gsf.2018.07.006.

Morrissey, L.J., Hand, M., Kelsey, D.E., 2015. Multi-stage metamorphism in the Rayner–Eastern Ghats Terrane: P–T– constraints from the northern Prince Charles Mountains, east Antarctica. Precambrian Research 267, 137–163. doi:10.1016/j.precamres.2015.06.003.

Morrissey, L.J., Hand, M., Kelsey, D.E., 2017. A curious case of agreement between conventional thermobarometry and phase equilibria modelling in granulites: New constraints *P-T* estimates in the Antarctica segment of the Musgrave-Albany-Fraser-Wilkes Orogen. Journal of Metamorphic Geology 35, 1023–1050. doi:10.1111/jmg.12266.

Mortimer, N., 2004. New Zealand's Geological Foundations. Gondwana Research 7, 261–272. doi:10.1016/s1342-937x(05)70324-5.

Mulder, J.A., Halpin, J.A., Daczko, N.R., Orth, K., Meffre, S., Thompson, J.M., Morrissey, L.J., 2019. A Multiproxy provenance approach to uncovering the assembly of East Gondwana in Antarctica. Geology 47, 645–649. doi:10.1130/g45952.1.

Mulder, J.A., Karlstrom, K.E., Halpin, J.A., Merdith, A.S., Spencer, C.J., Berry, R.F., McDonald, B., 2018. Rodinian devil in disguise: Correlation of 1.25–1.10 Ga strata between Tasmania and Grand Canyon. Geology 46, 991–994. doi:10.1130/g45225.1.

Muttoni, G., Kent, D.V., Garzanti, E., Brack, P., Abrahamsen, N., Gaetani, M., 2003. Early Permian Pangea 'B' to Late Permian Pangea 'A'. Earth and Planetary Science Letters 215, 379–394. doi:10.1016/s0012-821x(03)00452-7.

Naimi-Ghassabian, N., Khatib, M.M., Nazari, H., Heyhat, M.R., 2018. Regional variations and earthquake frequency–magnitude distribution and fractal dimension in the North of Central-East Iran Blocks (NCEIB). Arabian Journal of Geosciences 11. doi:10.1007/s12517-018-3506-6.

Nance, R.D., Gutiérrez-Alonso, G., Keppie, J.D., Linnemann, U., Murphy, J.B., Quesada, C., Strachan, R.A., Woodcock, N.H., 2012. A brief history of the Rheic Ocean. Geoscience Frontiers 3, 125–135. doi:10.1016/j.gsf.2011.11.008.

Nedel, I.M., Fuck, R.A., Ruiz, A.S., Matos, R., Ferreira, A.C.D., 2020. U–Pb geochronology and geochemistry of Grenville-age plutons in the Sunsas Belt - Bolivia, SW Amazonian Craton: Tectonic and magmatic implications. Journal of South American Earth Sciences 104, 102845. doi:10.1016/j.jsames.2020.102845.

Neill, I., Kerr, A.C., Hastie, A.R., Stanek, K.P., Millar, I.L., 2011. Origin of the Aves Ridge and Dutch–Venezuelan Antilles: interaction of the Cretaceous 'Great Arc' and Caribbean–Colombian Oceanic Plateau? Journal of the Geological Society 168, 333–348. doi:10.1144/0016-76492010-067.

Nixon, A., Glorie, S., Collins, A., Blades, M., Simpson, A., Whelan, J., 2022. Inter-cratonic geochronological and geochemical correlations of the Derim Derim–Galiwinku/Yanliao reconstructed Large Igneous Province across the North Australian and North China cratons. Gondwana Research 103, 473–486. doi:10.1016/j.gr.2021.10.027.

O'Donnell, J., Stuart, G., Brisbourne, A., Selway, K., Yang, Y., Nield, G., Whitehouse, P., Nyblade, A., Wiens, D., Aster, R., Anandakrishnan, S., Huerta, A., Wilson, T., Winberry, J., 2019. The uppermost mantle seismic velocity structure of West Antarctica from Rayleigh wave tomography: Insights into tectonic structure and geothermal heat flow. Earth and Planetary Science Letters 522, 219–233. doi:10.1016/j.epsl.2019.06.024.

Ontario Geological Survey, 2011. 1: 250 000 Scale Bedrock Geology of Ontario-Revision 1. Miscellaneous Release - Data MRD 126-REV-1. Ontario Geological Survey.

Oxman, V.S., 2003. Tectonic evolution of the Mesozoic Verkhoyansk–Kolyma belt (NE Asia). Tectonophysics 365, 45–76. doi:10.1016/s0040-1951(03)00064-7.

Pant, N.C., Dasgupta, S., 2017. An introduction to the crustal evolution of India and Antarctica: the supercontinent connection. Geological Society, London, Special Publications 457, 1–6. doi:10.1144/sp457.14.

Paulsen, T., Encarnación, J., Grunow, A.M., Valencia, V.A., Pecha, M.E., Benowitz, J., Layer, P., 2020. New ages from the Shackleton Glacier area and their context in the regional tectonomagmatic evolution of the Ross orogen of Antarctica. International Geology Review 63, 1596–1618. doi:10.1080/00206814.2020.1786737.

Pawlewicz, M.J., Steinshouer, D.W., Gautier, D.L., 1997. Map showing geology, oil and gas fields, and geologic provinces of Europe including Turkey. Open-file Report 97-470I. US Geological Survey. doi:10.3133/ofr97470i.

Pawley, M.J., Dutch, R.A., Wise, T.W., 2020. The relationship between crustal architecture, deformation, and magmatism in the Coompana Province, Australia. Tectonics 39. doi:10.1029/2019tc005593.

Payne, J.L., Hand, M., Barovich, K.M., Reid, A., Evans, D.A.D., 2009. Correlations and reconstruction models for the 2500-1500 Ma evolution of the Mawson Continent. Geological Society, London, Special Publications 323, 319–355. doi:10.1144/sp323.16.

Payne, J.L., Morrissey, L.J., Tucker, N.M., Roche, L.K., Szpunar, M.A., Neroni, R., 2021. Granites and gabbros at the dawn of a coherent Australian continent. Precambrian Research 359, 106189. doi:10.1016/j.precamres.2021.106189.

Pease, V., 2021. Eastern Europe: The Timanian and Uralian Orogens, in: Encyclopedia of Geology. Elsevier, pp. 302–310. doi:10.1016/b978-0-08-102908-4.00028-x.

Pehrsson, S.J., Berman, R.G., Eglington, B., Rainbird, R., 2013. Two Neoarchean supercontinents revisited: The case for a Rae family of cratons. Precambrian Research 232, 27–43. doi:10.1016/j.precamres.2013.02.005.

Pehrsson, S.J., Buchan, K.L., Eglington, B.M., Berman, R.M., Rainbird, R.H., 2014. Did plate tectonics shutdown in the Palaeoproterozoic? A view from the Siderian geologic record. Gondwana Research 26, 803–815. doi:10.1016/j.gr.2014.06.001.

Pelletier, J., Broxton, P., Hazenberg, P., Zeng, X., Troch, P., Niu, G., Williams, Z., Brunke, M., Gochis, D., 2016. Global 1-km Gridded Thickness of Soil, Regolith, and Sedimentary Deposit Layers. doi:10.3334/ORNLDAAC/1304.

Peron-Pinvidic, G., Gernigon, L., Gaina, C., Ball, P., 2012. Insights from the Jan Mayen system in the Norwegian-Greenland sea-I. Mapping of a microcontinent. Geophysical Journal International 191, 385–412. doi:10.1111/j.1365-246x.2012.05639.x.

Persits, F., Ahlbrandt, T.S., Tuttle, M.L., Charpentier, R.R., Brownfield, M.E., Takahashi, K.I., 1997a. Maps showing geology, oil and gas fields and geological provinces of Africa. Open-file Report 97-470A. US Geological Survey. doi:10.3133/ofr97470a.

Persits, F., Ulmishek, G., Steinshouer, D., 1997b. Maps showing geology, oil and gas fields and geologic provinces of the former Soviet Union. Open-file Report 97-470E. US Geological Survey. doi:10.3133/ofr97470e.

Pesonen, L., Mertanen, S., Veikkolainen, T., 2012. Paleo-Mesoproterozoic Supercontinents — A Paleomagnetic View. Geophysica 48, 5–47.

Peucat, J., Ménot, R., Monnier, O., Fanning, C., 1999. The Terre Adélie basement in the East-Antarctica Shield: geological and isotopic evidence for a major 1.7Ga thermal event: comparison with the Gawler Craton in South Australia. Precambrian Research 94, 205–224. doi:10.1016/s0301-9268(98)00119-3.

Peucat, J.J., Barbosa, J.S.F., de Araújo Pinho, I.C., Paquette, J.L., Martin, H., Fanning, C.M., de Menezes Leal, A.B., Cruz, S., 2011. Geochronology of granulites from the south Itabuna-Salvador-Curaçá Block, São Francisco Craton (Brazil): Nd isotopes and U–Pb zircon ages. Journal of South American Earth Sciences 31, 397–413. doi:10.1016/j.jsames.2011.03.009.

Phillips, G., Kelsey, D.E., Corvino, A.F., Dutch, R.A., 2009. Continental reworking during overprinting orogenic events, southern Prince Charles Mountains, East Antarctica. Journal of Petrology 50, 2017–2041. doi:10.1093/petrology/egp065.

Pierce, E., Hemming, S., Williams, T., van de Flierdt, T., Thomson, S., Reiners, P., Gehrels, G., Brachfeld, S., Goldstein, S., 2014. A comparison of detrital U–Pb zircon, 40Ar/39Ar hornblende, 40Ar/39Ar biotite ages in marine sediments off East Antarctica: Implications for the geology of subglacial terrains and provenance studies. Earth-Science Reviews 138, 156–178. doi:10.1016/j.earscirev.2014.08.010.

Pilia, S., Rawlinson, N., Cayley, R.A., Bodin, T., Musgrave, R., Reading, A.M., Direen, N.G., Young, M.K., 2015. Evidence of micro-continent entrainment during crustal accretion. Scientific Reports 5. doi:10.1038/srep08218.

Pisarevsky, S.A., Elming, S.Å., Pesonen, L.J., Li, Z.X., 2014. Mesoproterozoic paleogeography: Supercontinent and beyond. Precambrian Research 244, 207–225. doi:10.1016/j.precamres.2013.05.014.

Pisarevsky, S.A., Wingate, M.T.D., Harris, L.B., 2003. Late Mesoproterozoic (ca1.2 Ga) palaeomagnetism of the Albany-Fraser orogen: no pre-Rodinia Australia-Laurentia connection. Geophysical Journal International 155, F6–F11. doi:10.1046/j.1365-246x.2003.02074.x.

Pollastro, R., Persits, F., Steinshouer, D., 1997. Maps showing geology, oil and gas fields, and geologic provinces of Iran. Open-file report. US Geological Survey. doi:10.3133/ofr97470g. 97-470G.

Pollastro, R.M., Karshbaum, A.S., Viger, R.J., 1999. Maps showing geology, oil and gas fields and geologic provinces of the Arabian Peninsula. Open-file Report 97-470B. US Geological Survey. doi:10.3133/ofr97470b.

Pourteau, A., Smit, M.A., Li, Z.X., Collins, W.J., Nordsvan, A.R., Volante, S., Li, J., 2018. 1.6 Ga crustal thickening along the final Nuna suture. Geology 46, 959–962. doi:10.1130/g45198.1.

Profeta, L., Ducea, M.N., Chapman, J.B., Paterson, S.R., Gonzales, S.M.H., Kirsch, M., Petrescu, L., DeCelles, P.G., 2015. Quantifying crustal thickness over time in magmatic arcs. Scientific Reports 5. doi:10.1038/srep17786.

Puetz, S.J., 2018. A relational database of global U–Pb ages. Geoscience Frontiers 9, 877–891. doi:10.1016/j.gsf.2017.12.004.

Pyle, D.G., Christie, D.M., Mahoney, J.J., 1992. Resolving an isotopic boundary within the Australian-Antarctic discordance. Earth and Planetary Science Letters 112, 161–178. doi:10.1016/0012-821x(92)90014-m.

Ramos, V., Aleman, A., 2000. Tectonic evolution of the Andes, in: Cordani, U., Milani, E., Filho, T., Campos, A. (Eds.), Tectonic Evolution of South America. Geological Survey of Brazil, pp. 635–685.

Rathnayake, S., Tenzer, R., Eshagh, M., Pitoňák, M., 2019. Gravity maps of the lithospheric structure beneath the Indian Ocean. Surveys in Geophysics 40, 1055–1093. doi:10.1007/s10712-019-09564-6.

Robertson, A.H.F., Ustaömer, T., Pickett, E.A., Collins, A.S., Andrew, T., Dixon, J.E., 2004. Testing models of Late Palaeozoic–Early Mesozoic orogeny in Western Turkey: support for an evolving open-Tethys model. Journal of the Geological Society 161, 501–511. doi:10.1144/0016-764903-080.

Roest, W.R., Collette, B.J., 1986. The Fifteen Twenty Fracture Zone and the North American–South American plate boundary. Journal of the Geological Society 143, 833–843. doi:10.1144/gsjgs.143.5.0833.

da Rosa-Costa, L.T., Lafon, J.M., Cocherie, A., Delor, C., 2008. Electron microprobe u–th–pb monazite dating of the transamazonian metamorphic overprint on archean rocks from the amapá block, southeastern guiana shield, northern brazil. Journal of South American Earth Sciences 26, 445–462. doi:10.1016/j.jsames.2008.05.007.

Royer, J., Gordon, R., 1997. The motion and boundary between the Capricorn and Australian Plates. Science 277, 1268–1274. doi:10.1126/science.277.5330.1268.

Rubin, K., 2016. Mid-ocean Ridge Magmatism and Volcanism, in: Harff, J., Meschede, M., Petersen, S., Thiede, J. (Eds.), Encyclopedia of Marine Geosciences. Springer Netherlands, pp. 1–28. doi:10.1007/978-94-007-6238-1_28.

Ruppel, A.S., Jacobs, J., Läufer, A., Ratschbacher, L., Pfänder, J.A., Sonntag, B.L., Krasniqi, K., Elburg, M., Krohne, N., Damaske, D., Lisker, F., 2020. Protracted late Neoproterozic – early Palaeozoic deformation and cooling history of Sør Rondane, East Antarctica, from 40Ar/39Ar and U–Pb geochronology. Geological Magazine 158, 635–655. doi:10.1017/s0016756820000746.

Rusmore, M.E., Bogue, S.W., Dodson, K., Farley, K.A., Woodsworth, G.J., 2010. Deformation of continental crust along a transform boundary, Coast Mountains, British Columbia. Tectonics 29, TC4007. doi:10.1029/2009tc002502.

Salminen, J., Pehrsson, S., Evans, D.A., Wang, C., 2021. Neoarchean–Paleoproterozoic supercycles, in: Ancient Supercontinents and the Paleogeography of Earth. Elsevier, pp. 465–498. doi:10.1016/b978-0-12-818533-9.00014-x.

Sanchez, G., Halpin, J.A., Gard, M., Hasterok, D., Stål, T., Raimondo, T., Peters, S., Burton-Johnson, A., 2021. PetroChron Antarctica: A geological database for interdisciplinary use. Geochemistry, Geophysics, Geosystems 22. doi:10.1029/2021gc010154.

Sandiford, M., Hand, M., McLaren, S., 2001. Tectonic feedback, intraplate orogeny and the geochemical structure of the crust: a central Australian perspective, in: Miller, J., Holdsworth, J., Buick, I., Hand, M. (Eds.), Continental Reactivation and Reworking. Geological Society of London. volume 184 of *Spec. Pub.*, pp. 195–218. doi:10.1144/gsl.sp.2001.184.01.10.

Santos, J., Rizzotto, G., Potter, P., McNaughton, N., Matos, R., Hartmann, L., Chemale, F., Quadros, M., 2008. Age and autochthonous evolution of the Sunsás Orogen in West Amazon Craton based on mapping and U–Pb geochronology. Precambrian Research 165, 120–152. doi:10.1016/j.precamres.2008.06.009.

Saria, E., Calais, E., Stamps, D.S., Delvaux, D., Hartnady, C.J.H., 2014. Present-day kinematics of the East African Rift. Journal of Geophysical Research: Solid Earth 119, 3584–3600. doi:10.1002/2013jb010901.

Savko, K.A., Samsonov, A.V., Sal'nikova, E.B., Kotov, A.B., Bazikov, N.S., 2015. HT/LP metamorphic zoning in the eastern voronezh crystalline massif: Age and parameters of metamorphism and its geodynamic environment. Petrology 23, 559–575. doi:10.1134/s0869591115050045.

Scheinert, M., Ferraccioli, F., Schwabe, J., Bell, R., Studinger, M., Damaske, D., Jokat, W., Aleshkova, N., Jordan, T., Leitchenkov, G., Blankenship, D.D., Damiani, T.M., Young, D., Cochran, J.R., Richter, T.D., 2016. New antarctic gravity anomaly grid for enhanced geodetic and geophysical studies in antarctica. Geophysical Research Letters 43, 600–610. doi:10.1002/2015gl067439.

Schenk, C.J., Viger, R.J., Anderson, C.P., 1999. Maps showing geology, oil and gas fields and geologic provinces of the South America region. Open-file Report 97-470D. US Geological Survey. doi:10.3133/ofr97470d.

Schepers, G., van Hinsbergen, D.J.J., Spakman, W., Kosters, M.E., Boschman, L.M., McQuarrie, N., 2017. South-American plate advance and forced Andean trench retreat as drivers for transient flat subduction episodes. Nature Communications 8. doi:10.1038/ncomms15249.

Schmid, S.M., Fügenschuh, B., Kounov, A., Maţenco, L., Nievergelt, P., Oberhänsli, R., Pleuger, J., Schefer, S., Schuster, R., Tomljenović, B., Ustaszewski, K., van Hinsbergen, D.J., 2020. Tectonic units of the Alpine collision zone between Eastern Alps and western Turkey. Gondwana Research 78, 308–374. doi:10.1016/j.gr.2019.07.005.

Schultz, M.E., Chacko, T., Heaman, L.M., Sandeman, H.A., Simonetti, A., Creaser, R.A., 2007. Queen Maud block: A newly recognized Paleoproterozoic (2.4–2.5 Ga) terrane in northwest Laurentia. Geology 35, 707. doi:10.1130/g23629a.1.

Schweickert, R., Lahren, M., Smith, K., Howle, J., Ichinose, G., 2004. Transtensional deformation in the Lake Tahoe region, California and Nevada, USA. Tectonophysics 392, 303–323. doi:10.1016/j.tecto.2004.04.019.

Scrimgeour, I.R., Kinny, P.D., Close, D.F., Edgoose, C.J., 2005. High-T granulites and polymetamorphism in the southern Arunta Region, central Australia: Evidence for a 1.64 Ga accretional event. Precambrian Research 142, 1–27. doi:10.1016/j.precamres.2005.08.005.

Sears, J.W., Price, R.A., 2003. Tightening the Siberian connection to western Laurentia. Geological Society of America Bulletin 115, 943–953. doi:10.1130/b25229.1.

Sedlock, R.L., Ortega-Gutiérrez, F., Speed, R.C., 1993. Tectonostratigraphic Terranes and Tectonic Evolution of Mexico. Geological Society of America. doi:10.1130/spe278.

Şengör, A.M.C., Lom, N., Zabcı, C., Sunal, G., Öner, T., 2020. Reconstructing orogens without biostratigraphy: The Saharides and continental growth during the final assembly of Gondwana-Land. Proceedings of the National Academy of Sciences 117, 32278–32284. doi:10.1073/pnas.2015117117.

Sengör, A.M.C., Natal'in, B.A., 1996. Turkik-type orogeny and its role in the making of the continental crust. Annual Review of Earth and Planetary Sciences 24, 263–337. doi:10.1146/annurev.earth.24.1.263.

Seton, M., Müller, R.D., Zahirovic, S., Williams, S., Wright, N.M., Cannon, J., Whittaker, J.M., Matthews, K.J., McGirr, R., 2020. A global data set of present-day oceanic crustal age and seafloor spreading parameters. Geochemistry, Geophysics, Geosystems 21. doi:10.1029/2020gc009214.

Sheppard, S., Occhipinti, S., Nelson, D., 2005. Intracontinental reworking in the Capricorn Orogen, Western Australia: the 1680–1620 Ma Mangaroon Orogeny. Australian Journal of Earth Sciences 52, 443–460. doi:10.1080/08120090500134589.

Sheppard, S., Rasmussen, B., Muhling, J.R., Farrell, T.R., Fletcher, I.R., 2007. Grenvillian-aged orogenesis in the Palaeoproterozoic Gascoyne Complex, Western Australia: 1030–950 Ma reworking of the Proterozoic Capricorn Orogen. Journal of Metamorphic Geology 25, 477–494. doi:10.1111/j.1525-1314.2007.00708.x.

Shi, X., Tapponnier, P., Wang, T., Wei, S., Wang, Y., Wang, X., Jiao, L., 2019. Triple junction kinematics accounts for the 2016 Mw7.8 Kaikoura earthquake rupture complexity. Proceedings of the National Academy of Sciences 116, 26367–26375. doi:10.1073/pnas.1916770116.

da Silva Schmitt, R., de Araújo Fragoso, R., Collins, A.S., 2018. Suturing Gondwana in the Cambrian: The orogenic events of the final amalgamation, in: Regional Geology Reviews. Springer International Publishing, pp. 411–432. doi:10.1007/978-3-319-68920-3_15.

Sobh, M., Ebbing, J., Mansi, A.H., Götze, H.J., Emry, E.L., Abdelsalam, M.G., 2020. The lithospheric structure of the saharan metacraton from 3-d integrated geophysical-petrological modeling. Journal of Geophysical Research: Solid Earth 125. doi:10.1029/2019jb018747.

Song, D., Xiao, W., Collins, A.S., Glorie, S., Han, C., Li, Y., 2018. Final subduction processes of the Paleo-Asian Ocean in the Alxa Tectonic Belt (NW China): Constraints from field and chronological data of Permian arc-related volcano-sedimentary rocks. Tectonics 37, 1658–1687. doi:10.1029/2017tc004919.

Song, D., Xiao, W., Windley, B.F., Mao, Q., Ao, S., Wang, H.Y.C., Li, R., 2021. Closure of the Paleo-Asian Ocean in the Middle-Late Triassic (Ladinian-Carnian): Evidence from provenance analysis of retroarc sediments. Geophysical Research Letters 48. doi:10.1029/2021gl094276.

Spaggiari, C.V., Smithies, R.H., Kirkland, C.L., Wingate, M.T., England, R.N., Lu, Y.J., 2018. Buried but preserved: The Proterozoic Arubiddy Ophiolite, Madura Province, Western Australia. Precambrian Research 317, 137–158. doi:10.1016/j.precamres.2018.08.025.

St-Onge, M.R., Searle, M.P., Wodicka, N., 2006. Trans-Hudson Orogen of North America and Himalaya-Karakoram-Tibetan Orogen of Asia: Structural and thermal characteristics of the lower and upper plates. Tectonics 25, n/a–n/a. doi:10.1029/2005tc001907.

Stagg, H., Alcock, M., Borissova, I., Moore, A., 2002. Geological framework of the southern Lord Howe Rise and adjacent areas. Record 2002/25. Geoscience Australia. Canberra.

Stål, T., Reading, A.M., Halpin, J.A., Whittaker, J.M., 2019. A multivariate approach for mapping lithospheric domain boundaries in East Antarctica. Geophysical Research Letters 46, 10404–10416. doi:10.1029/2019gl083453.

Stampfli, G., Hochard, C., Vérard, C., Wilhem, C., vonRaumer, J., 2013. The formation of Pangea. Tectonophysics 593, 1–19. doi:10.1016/j.tecto.2013.02.037.

Stamps, D., Kreemer, C., Fernandes, R., Rajaonarison, T., Rambolamanana, G., 2021. Redefining East African Rift System kinematics. Geology 49, 150–155. doi:10.1130/g47985.1.

Stamps, D.S., Saria, E., Kreemer, C., 2018. A geodetic strain rate model for the East African Rift system. Scientific Reports 8. doi:10.1038/s41598-017-19097-w.

Steinshouer, D.W., Qiang, J., McCabe, P.J., Ryder, R.T., 1999. Maps showing geology, oil and gas fields, and geologic provinces of the Asia Pacific region. Open-file Report 97-470F. US Geological Survey. doi:10.3133/ofr97470f.

Stern, R.J., 1994. Arc assembly and continental collision in the Neoproterozoic East African Orogen: Implications for the consolidation of Gondwanaland. Annual Review of Earth and Planetary Sciences 22, 319–351. doi:10.1146/annurev.ea.22.050194.001535.

Straume, E.O., Gaina, C., Medvedev, S., Hochmuth, K., Gohl, K., Whittaker, J.M., Fattah, R.A., Doornenbal, J.C., Hopper, J.R., 2019. GlobSed: Updated total sediment thickness in the world's oceans. Geochemistry, Geophysics, Geosystems 20, 1756–1772. doi:10.1029/2018gc008115.

Styron, R., Pagani, M., 2020. The GEM global active faults database. Earthquake Spectra 36, 160–180. doi:10.1177/8755293020944182.

Sun, L., Mann, P., Bird, D.E., 2020. Integration of tectonic geomorphology and crustal structure across the active obliquely collisional zone on the island of Hispaniola, northeastern Caribbean. Geological Society, London, Special Publications , SP504–2019–242doi:10.1144/sp504-2019-242.

Symeou, V., Homberg, C., Nader, F.H., Darnault, R., Lecomte, J.C., Papadimitriou, N., 2018. Longitudinal and temporal evolution of the tectonic style along the Cyprus Arc system, assessed through 2-D reflection seismic interpretation. Tectonics 37, 30–47. doi:10.1002/2017tc004667.

Szwillus, W., Afonso, J.C., Ebbing, J., Mooney, W.D., 2019. Global crustal thickness and velocity structure from geostatistical analysis of seismic data. Journal of Geophysical Research: Solid Earth 124, 1626–1652. doi:10.1029/2018jb016593.

Tagami, T., Hasebe, N., 1999. Cordilleran-type orogeny and episodic growth of continents: Insights from the circum-pacific continental margins. Island Arc 8, 206–217. doi:10.1046/j.1440-1738.1999.00232.x.

Tamblyn, R., Hasterok, D., Hand, M., Gard, M., 2021. Mantle heating at ca. 2 Ga by continental insulation: Evidence from granites and eclogites. Geology 50, 91–95. doi:10.1130/g49288.1.

Tang, M., Ji, W.Q., Chu, X., Wu, A., Chen, C., 2020. Reconstructing crustal thickness evolution from europium anomalies in detrital zircons. Geology 49, 76–80. doi:10.1130/g47745.1.

Tetley, M.G., Li, Z.X., Matthews, K.J., Williams, S.E., Müller, R.D., 2020. Decoding Earth's plate tectonic history using sparse geochemical data. Geoscience Frontiers 11, 265–276. doi:10.1016/j.gsf.2019.05.002.

Thiessen, E.J., Gibson, H.D., Regis, D., Pehrsson, S.J., 2018. Deformation and extensional exhumation of 1.9 Ga high-pressure granulites along the Wholdaia Lake shear zone, south Rae craton, Northwest Territories, Canada. Lithosphere 10, 641–661. doi:10.1130/l704.1.

Tiddy, C.J., Betts, P.G., Neumann, M.R., Murphy, F.C., Stewart, J., Giles, D., Sawyer, M., Freeman, H., Jourdan, F., 2020. Interpretation of a ca. 1600–1580 Ma metamorphic core complex in the northern Gawler Craton, Australia. Gondwana Research 85, 263–290. doi:10.1016/j.gr.2020.04.008.

Tohver, E., Teixeira, W., van der Pluijm, B., Geraldes, M.C., Bettencourt, J.S., Rizzotto, G., 2006. Restored transect across the exhumed Grenville orogen of Laurentia and Amazonia, with implications for crustal architecture. Geology 34, 669. doi:10.1130/g22534.1.

Topuz, G., Candan, O., Okay, A.I., von Quadt, A., Othman, M., Zack, T., Wang, J., 2020. Silurian anorogenic basic and acidic magmatism in Northwest Turkey: Implications for the opening of the Paleo-Tethys. Lithos 356-357, 105302. doi:10.1016/j.lithos.2019.105302.

Torsvik, T.H., Amundsen, H., Hartz, E.H., Corfu, F., Kusznir, N., Gaina, C., Doubrovine, P.V., Steinberger, B., Ashwal, L.D., Jamtveit, B., 2013. A Precambrian microcontinent in the Indian Ocean. Nature Geoscience 6, 223–227. doi:10.1038/ngeo1736.

Torsvik, T.H., Andersen, T.B., 2002. The Taimyr fold belt, Arctic Siberia: timing of pre-fold remagnetisation and regional tectonics. Tectonophysics 352, 335–348. doi:10.1016/s0040-1951(02)00274-3.

Torsvik, T.H., Cocks, L.R.M., 2016. Earth History and Palaeogeography. Cambridge University Press. doi:10.1017/9781316225523.

Tretiakova, I.G., Belousova, E.A., Malkovets, V.G., Griffin, W.L., Piazolo, S., Pearson, N.J., O'Reilly, S.Y., Nishido, H., 2017. Recurrent magmatic activity on a lithosphere-scale structure: Crystallization and deformation in kimberlitic zircons. Gondwana Research 42, 126–132. doi:10.1016/j.gr.2016.10.006.

Tuisku, P., Huhma, H., 2006. Evolution of migmatitic granulite complexes: Implications from Lapland Granulite Belt, Part II: Isotopic dating. Bulletin of the Geological Society of Finland 78, 143–175. doi:10.17741/bgsf/78.2.003.

Ueki, K., Hino, H., Kuwatani, T., 2018. Geochemical discrimination and characteristics of magmatic tectonic settings: A machine-learning-based approach. Geochemistry, Geophysics, Geosystems 19, 1327–1347. doi:10.1029/2017gc007401.

Ustaszewski, K., Kounov, A., Schmid, S.M., Schaltegger, U., Krenn, E., Frank, W., Fügenschuh, B., 2010. Evolution of the Adria-Europe plate boundary in the northern Dinarides: From continent-continent collision to back-arc extension. Tectonics 29, n/a–n/a. doi:10.1029/2010tc002668.

Vaes, B., Hinsbergen, D.J.J., Boschman, L.M., 2019. Reconstruction of subduction and back-arc spreading in the NW Pacific and Aleutian Basin: Clues to causes of Cretaceous and Eocene plate reorganizations. Tectonics 38, 1367–1413. doi:10.1029/2018tc005164.

Vallini, D.A., Cannon, W.F., Schulz, K.J., McNaughton, N.J., 2007. Thermal history of low metamorphic grade Paleoproterozoic sedimentary rocks of the Penokean orogen, Lake Superior region: Evidence for a widespread 1786Ma overprint based on xenotime geochronology. Precambrian Research 157, 169–187. doi:10.1016/j.precamres.2007.02.015.

Vernikovsky, V., Vernikovskaya, A., Wingate, M., Popov, N., Kovach, V., 2007. The 880–864Ma granites of the Yenisey Ridge, western Siberian margin: Geochemistry, SHRIMP geochronology, and tectonic implications. Precambrian Research 154, 175–191. doi:10.1016/j.precamres.2006.12.006.

Vernikovsky, V.A., Vernikovskaya, A., Kotov, A., Sal'nikova, E., Kovach, V., 2003. Neoproterozoic accretionary and collisional events on the western margin of the Siberian craton: new geological and geochronological evidence from the Yenisey Ridge. Tectonophysics 375, 147–168. doi:10.1016/s0040-1951(03)00337-8.

Volante, S., Pourteau, A., Collins, W.J., Blereau, E., Li, Z.X., Smit, M., Evans, N.J., Nordsvan, A.R., Spencer, C.J., McDonald, B.J., Li, J., Günter, C., 2020. Multiple P–T–d–t paths reveal the evolution of the final Nuna assembly in northeast Australia. Journal of Metamorphic Geology 38, 593–627. doi:10.1111/jmg.12532.

Wan, Y., Liu, D., Dong, C., Liu, S., Wang, S., Yang, E., 2011. U–Th–Pb behavior of zircons under high-grade metamorphic conditions: A case study of zircon dating of meta-diorite near Qixia, eastern Shandong. Geoscience Frontiers 2, 137–146. doi:10.1016/j.gsf.2011.02.004.

Wandrey, C.J., Law, B.E., 1998. Maps showing geology, oil and gas fields and geologic provinces of South Asia. Open-file Report 97-470C. US Geological Survey. doi:10.3133/ofr97470c.

Wang, C., Li, Z.X., Peng, P., Pisarevsky, S., Liu, Y., Kirscher, U., Nordsvan, A., 2019. Long-lived connection between the north china and north australian cratons in supercontinent nuna: paleomagnetic and geological constraints. Science Bulletin 64, 873–876. doi:10.1016/j.scib.2019.04.028.

Wang, C.C., Jacobs, J., Elburg, M.A., Läufer, A., Thomas, R.J., Elvevold, S., 2020. Grenville-age continental arc magmatism and crustal evolution in central Dronning Maud Land (East Antarctica): Zircon geochronological and Hf–O isotopic evidence. Gondwana Research 82, 108–127. doi:10.1016/j.gr.2019.12.004.

Wang, Y., Fan, W., Zhang, G., Zhang, Y., 2013. Phanerozoic tectonics of the South China Block: Key observations and controversies. Gondwana Research 23, 1273–1305. doi:10.1016/j.gr.2012.02.019.

Weber, F., Gauthier-Lafaye, F., Whitechurch, H., Ulrich, M., Albani, A.E., 2016. The 2-Ga Eburnean Orogeny in Gabon and the opening of the Francevillian intracratonic basins: A review. Comptes Rendus Geoscience 348, 572–586. doi:10.1016/j.crte.2016.07.003.

Weller, O.M., Mottram, C.M., St-Onge, M.R., Möller, C., Strachan, R., Rivers, T., Copley, A., 2021. The metamorphic and magmatic record of collisional orogens. Nature Reviews Earth & Environment 2, 781–799. doi:10.1038/s43017-021-00218-z.

Weller, O.M., St-Onge, M.R., 2017. Record of modern-style plate tectonics in the palaeoproterozoic trans-hudson orogen. Nature Geoscience 10, 305–311. doi:10.1038/ngeo2904.

Whalen, J.B., Berman, R.G., Davis, W.J., Sanborn-Barrie, M., Nadeau, L., 2018. Bedrock geochemistry of the central Thelon Tectonic Zone, Nunavut. Technical Report. doi:10.4095/306385.

White, L.F., Bailey, I., Foster, G.L., Allen, G., Kelley, S.P., Andrews, J.T., Hogan, K., Dowdeswell, J.A., Storey, C.D., 2016. Tracking the provenance of Greenland-sourced, Holocene aged, individual sand-sized ice-rafted debris using the Pb-isotope compositions of feldspars and 40 Ar/ 39 Ar ages of hornblendes. Earth and Planetary Science Letters 433, 192–203. doi:10.1016/j.epsl.2015.10.054.

Whitmeyer, S., Karlstrom, K.E., 2007. Tectonic model for the Proterozoic growth of North America. Geosphere 3, 220. doi:10.1130/ges00055.1.

Wilde, S.A., Zhao, G., Sun, M., 2002. Development of the North China Craton during the late Archaean and its final amalgamation at 1.8 Ga: some speculations on its position within a global palaeoproterozoic supercontinent. Gondwana Research 5, 85–94. doi:10.1016/s1342-937x(05)70892-3.

Willner, A.P., Gopon, M., Glodny, J., Puchkov, V.N., Schertl, H.P., 2019. Timanide (Ediacaran-Early Cambrian) metamorphism at the transition from eclogite to amphibolite facies in the Beloretsk Complex, SW-Urals, Russia. Journal of Earth Science 30, 1144–1165. doi:10.1007/s12583-019-1249-2.

Winberry, J.P., Anandakrishnan, S., 2004. Crustal structure of the West Antarctic rift system and Marie Byrd Land hotspot. Geology 32, 977. doi:10.1130/g20768.1.

Windley, B.F., Alexeiev, D., Xiao, W., Kröner, A., Badarch, G., 2007. Tectonic models for accretion of the Central Asian Orogenic Belt. Journal of the Geological Society 164, 31–47. doi:10.1144/0016-76492006-022.

Wingate, M.T.D., Pisarevsky, S.A., Evans, D.A.D., 2002. Rodinia connections between Australia and Laurentia: no SWEAT, no AUSWUS? Terra Nova 14, 121–128. doi:10.1046/j.1365-3121.2002.00401.x.

Wong, B.L., Morrissey, L.J., Hand, M., Fields, C.E., Kelsey, D.E., 2015. Grenvillian-aged reworking of late Paleoproterozoic crust of the southern North Australian Craton, central Australia: Implications for the assembly of Mesoproterozoic Australia. Precambrian Research 270, 100–123. doi:10.1016/j.precamres.2015.09.001.

Wu, F.Y., Yang, J.H., Xu, Y.G., Wilde, S.A., Walker, R.J., 2019. Destruction of the North China Craton in the Mesozoic. Annual Review of Earth and Planetary Sciences 47, 173–195. doi:10.1146/annurev-earth-053018-060342.

Wu, J.L., Zhang, H.F., Zhai, M.G., Guo, J.H., Liu, L., Yang, W.Q., Wang, H.Z., Zhao, L., Jia, X.L., Wang, W., 2016. Discovery of pelitic high-pressure granulite from Manjinggou of the Huai'an Complex, North China Craton: Metamorphic P–T evolution and geological implications. Precambrian Research 278, 323–336. doi:10.1016/j.precamres.2016.03.001.

Wynne, P., Bacchin, M., 2009. Index of Gravity Surveys (Second Edition). Geoscience Australia Record 2009/07. Geoscience Australia. Canberra, Australia.

Xiao, W., Windley, B.F., Sun, S., Li, J., Huang, B., Han, C., Yuan, C., Sun, M., Chen, H., 2015. A Tale of Amalgamation of Three Permo-Triassic Collage Systems in Central Asia: Oroclines, Sutures, and Terminal Accretion. Annual Review of Earth and Planetary Sciences 43, 477–507. doi:10.1146/annurev-earth-060614-105254.

Xu, Y., Zeyen, H., Hao, T., Santosh, M., Li, Z., Huang, S., Xing, J., 2016. Lithospheric structure of the North China Craton: Integrated gravity, geoid and topography data. Gondwana Research 34, 315–323. doi:10.1016/j.gr.2015.03.010.

Yang, B., Collins, A.S., Blades, M.L., Munson, T.J., Payne, J.L., Glorie, S., Farkaš, J., 2020. Tectonic controls on sedimentary provenance and basin geography of the Mesoproterozoic Wilton package, McArthur Basin, northern Australia. Geological Magazine 159, 179–198. doi:10.1017/s0016756820001223.

Yang, J.H., Zhang, M., Wu, F.Y., 2018. Mesozoic decratonization of the North China Craton by lithospheric delamination: Evidence from Sr-Nd-Hf-Os isotopes of mantle xenoliths of Cenozoic alkaline basalts in Yangyuan, Hebei Province, China. Journal of Asian Earth Sciences 160, 396–407. doi:10.1016/j.jseaes.2017.09.002.

Yin, A., Brandl, G., Kröner, A., 2019. Plate-tectonic processes at ca. 2.0 Ga: Evidence from >600 km of plate convergence. Geology 48, 103–107. doi:10.1130/g47070.1.

Yin, C., Zhao, G., Wei, C., Sun, M., Guo, J., Zhou, X., 2014. Metamorphism and partial melting of high-pressure pelitic granulites from the qianlishan complex: Constraints on the tectonic evolution of the khondalite belt in the north china craton. Precambrian Research 242, 172–186. doi:10.1016/j.precamres.2013.12.025.

Zahirovic, S., Seton, M., Müller, R.D., 2014. The Cretaceous and Cenozoic tectonic evolution of Southeast Asia. Solid Earth 5, 227–273. doi:10.5194/se-5-227-2014.

Žák, J., Verner, K., Janoušek, V., Holub, F.V., Kachlík, V., Finger, F., Hajná, J., Tomek, F., Vondrovic, L., Trubač, J., 2014. A plate-kinematic model for the assembly of the Bohemian Massif constrained by structural relationships around granitoid plutons. Geological Society, London, Special Publications 405, 169–196. doi:10.1144/sp405.9.

Zhang, S., Li, Z.X., Evans, D.A., Wu, H., Li, H., Dong, J., 2012. Pre-Rodinia supercontinent Nuna shaping up: A global synthesis with new paleomagnetic results from North China. Earth and Planetary Science Letters 353-354, 145–155. doi:10.1016/j.epsl.2012.07.034.

Zhang, S.H., Ernst, R.E., Munson, T.J., Pei, J., Hu, G., Liu, J.M., Zhang, Q.Q., Cai, Y.H., Zhao, Y., 2022. Comparisons of the Paleo-Mesoproterozoic large igneous provinces and black shales in the North China and North Australian cratons. Fundamental Research 2, 84–100. doi:10.1016/j.fmre.2021.10.009.

Zhang, T., Gordon, R.G., Mishra, J.K., Wang, C., 2017. The Malpelo Plate Hypothesis and implications for nonclosure of the Cocos-Nazca-Pacific plate motion circuit. Geophysical Research Letters 44, 8213–8218. doi:10.1002/2017gl073704.

Zhang, Z., Shu, Q., Yang, X., Wu, C., Zheng, C., Xu, J., 2019. Review on the tectonic terranes associated with metallogenic zones in southeast asia. Journal of Earth Science 30, 1–19. doi:10.1007/s12583-019-0858-0.

Zhao, G., Cawood, P.A., Li, S., Wilde, S.A., Sun, M., Zhang, J., He, Y., Yin, C., 2012. Amalgamation of the North China Craton: Key issues and discussion. Precambrian Research 222-223, 55–76. doi:10.1016/j.precamres.2012.09.016.

Zhao, G., Cawood, P.A., Wilde, S.A., Sun, M., 2002. Review of global 2.1–1.8 Ga orogens: implications for a pre-Rodinia supercontinent. Earth-Science Reviews 59, 125–162. doi:10.1016/S0012-8252(02)00073-9.

Zhao, G., Li, S., Sun, M., Wilde, S.A., 2011. Assembly, accretion, and break-up of the Palaeo-Mesoproterozoic Columbia supercontinent: record in the North China Craton revisited. International Geology Review 53, 1331–1356. doi:10.1080/00206814.2010.527631.

wei Zhou, H., Murphy, M.A., 2005. Tomographic evidence for wholesale underthrusting of India beneath the entire Tibetan plateau. Journal of Asian Earth Sciences 25, 445–457. doi:10.1016/j.jseaes.2004.04.007.

Zi, J.W., Sheppard, S., Muhling, J.R., Rasmussen, B., 2021. Refining the Paleoproterozoic tectonothermal history of the Penokean Orogen: New U-Pb age constraints from the Pembine-Wausau terrane, Wisconsin, USA. GSA Bulletin doi:10.1130/b36114.1.